Jan Lunze

Networked Control of Multi-Agent Systems: Application Studies

Figures

Edition MoRa

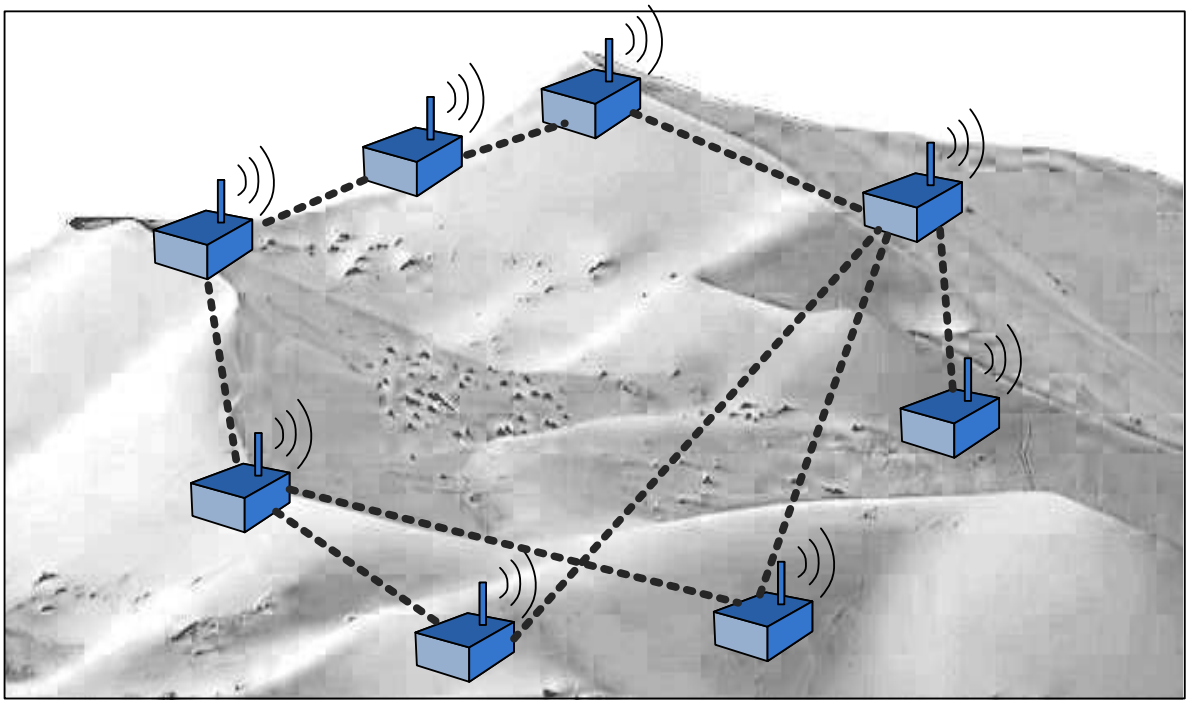

Fig. 0: Sensor network

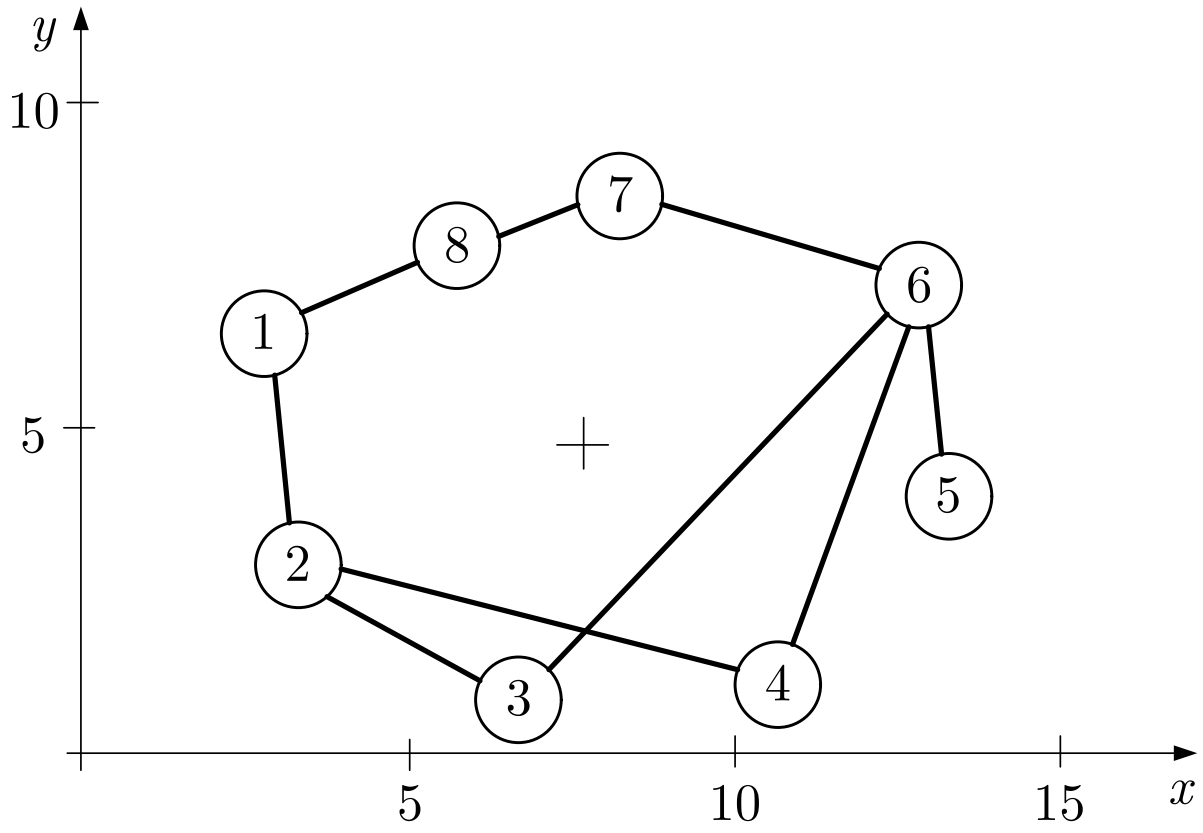

Fig. 1: Two communication graphs of sensor networks drawn in the x/y-coordinate system with the centroid marked by "+" (I)

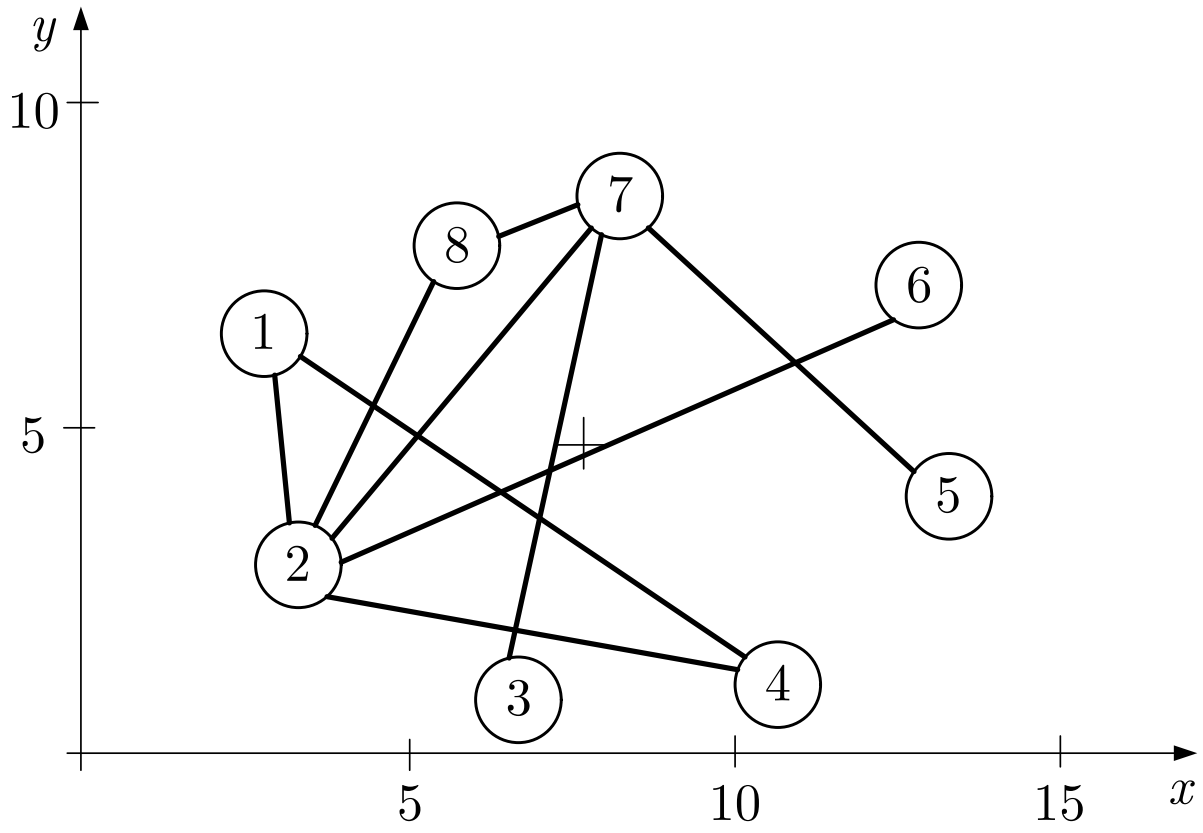

Fig. 1: Two communication graphs of sensor networks drawn in the x/y-coordinate system with the centroid marked by "+" (II)

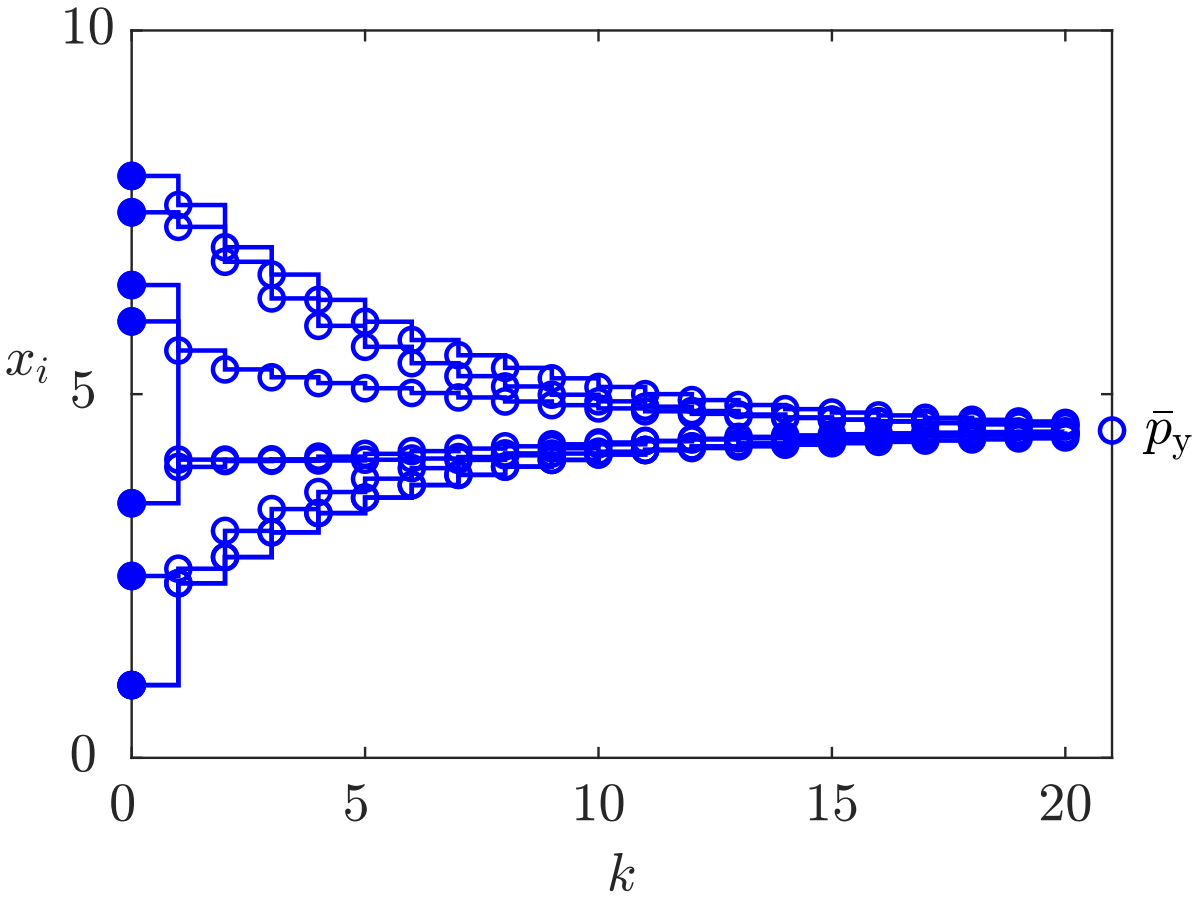

Fig. 2: Convergence of the sensor states towards the consensus value $\bar{p}_{\mathrm{y}}$ for the two communication graphs of Fig. 1 (I)

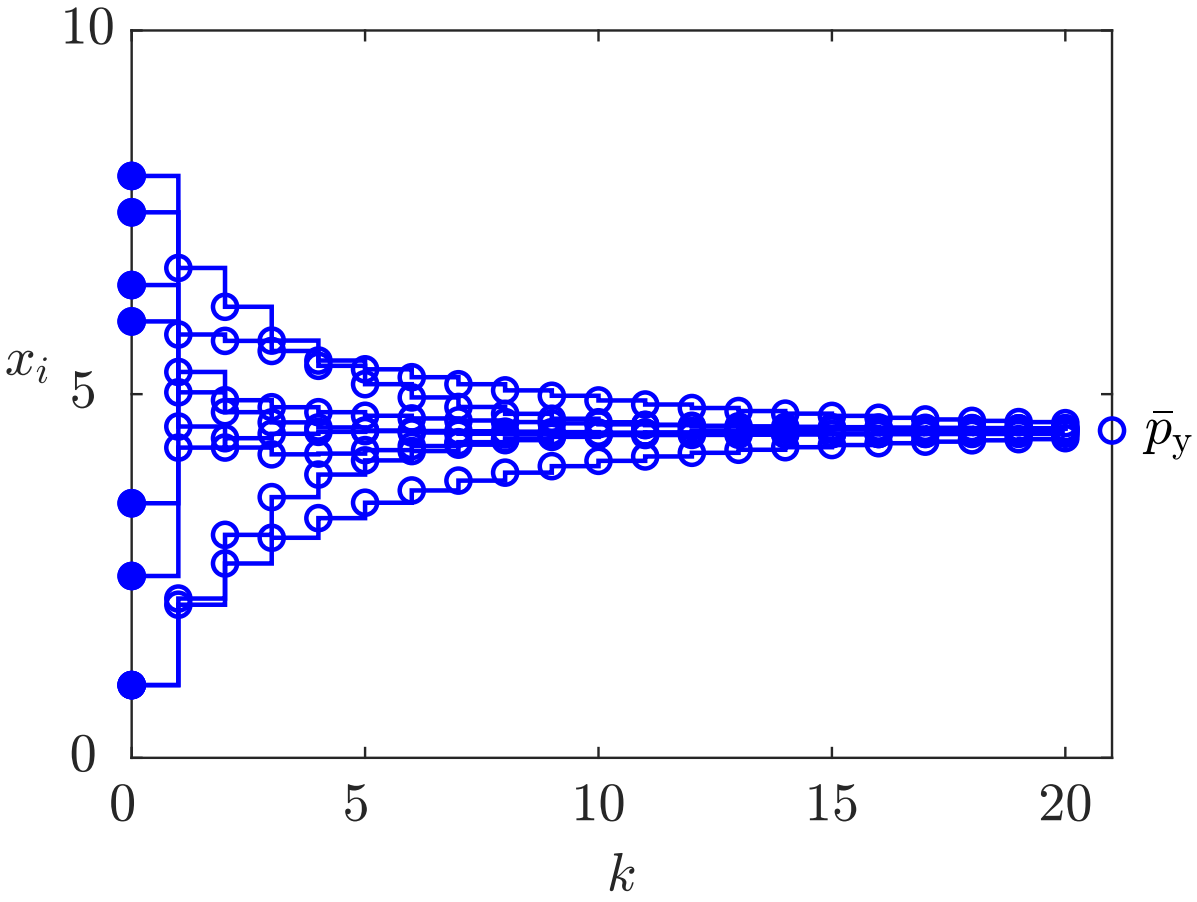

Fig. 2: Convergence of the sensor states towards the consensus value $\bar{p}_{\rm y}$ for the two communication graphs of Fig. 1 (II)

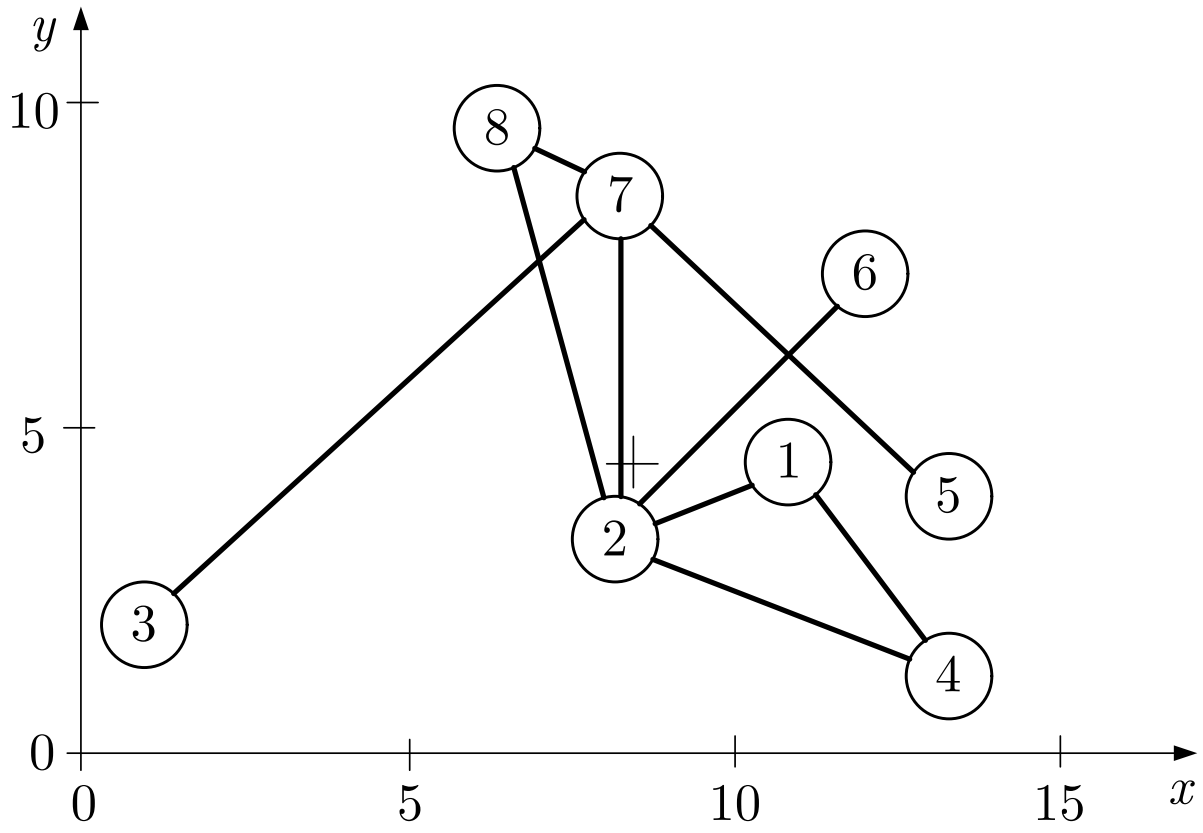

Fig. 3: Determination of a centroid that lies outside of the polygon. Communication graph of the sensor network

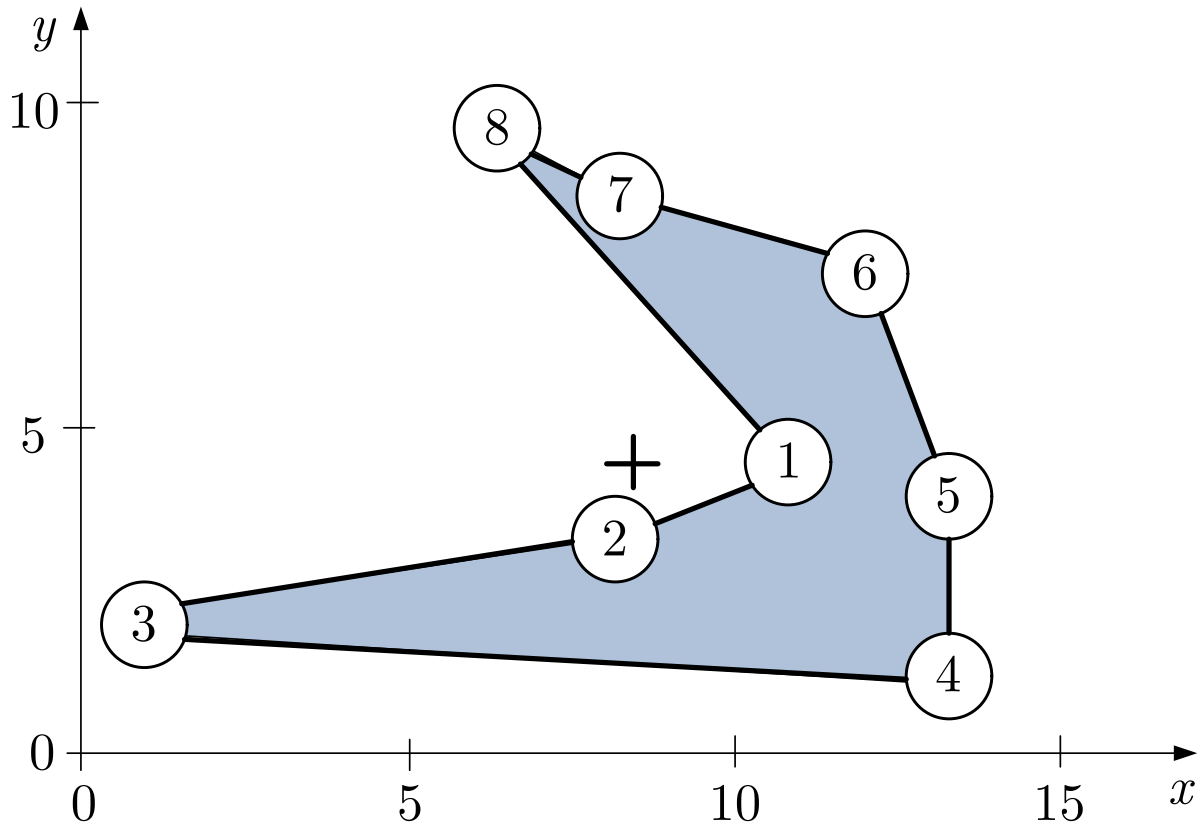

Fig. 3: Determination of a centroid that lies outside of the polygon. Polygon formed by the sensors

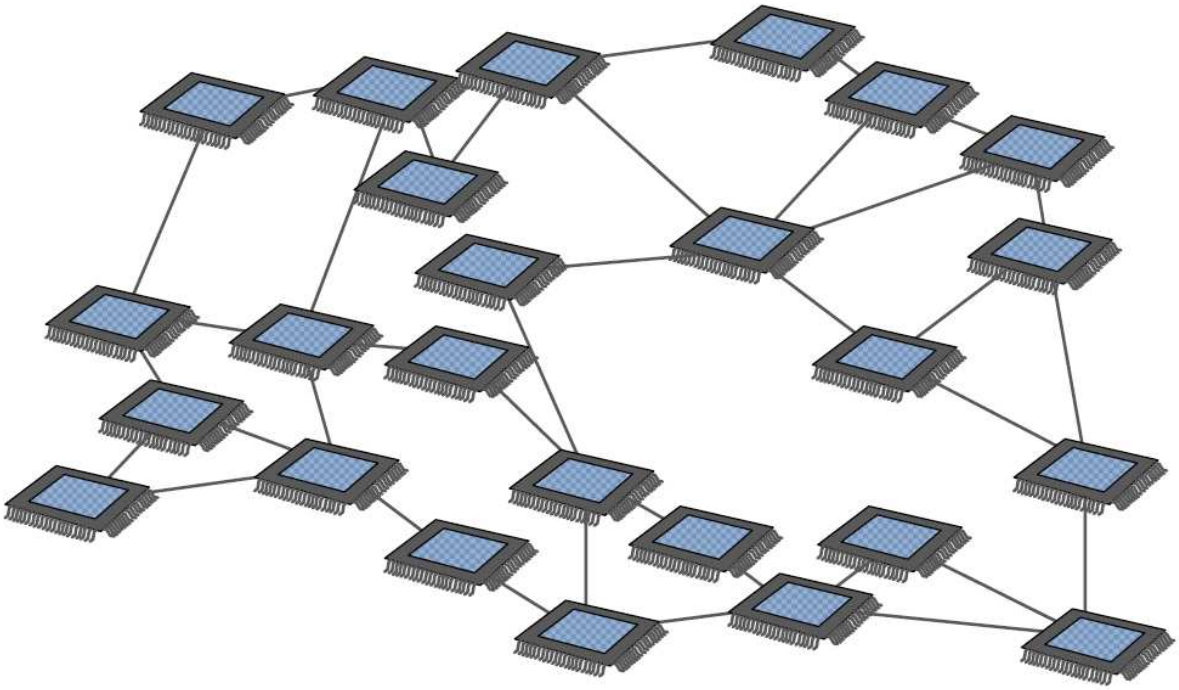

Fig. 0: Networked processors cooperate to solve a linear equation

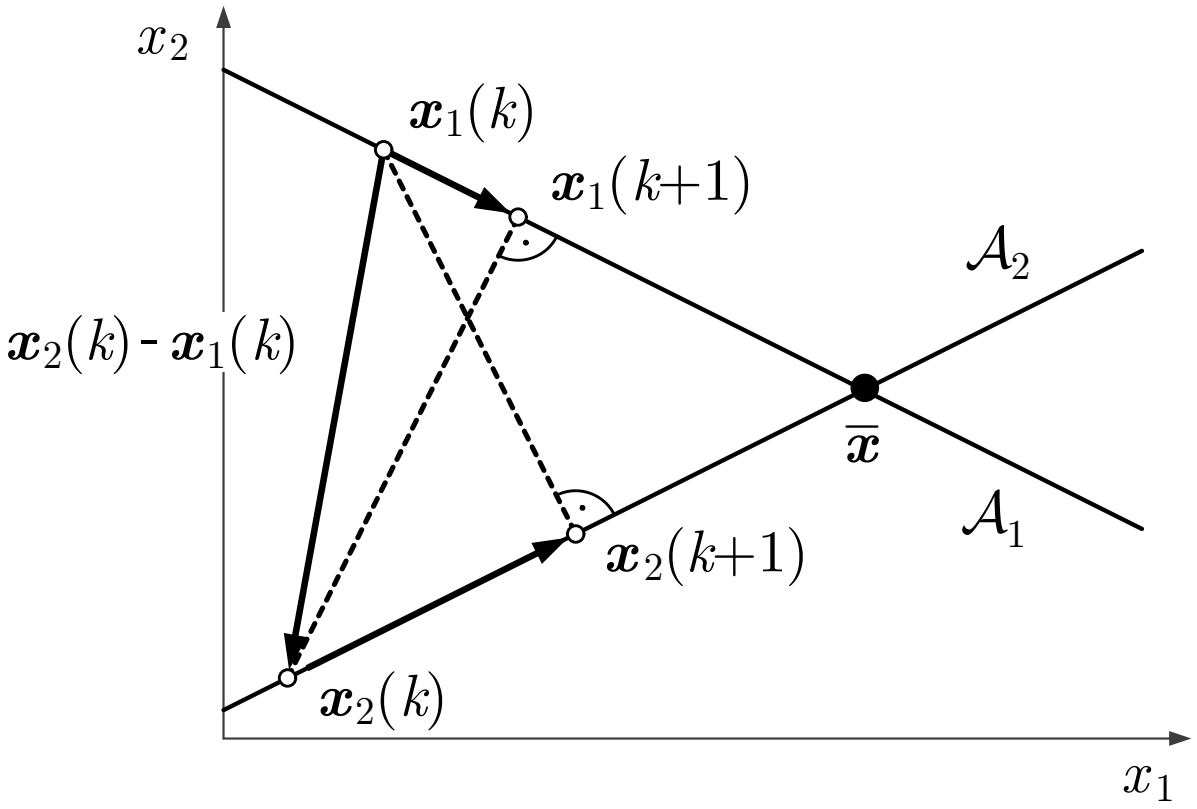

Fig. 1: One iteration steps of the distributed algorithm

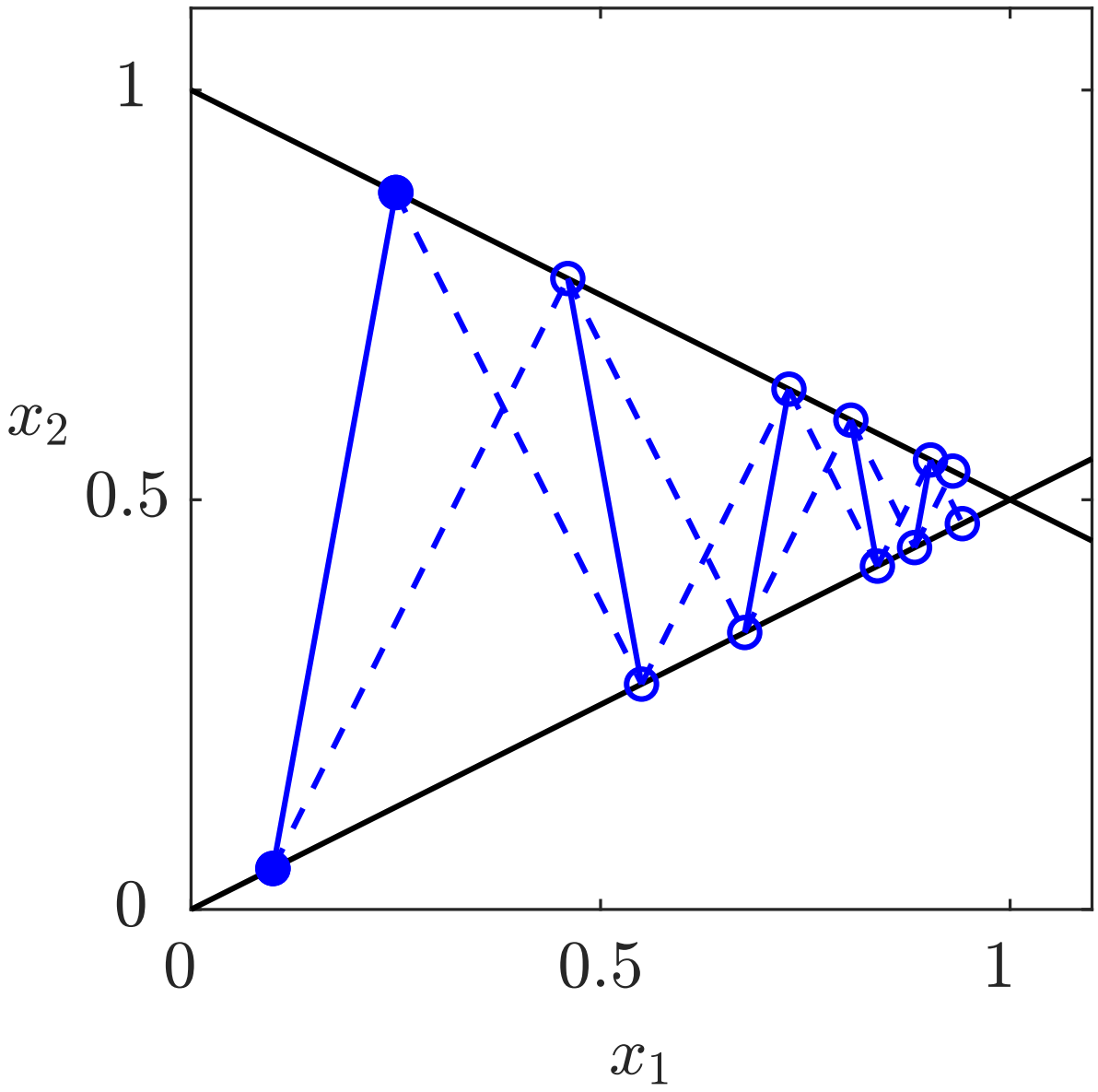

Fig. 1: One iteration steps of the distributed algorithm

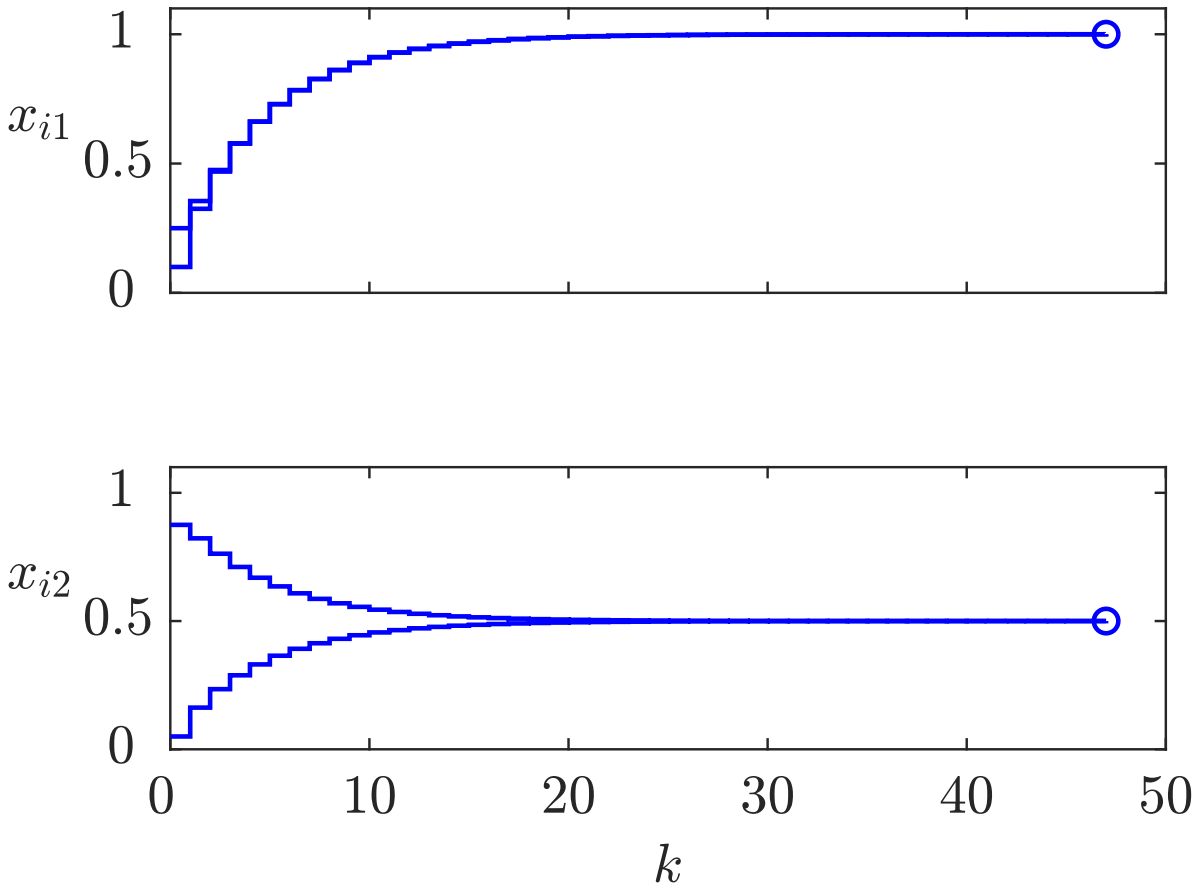

Fig. 2: Solution of a linear equation as a consensus problem

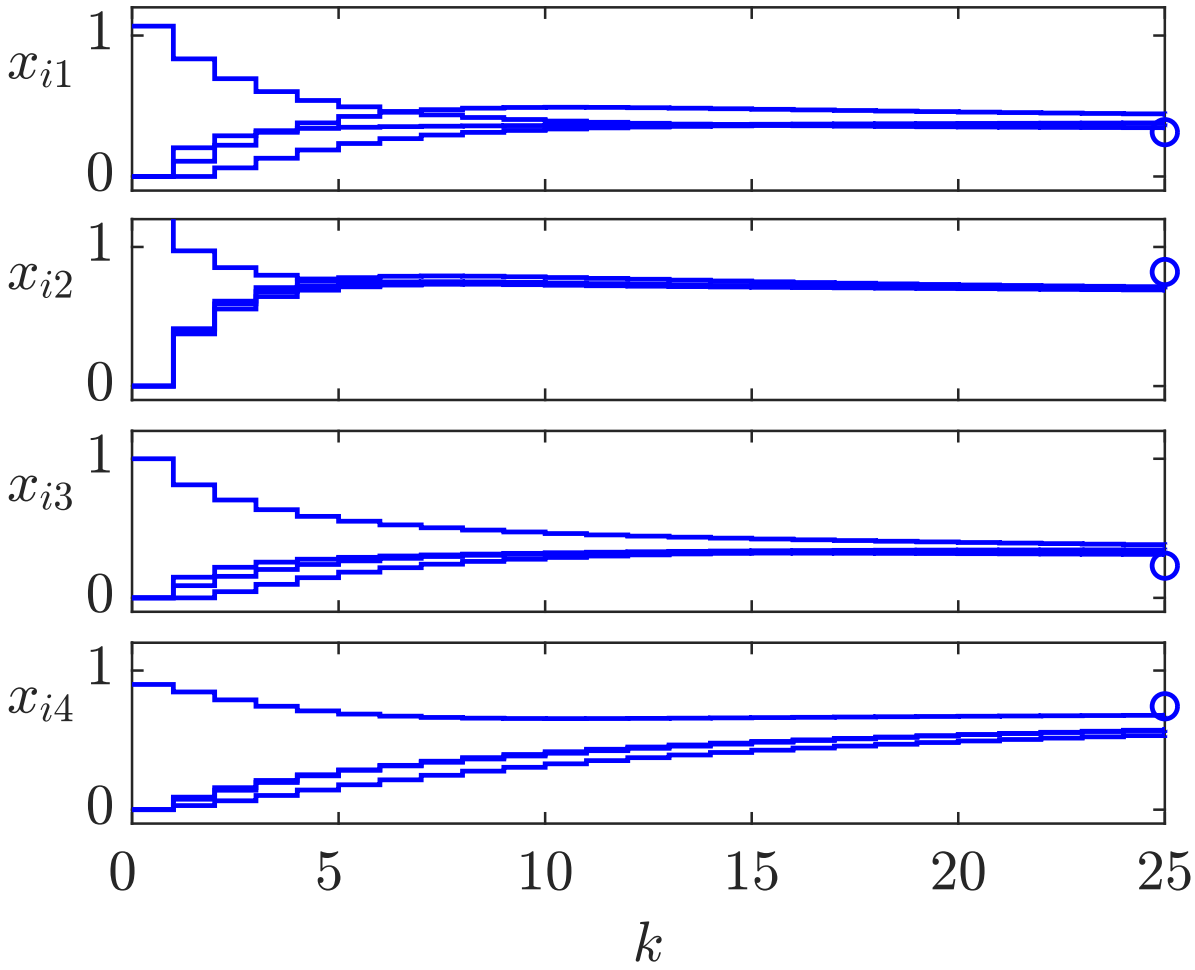

Fig. 3: Solution of a linear equation with two communication structures

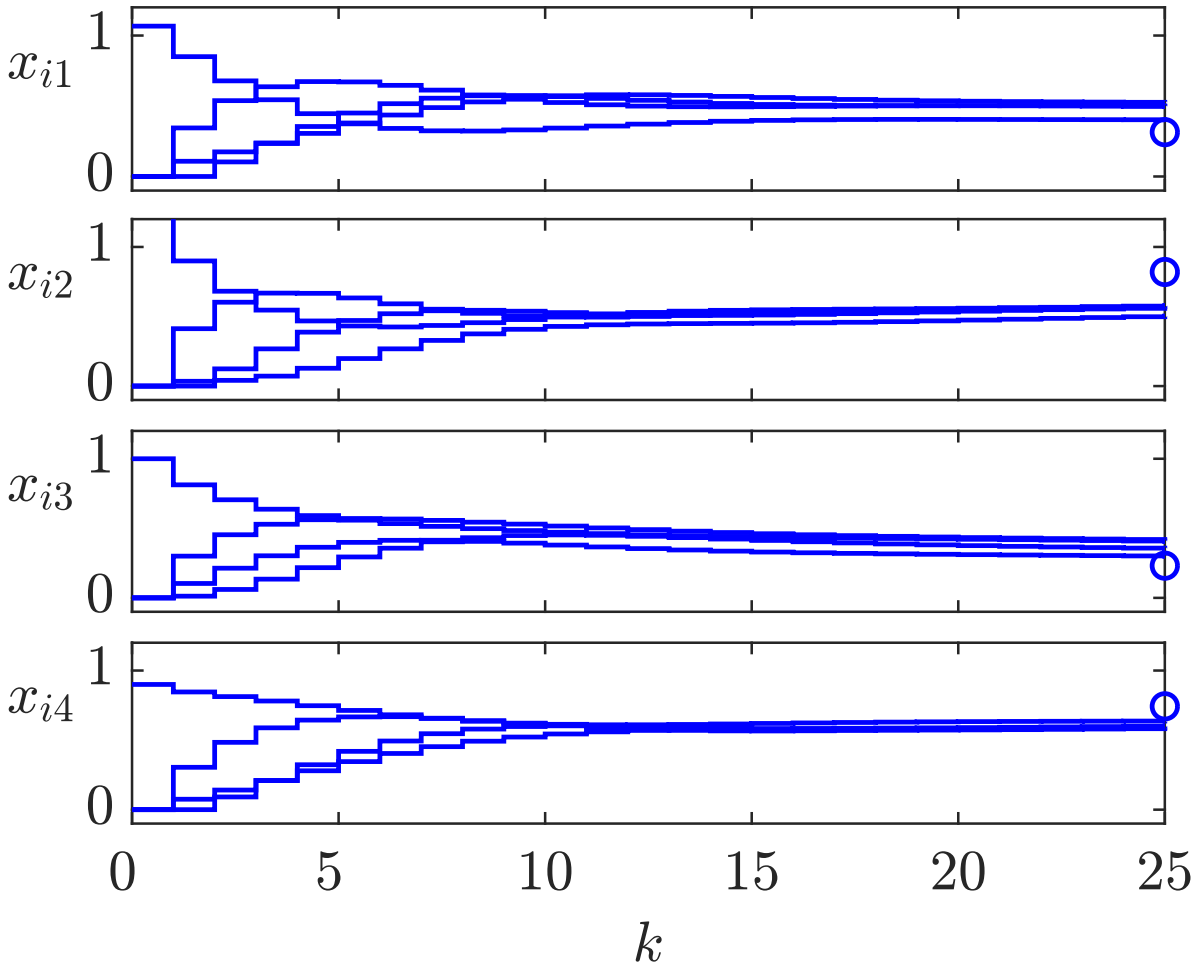

Fig. 3: Solution of a linear equation with two communication structures

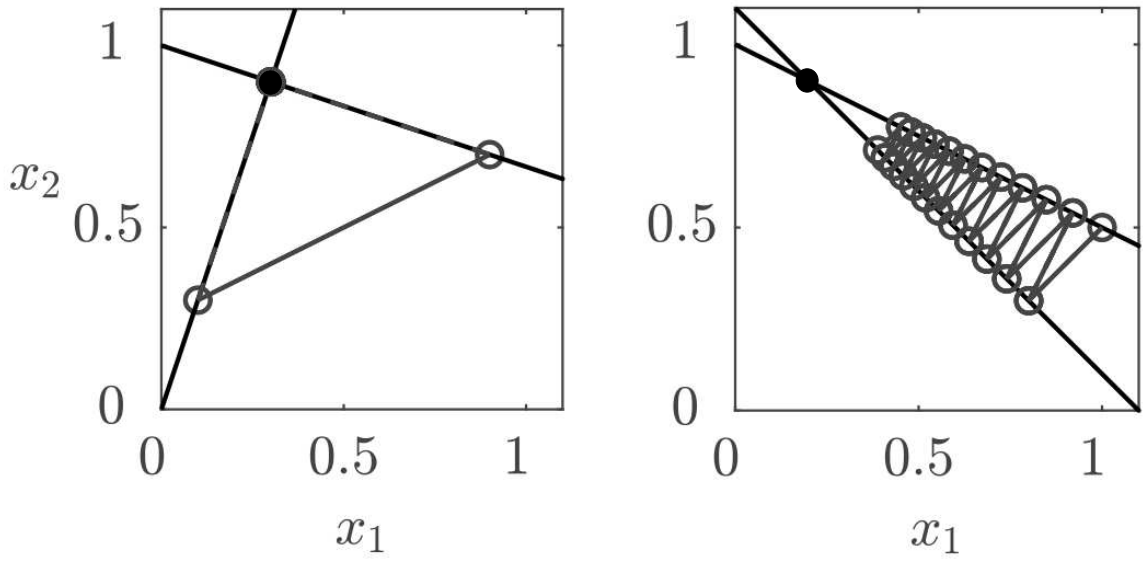

Fig. 4: Two examples with different convergence properties for the same communication structure

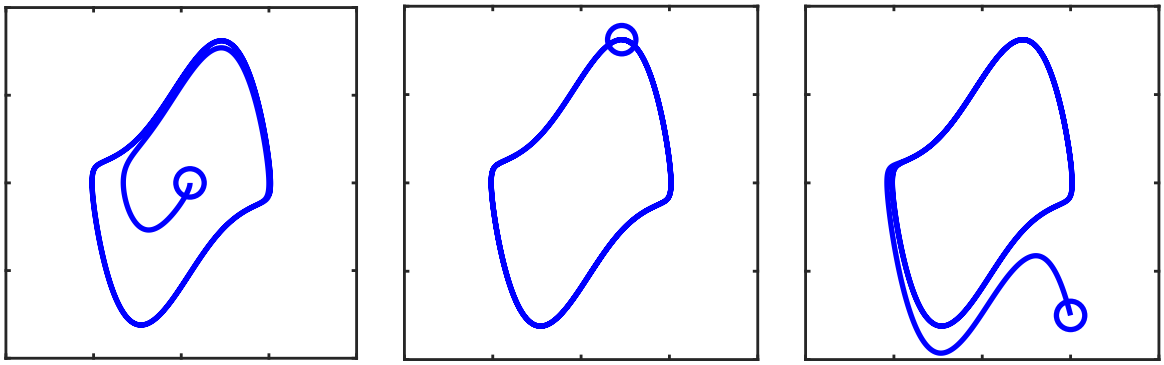

Fig. 0: Behaviour of van der Pol oscillators

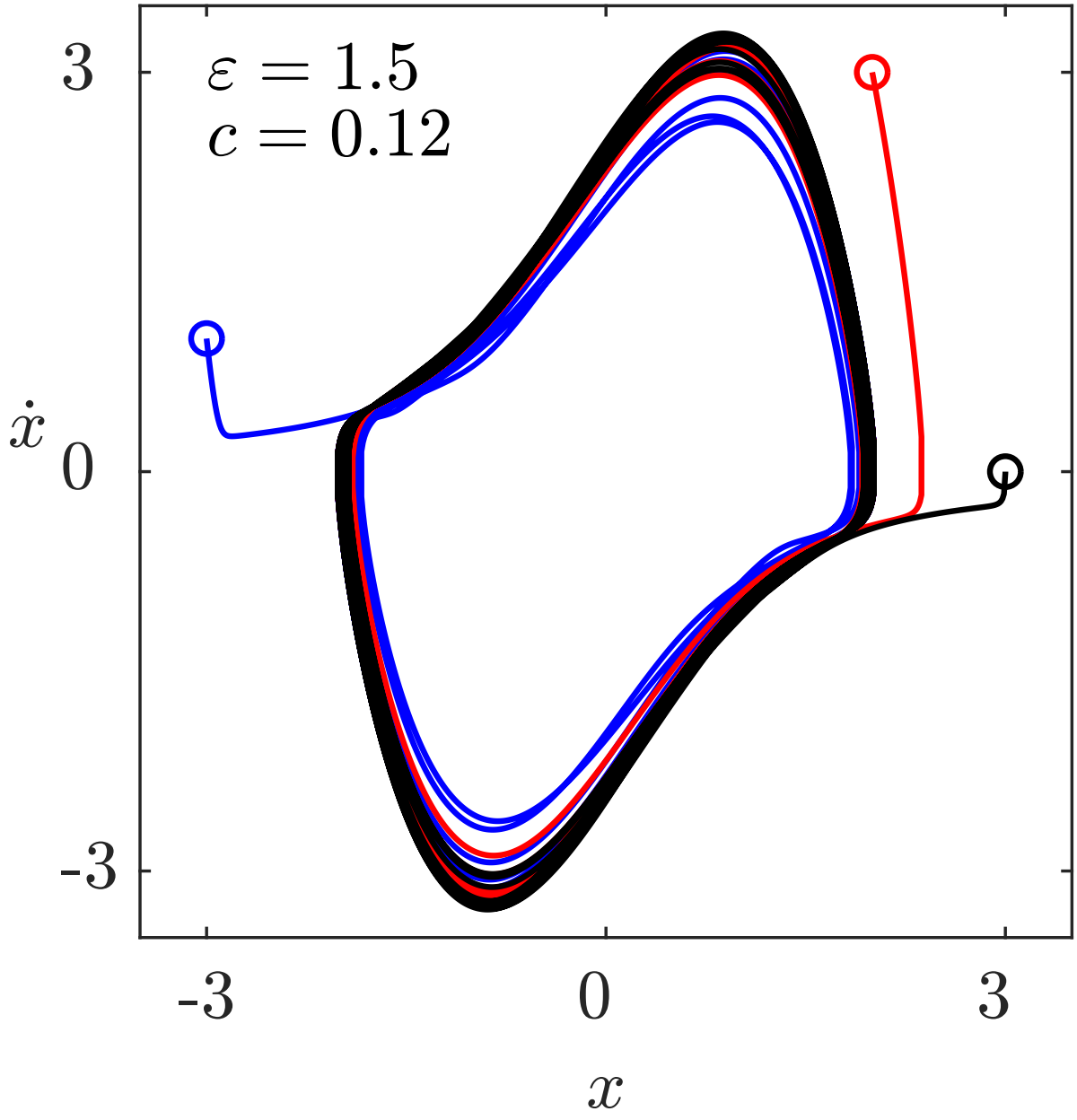

Fig. 1: Synchronisation of three van der Pol oscillators that are coupled in a directed ring

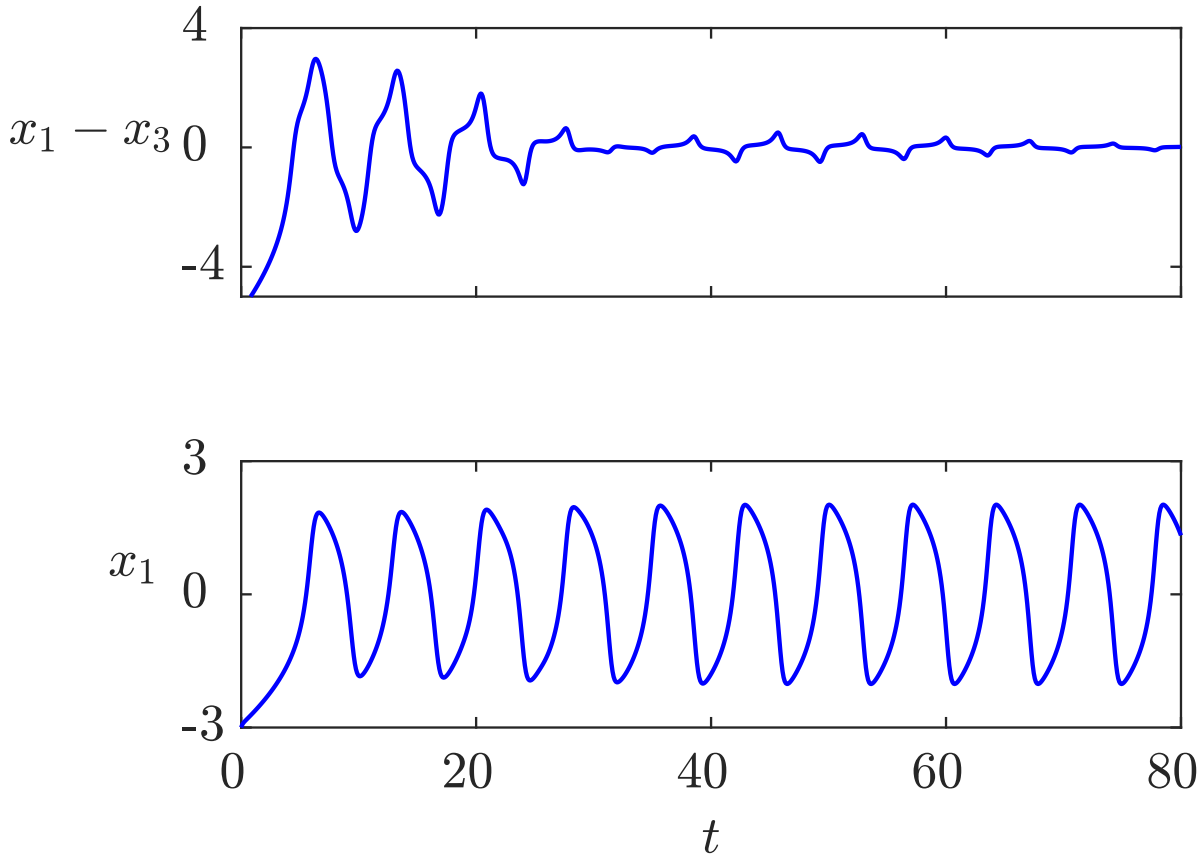

Fig. 1: Synchronisation of three van der Pol oscillators that are coupled in a directed ring

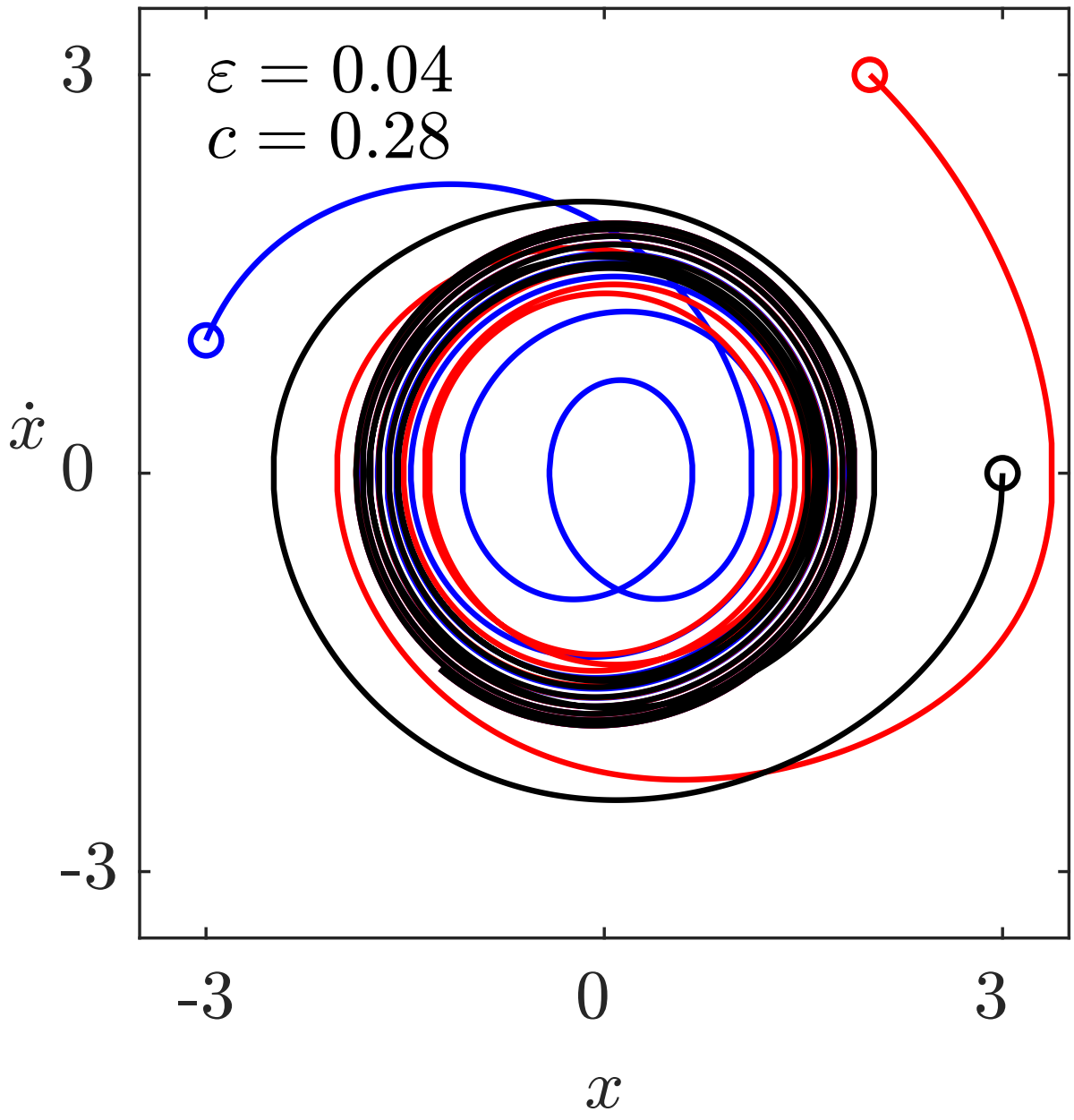

Fig. 2: Synchronisation of three van der Pol oscillators with small damping factor

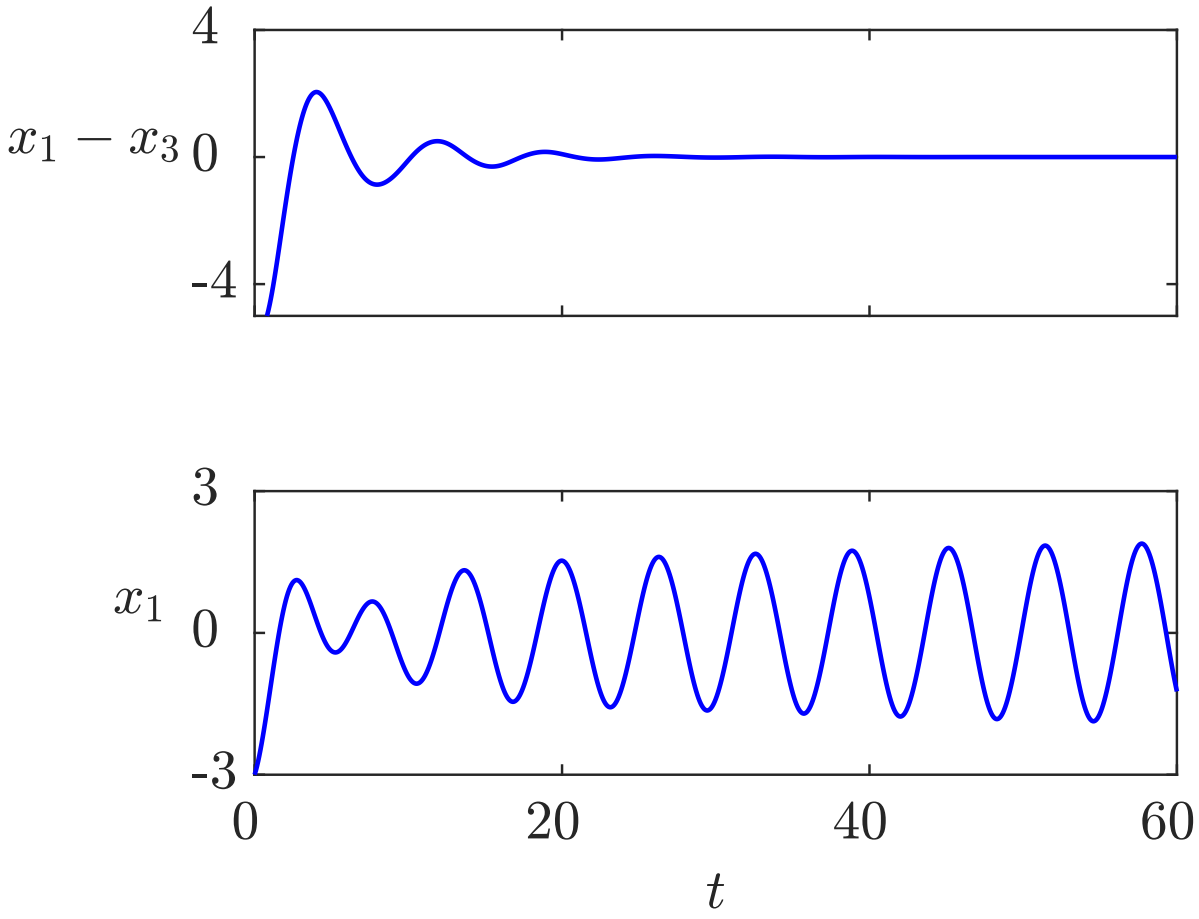

Fig. 2: Synchronisation of three van der Pol oscillators with small damping factor

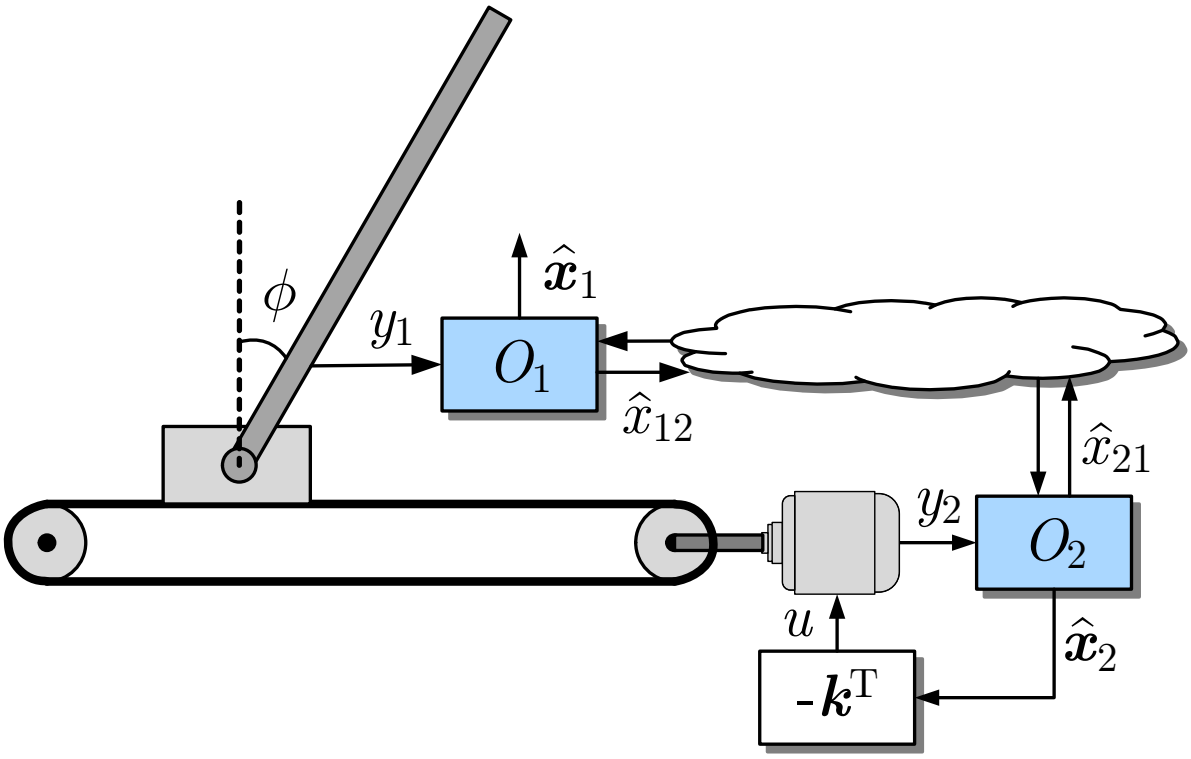

Fig. 0: Inverted pendulum with distributed state observers

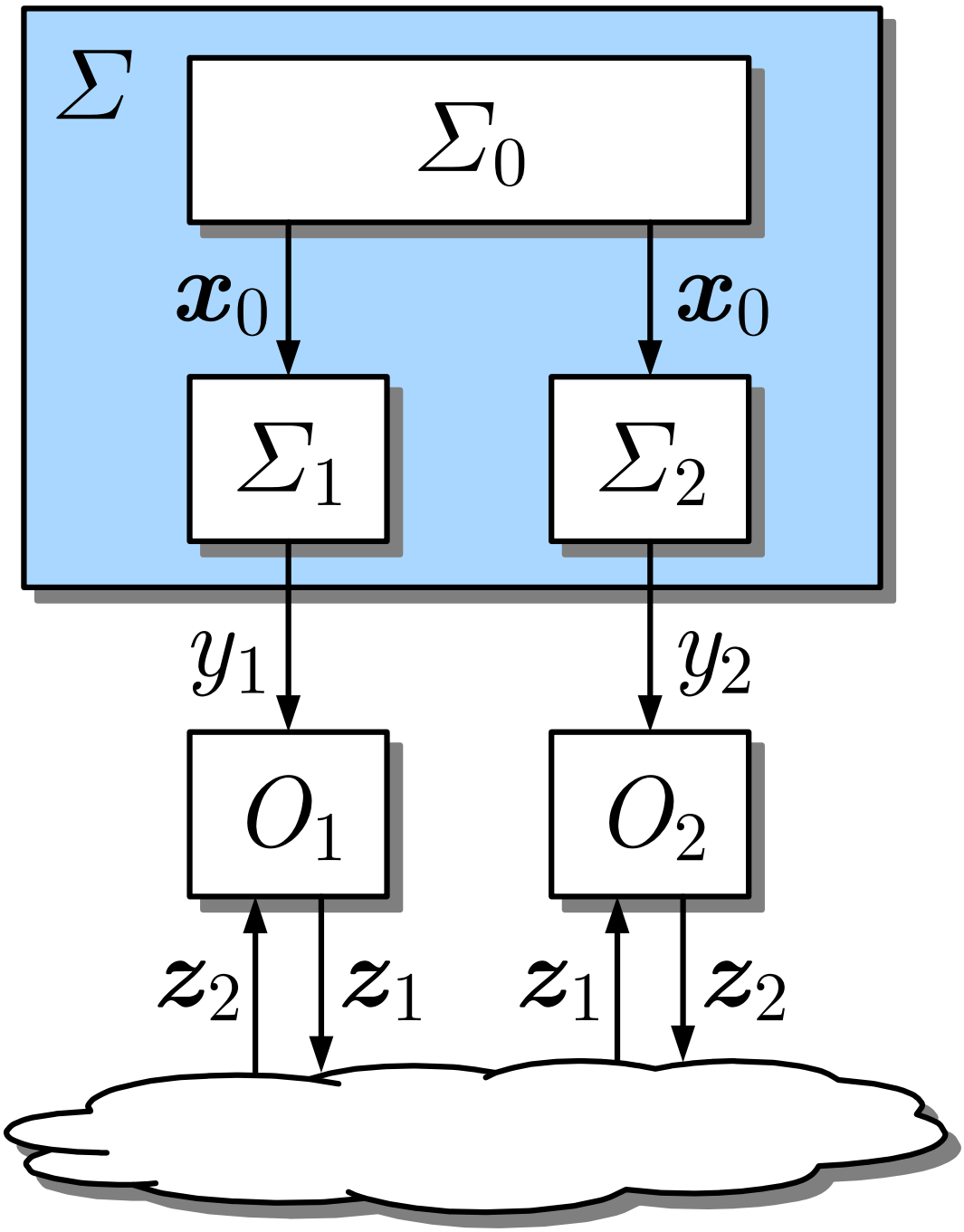

Fig. 1. Distributed observers for the system Σ

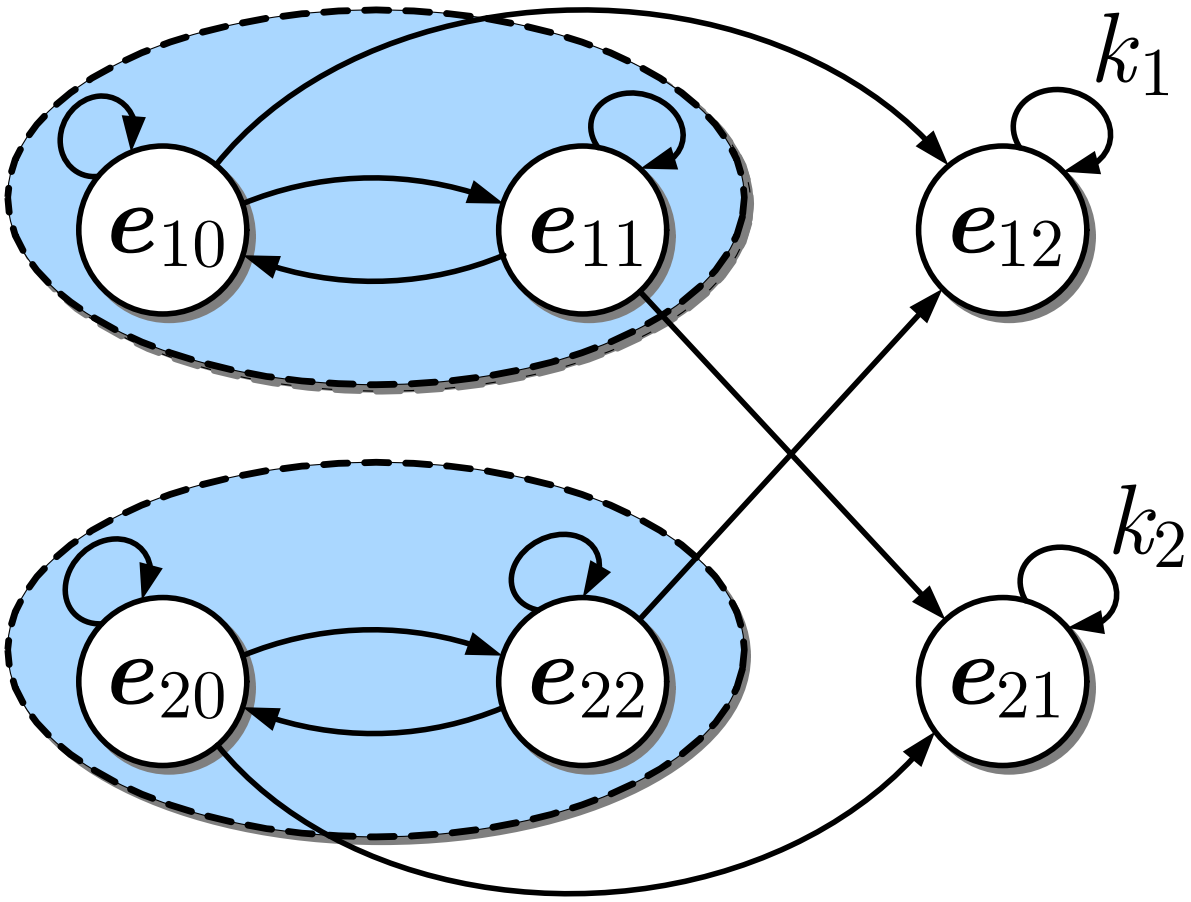

Fig. 2: Structure graph of the system matrix of the error representation

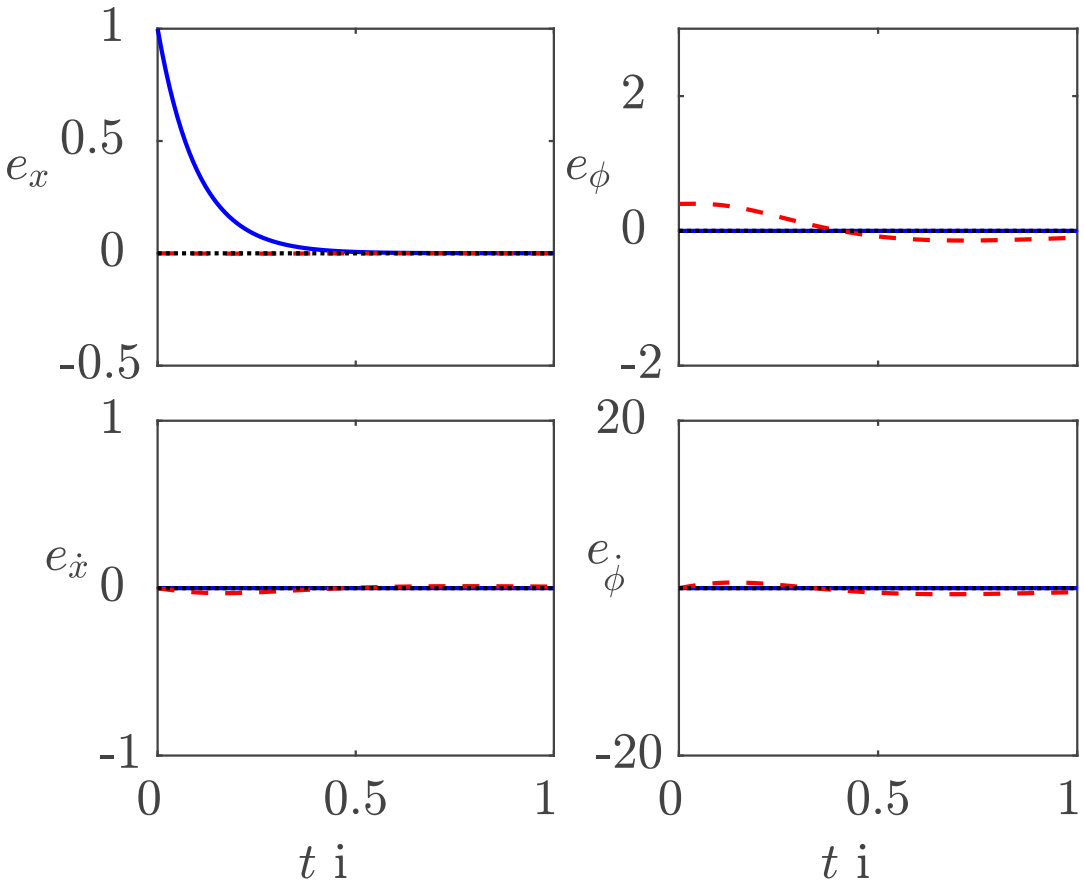

Fig. 3: Observation errors of the distributed state observer (O_1 —, O_2 - - -)

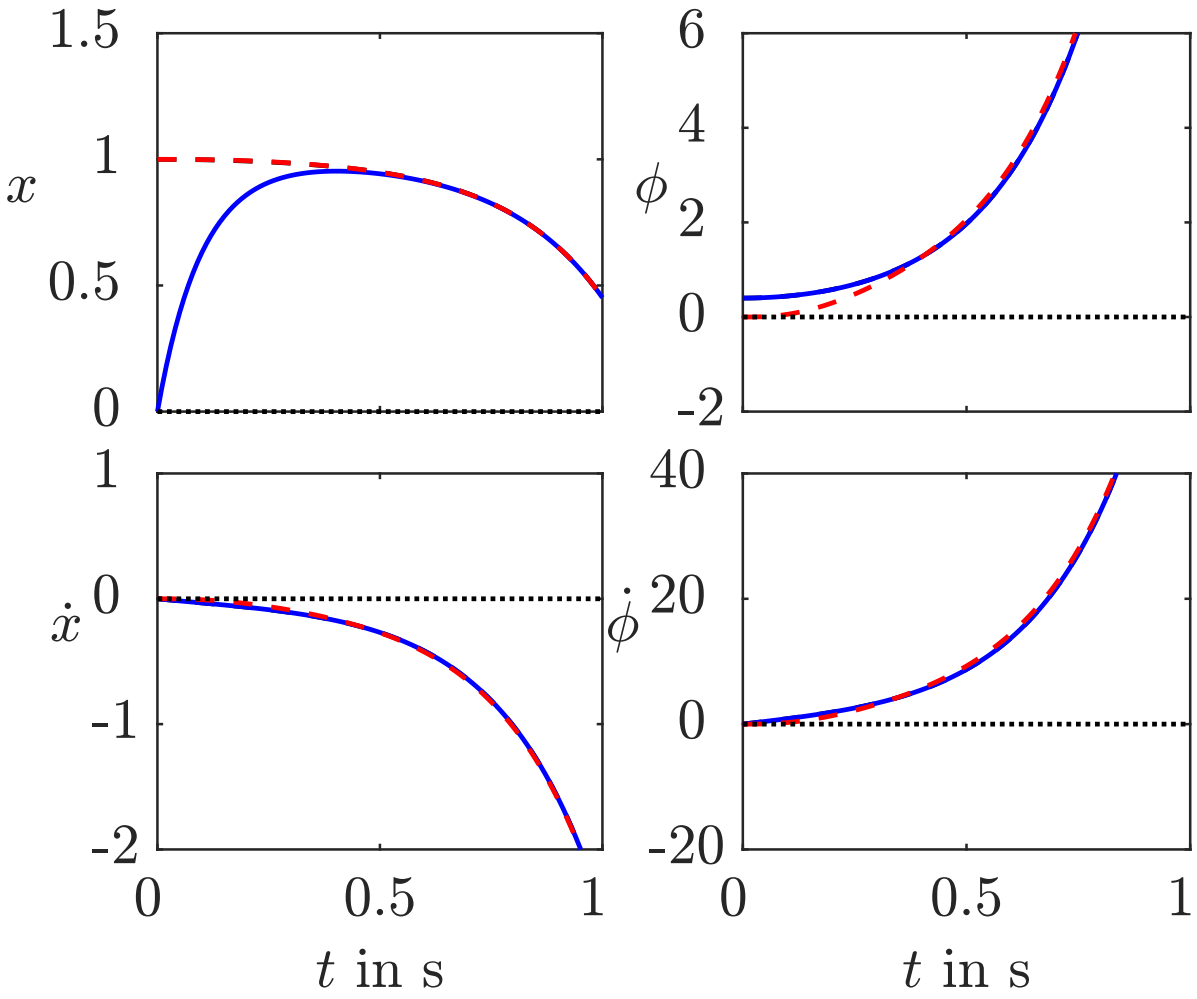

Fig. 4: Observation results obtained by the distributed observer

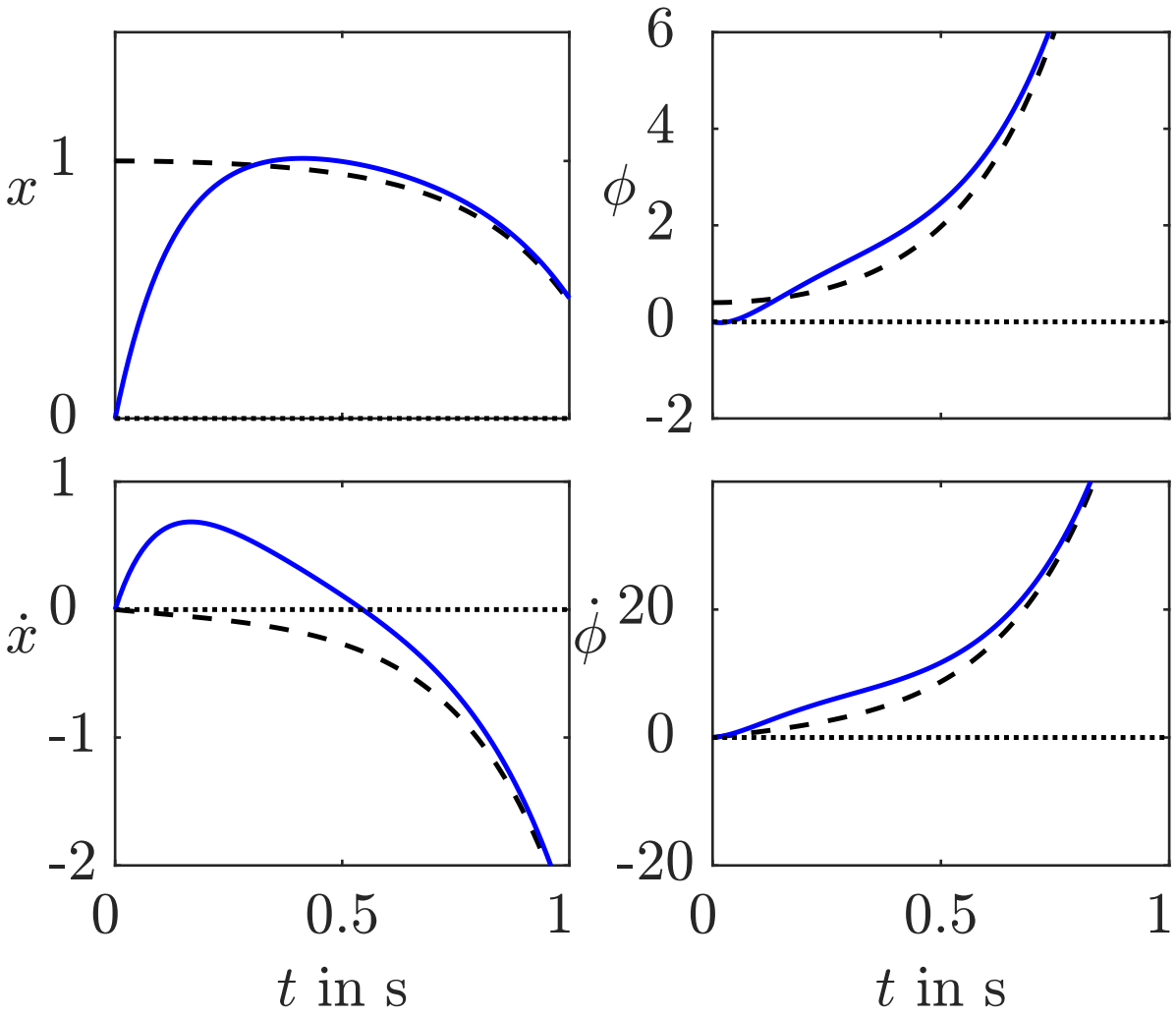

Fig. 4: Observation results obtained by a centralised state observer

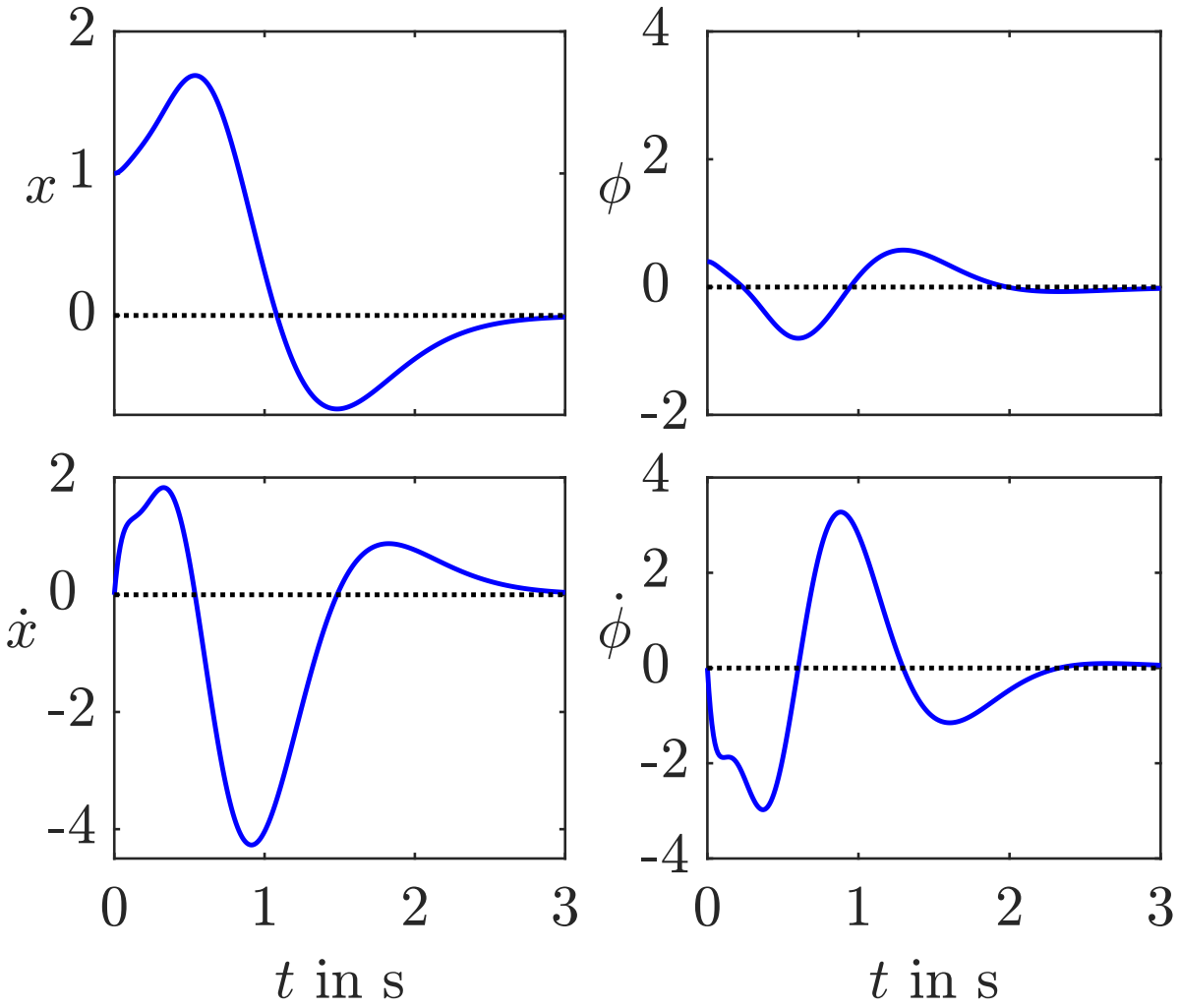

Fig. 5: Behaviour of the stabilised pendulum

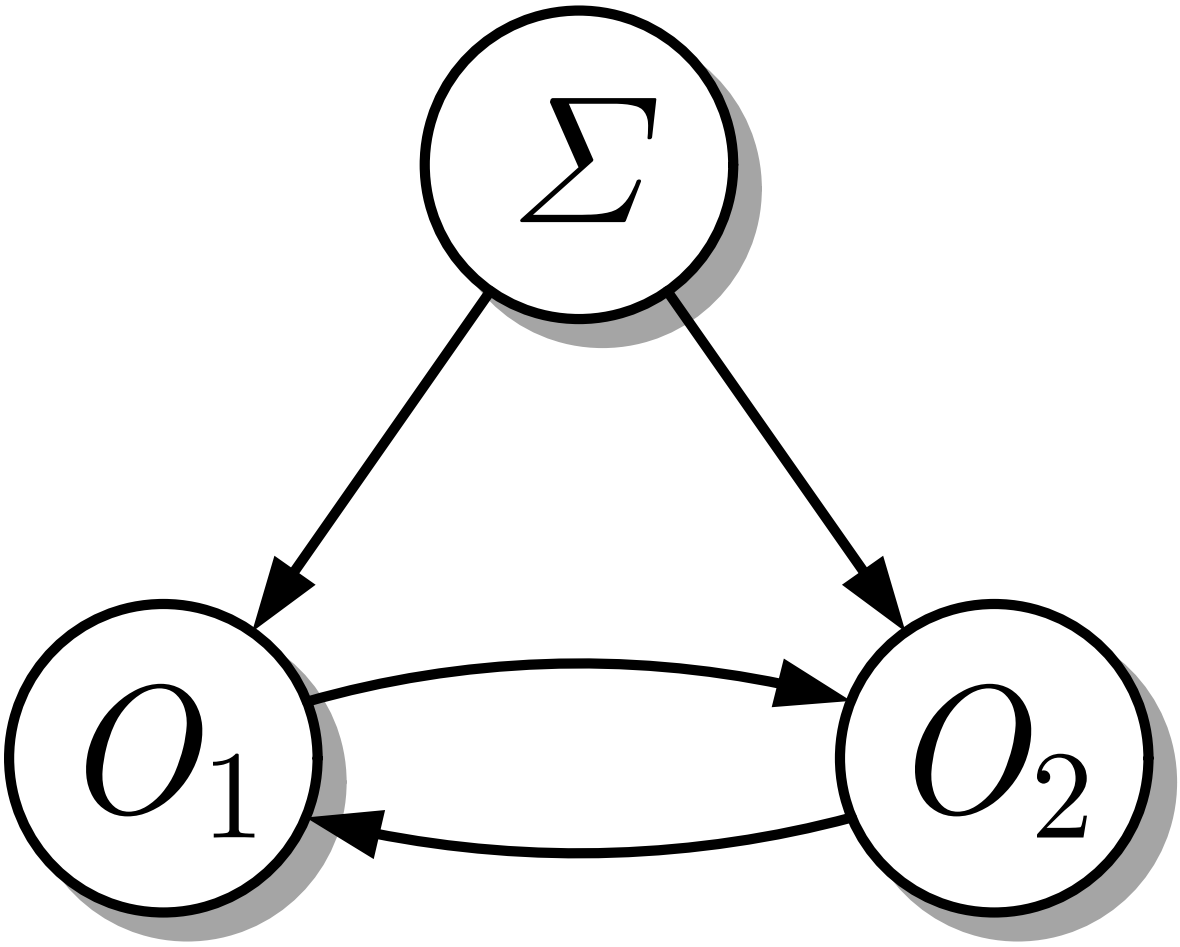

Fig. 6: Communication graph of the distributed state observer

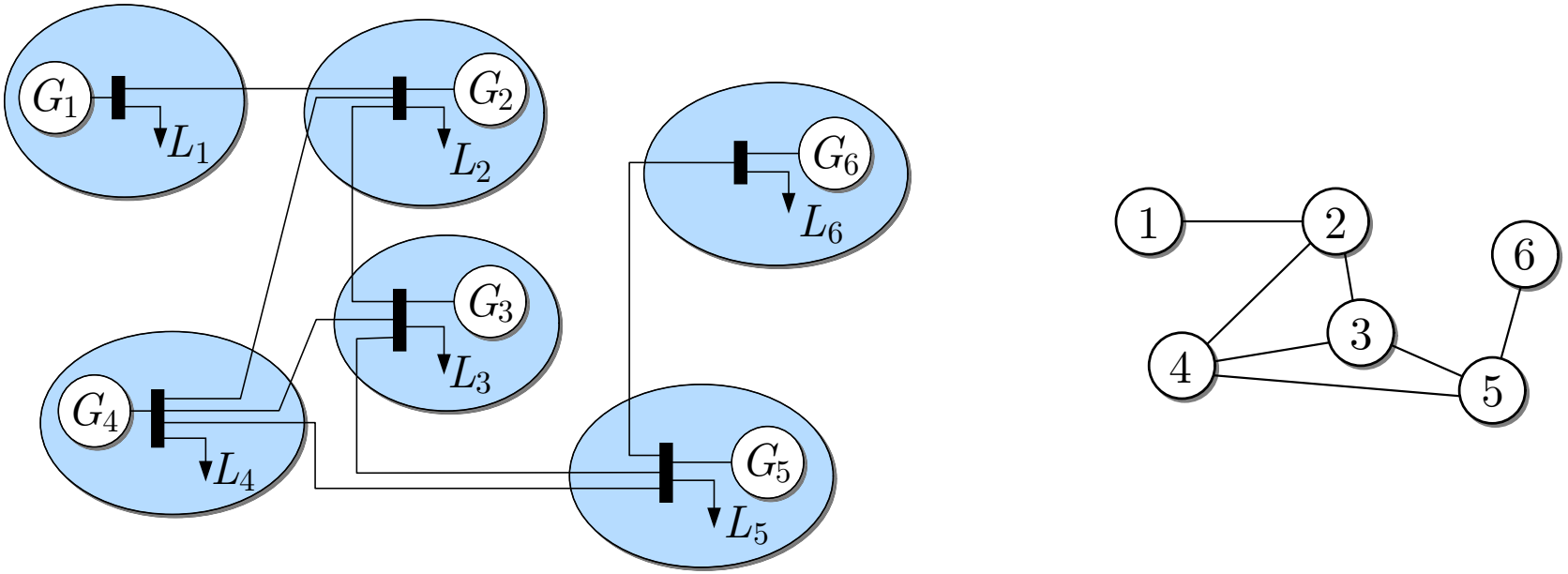

Fig. 0. Electrical power network

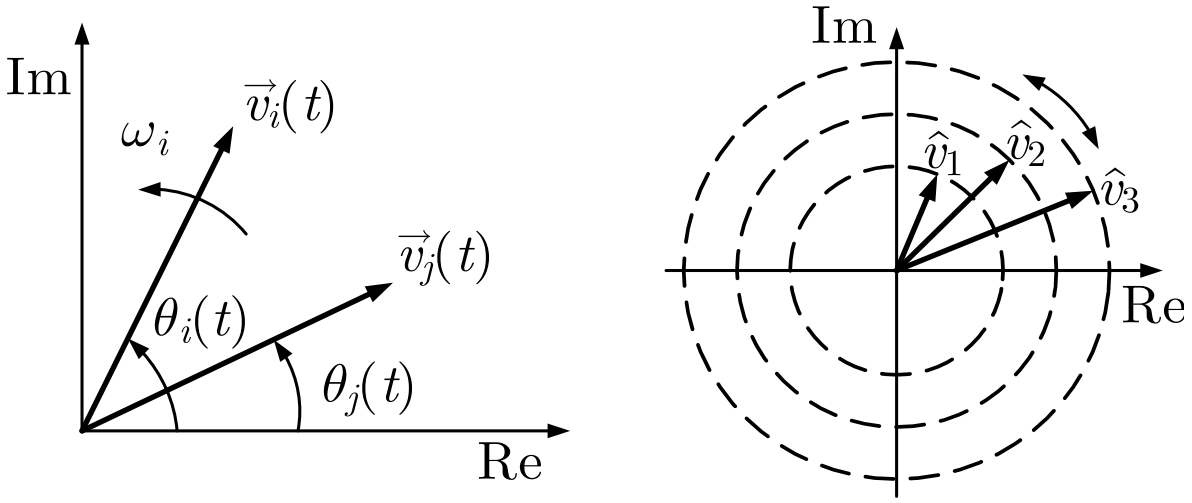

Fig. 1: Arrow diagram of the area voltages

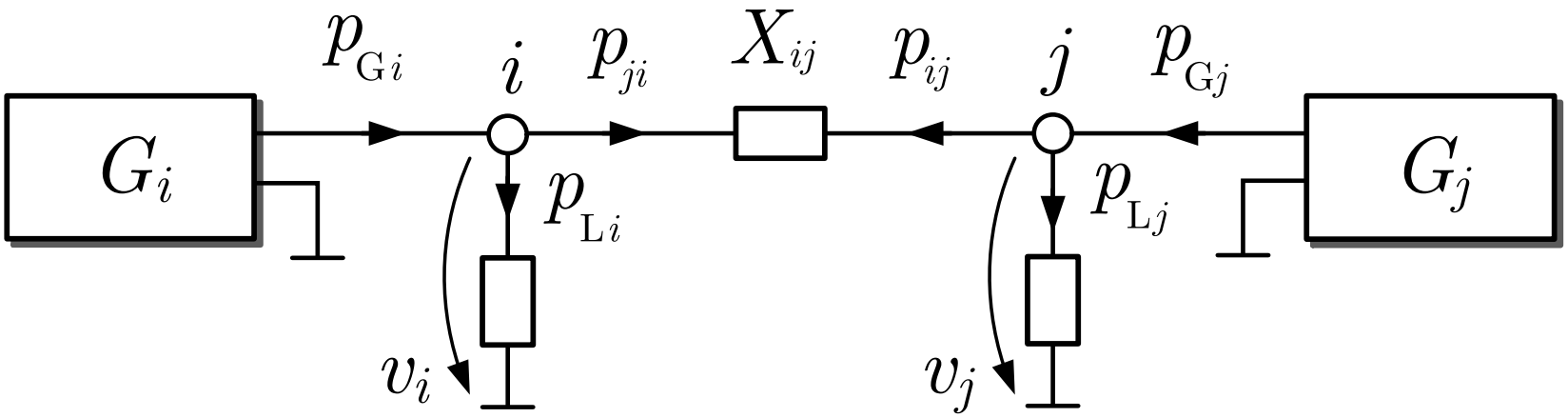

Fig. 2. Block diagram of two coupled areas

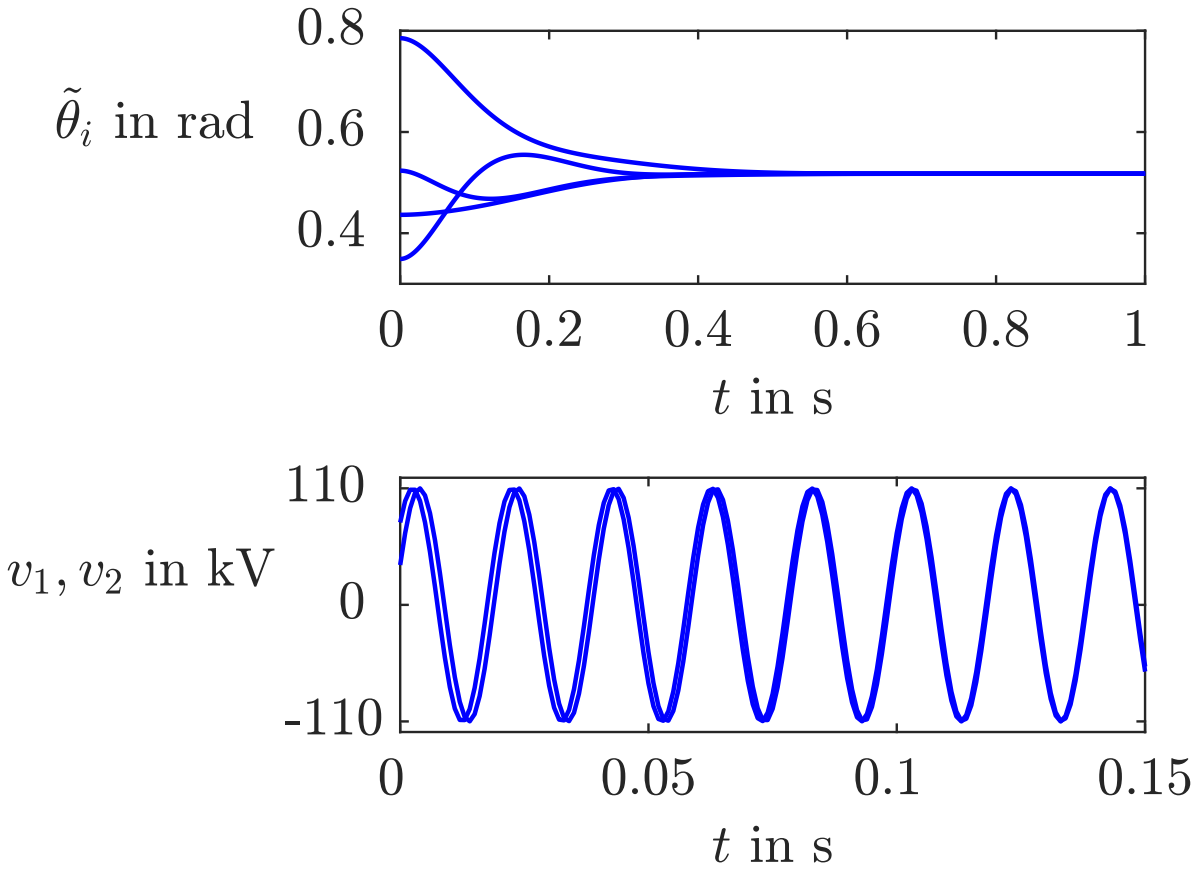

Fig. 3: Behaviour of the power network with balanced areas

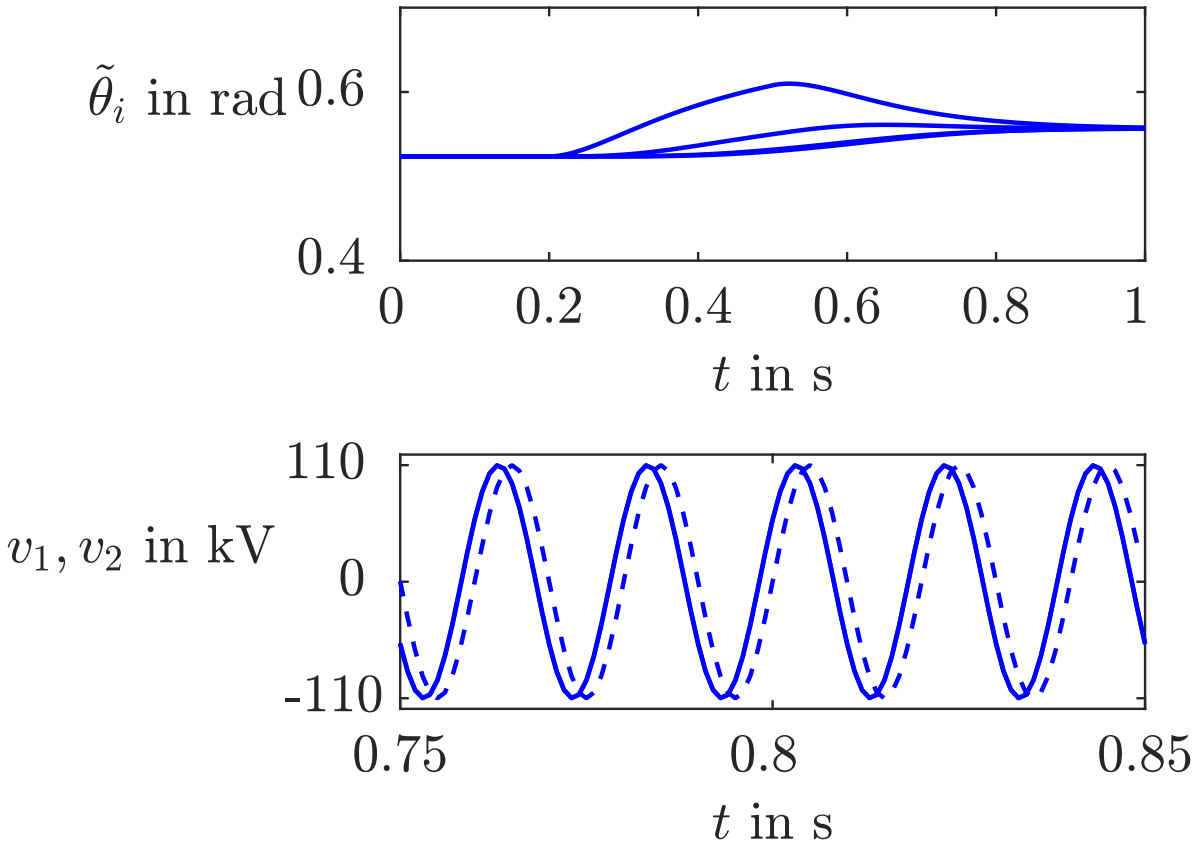

Fig. 4: Behaviour of the balanced power network subject to a disturbance

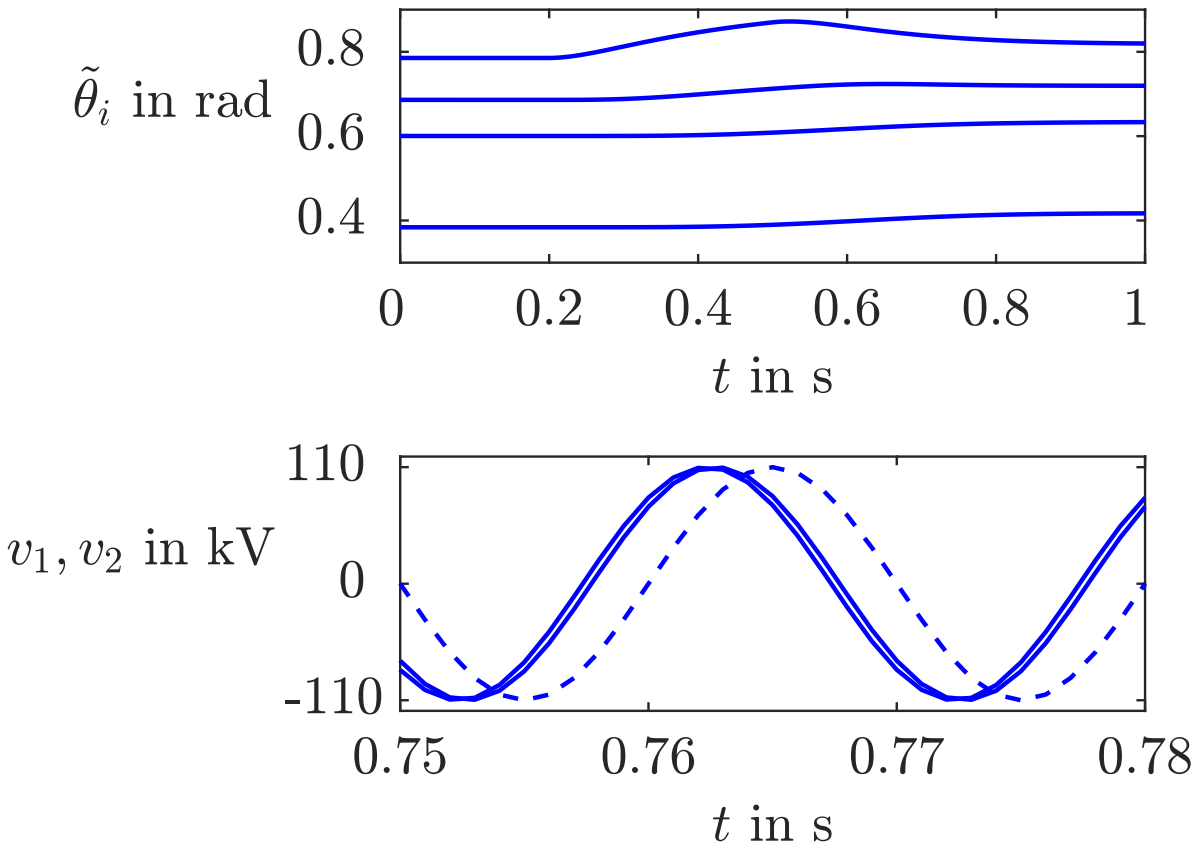

Fig. 5: Behaviour of the unbalanced power network

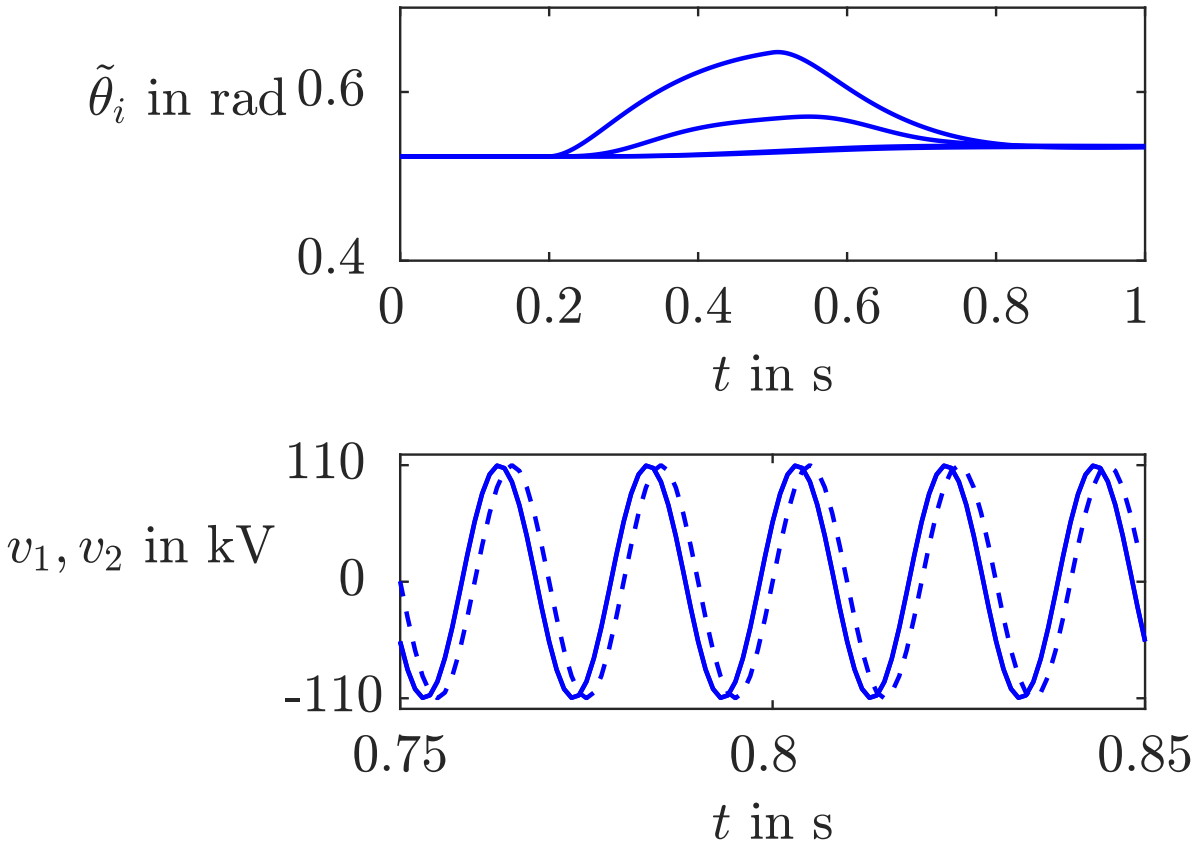

Fig. 6: Disturbance behaviour of a balanced power network with renewable energy sources

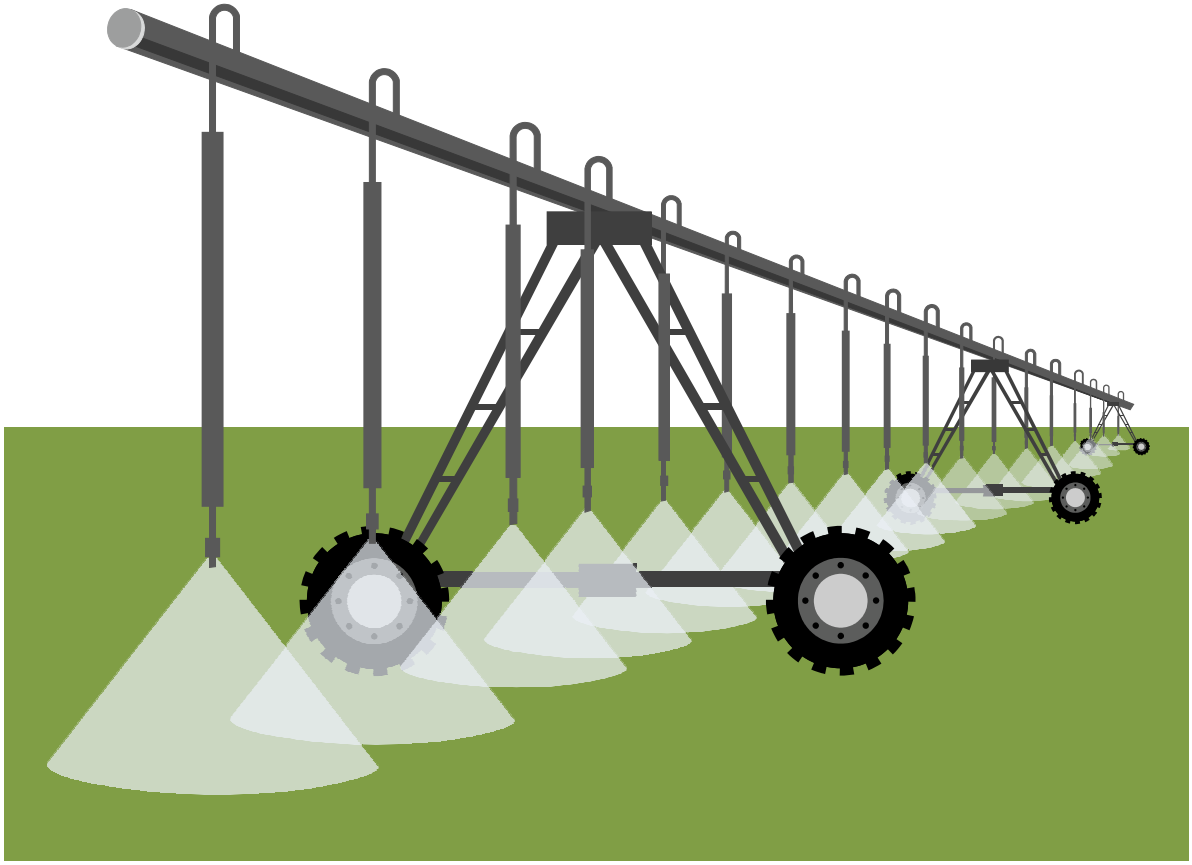

Fig. 0: Irrigation system

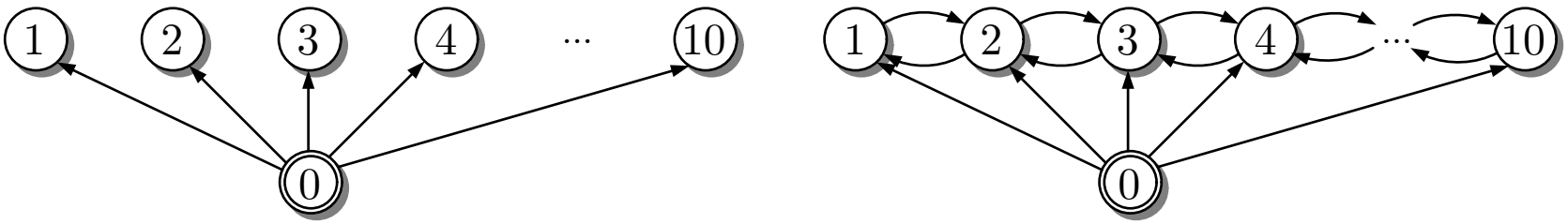

Fig. 1. Communication graph of the irrigation system

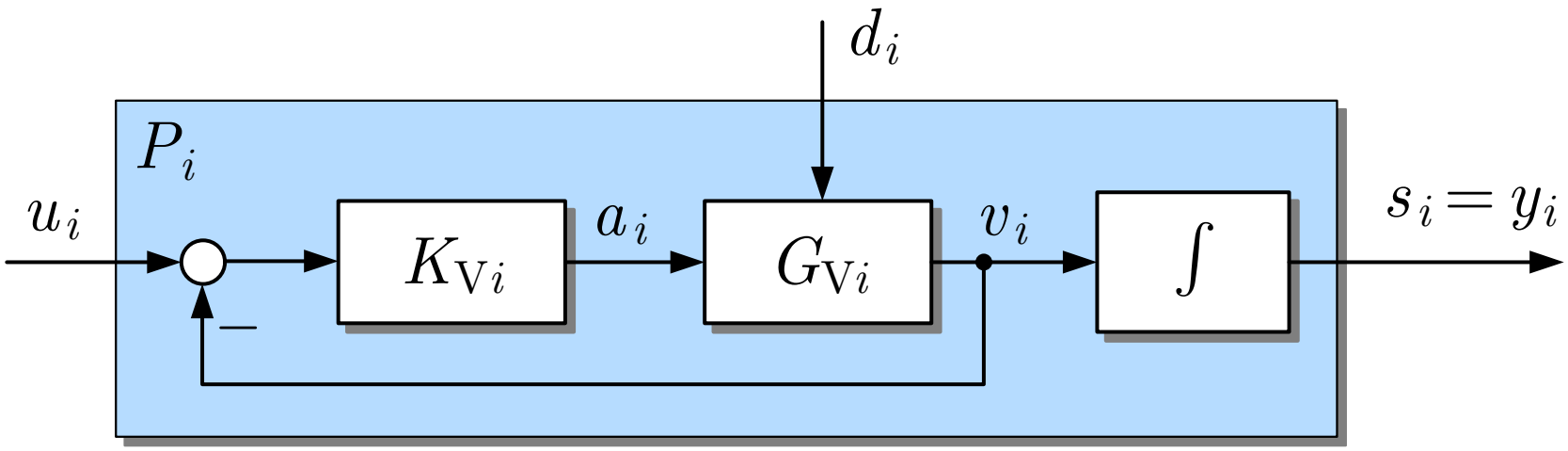

Fig. 2. Model of a single pillar

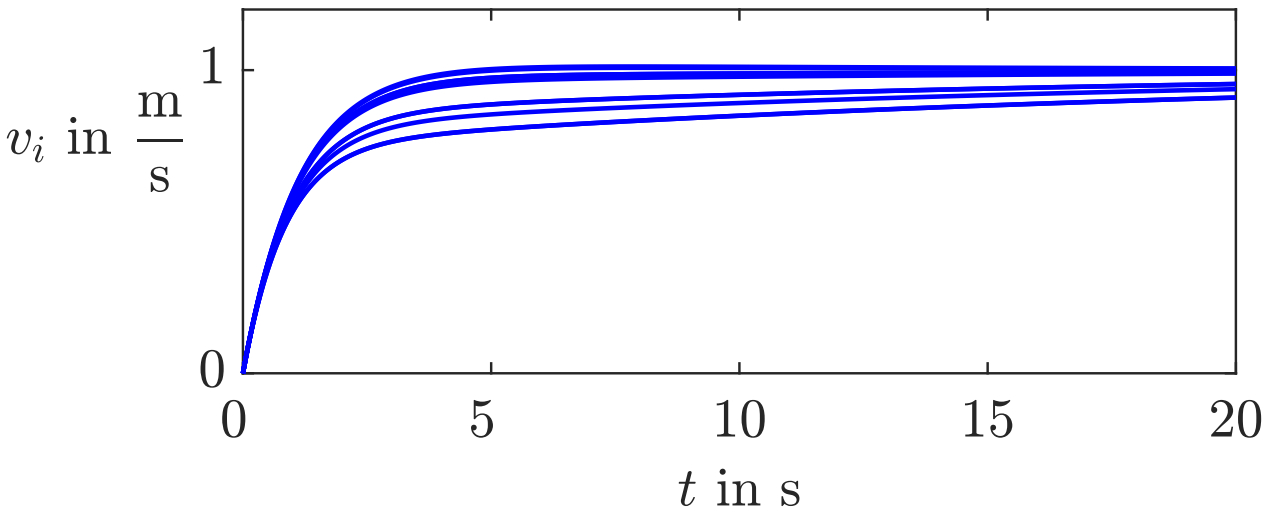

Fig. 3: Command step response of the ten pillars

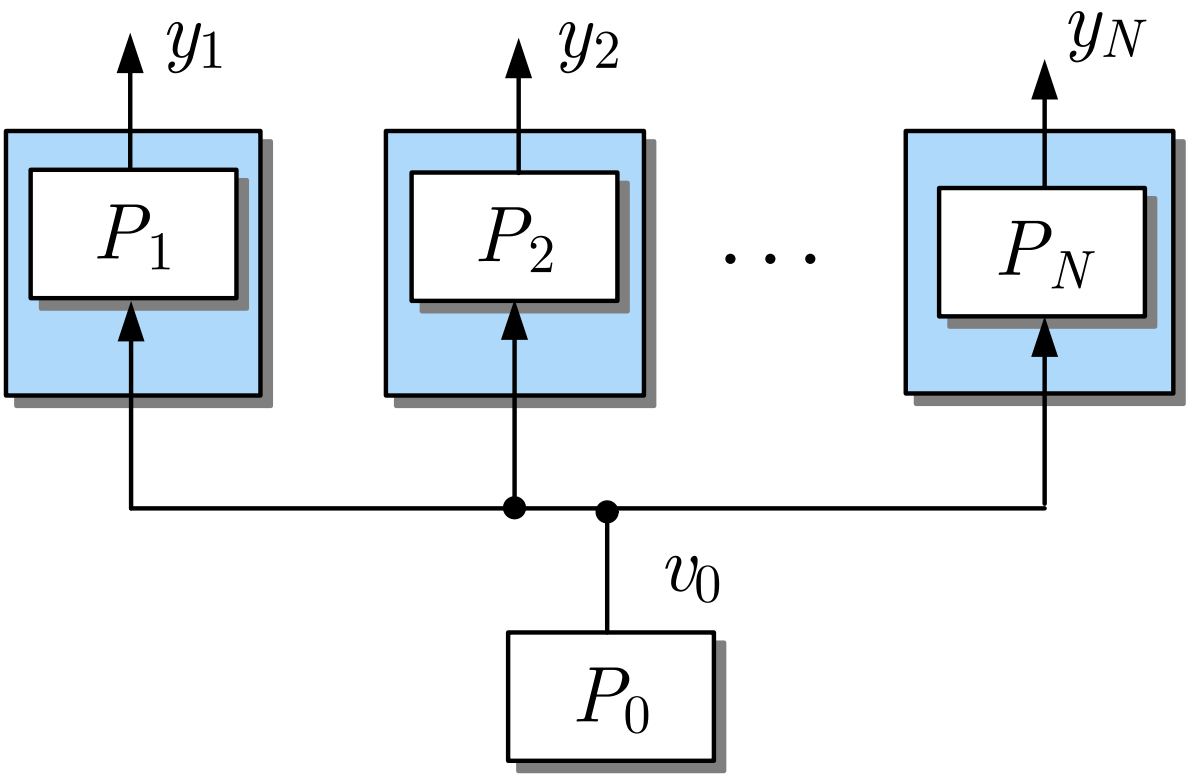

Fig. 4: Irrigation system with decentralised control

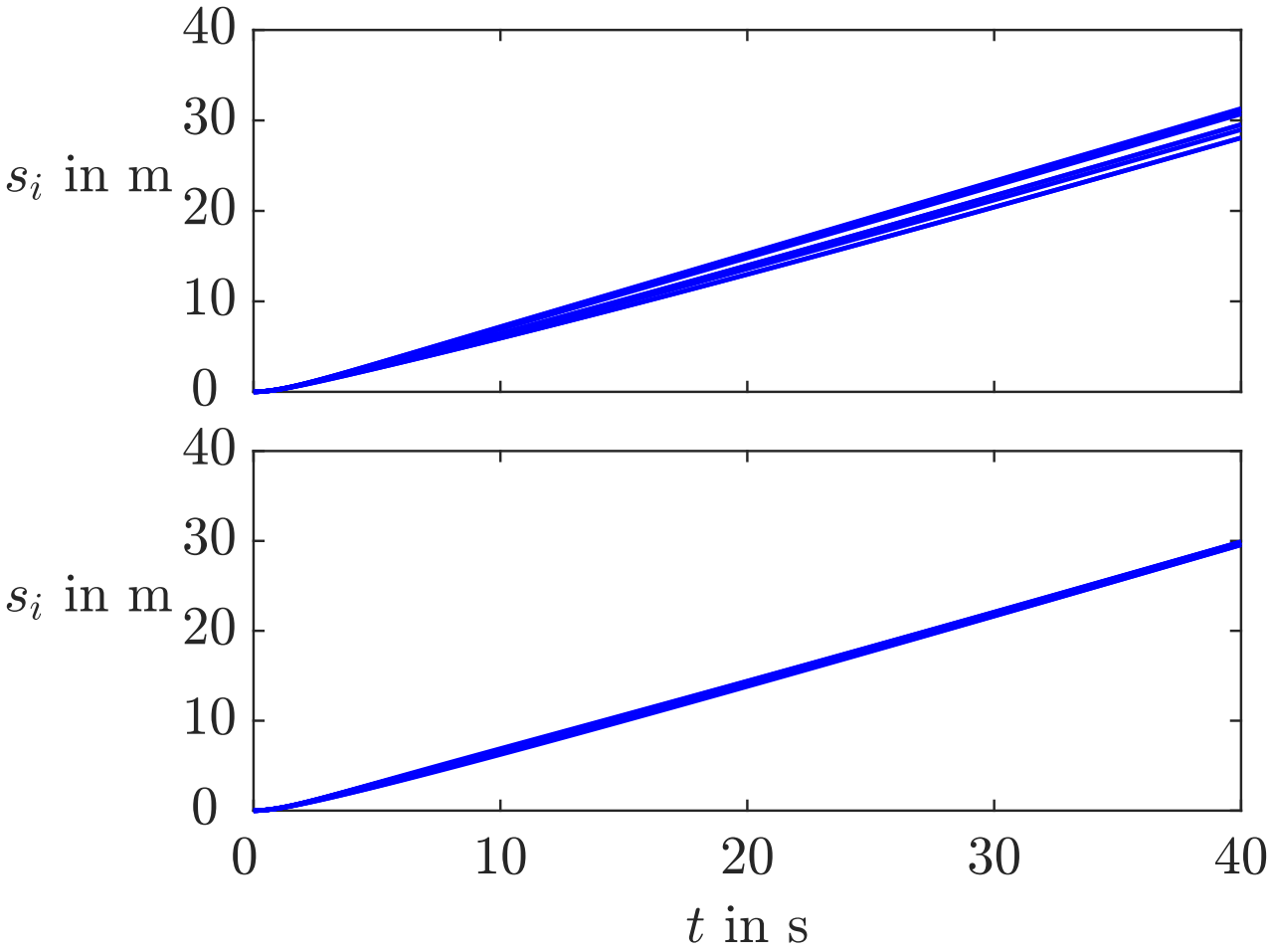

Fig. 5: Trajectories of ten undisturbed pillars with decentralised controller (top) and with networked controller (bottom) starting in the same initial position

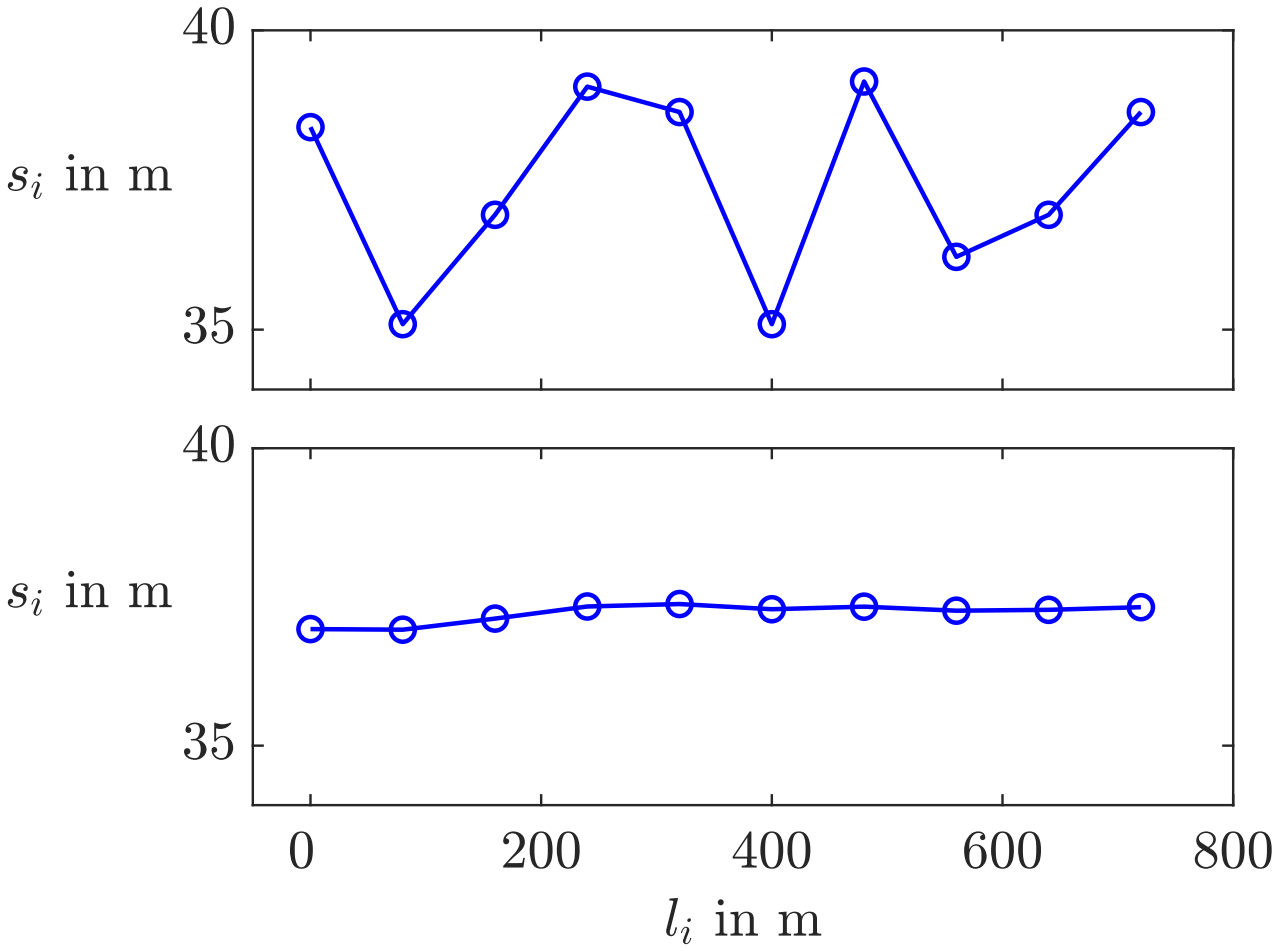

Fig. 6: Positions of the pillars at time $t = 40\,\mathrm{s}$

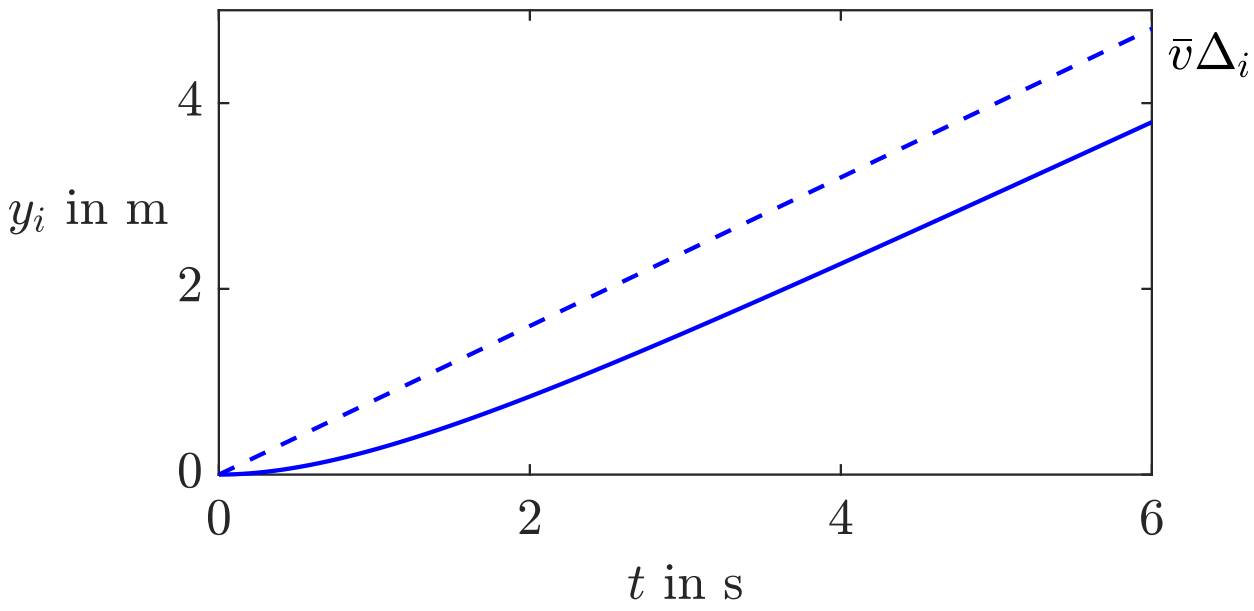

Fig. 7: Step response of a single pillar; Required position $s_{\rm ref}(t)$ (- - -) and true position $s_i(t)$ (—)

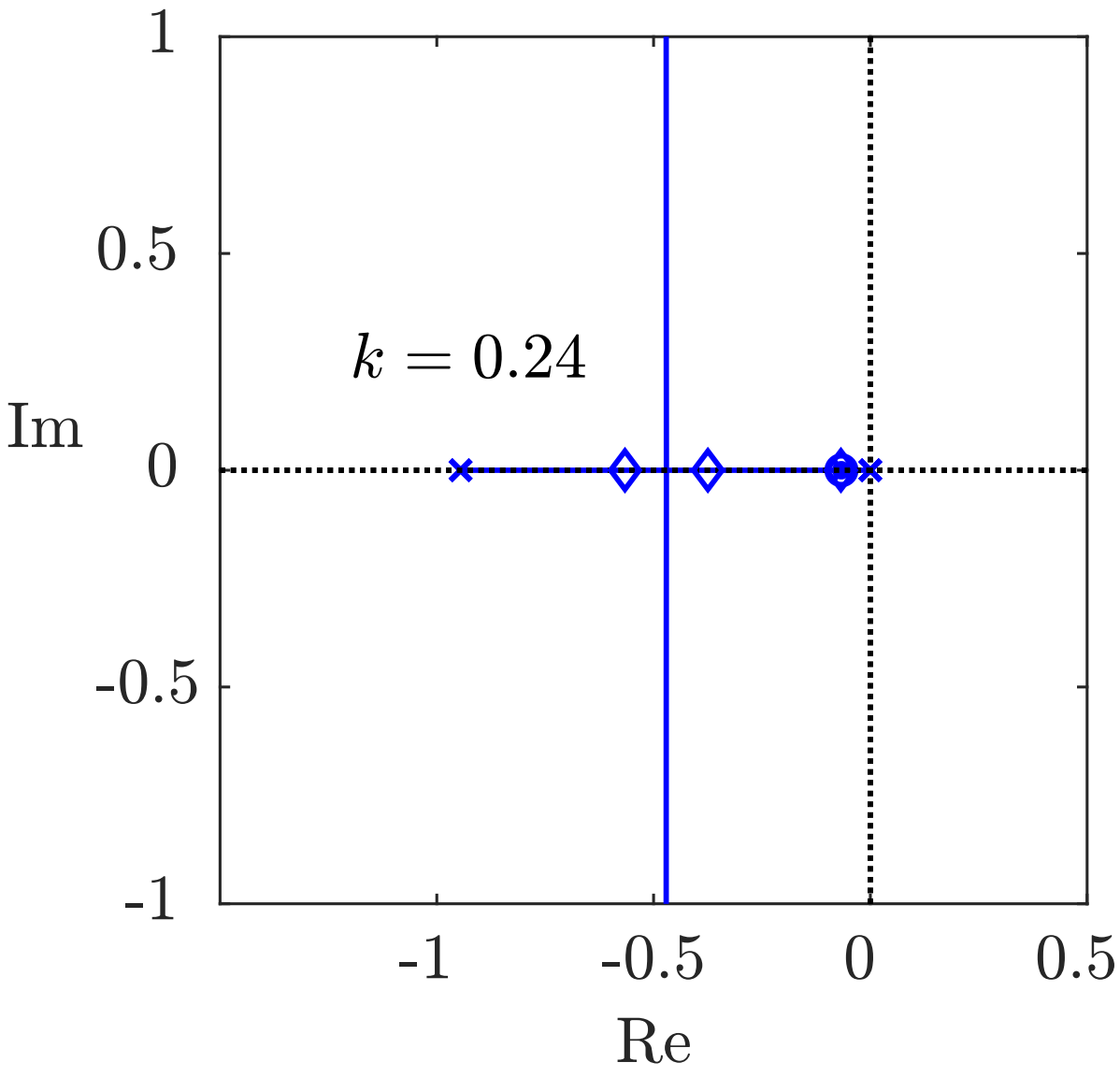

Fig. 8: Root locus of a single pillar with the closed-loop eigenvalues for $k = 0.24$ marked by $\diamond$

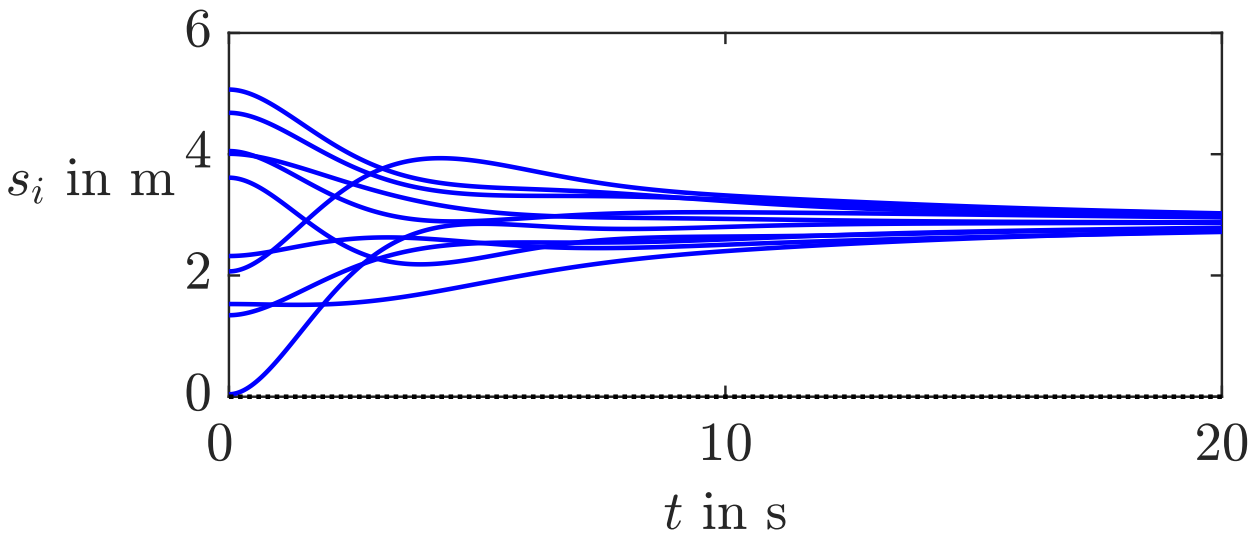

Fig. 9: Synchronisation of the undisturbed identical pillars

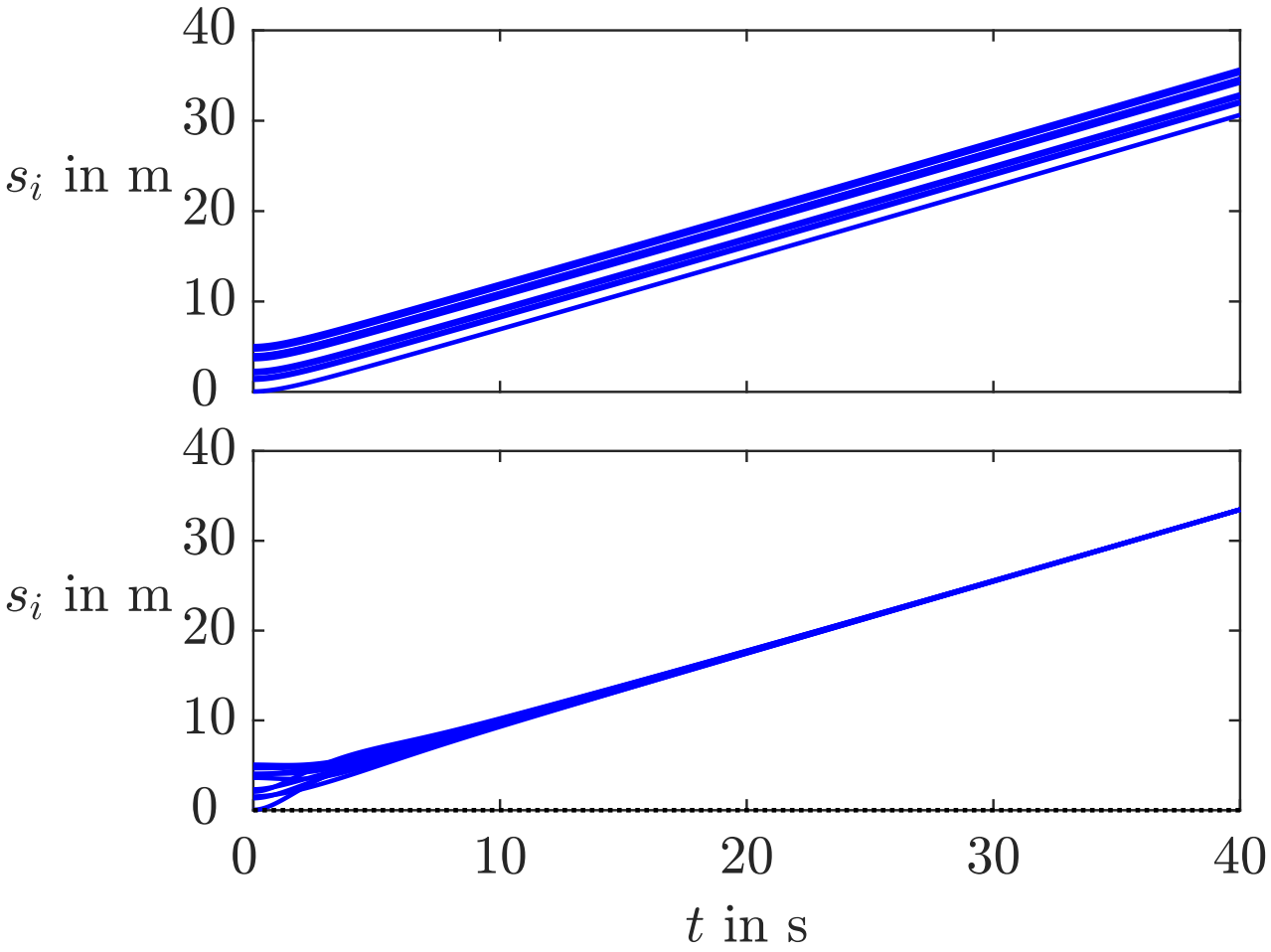

Fig. 10: Trajectories of ten undisturbed identical pillars with decentralised controller (top) and with networked controller (bottom)

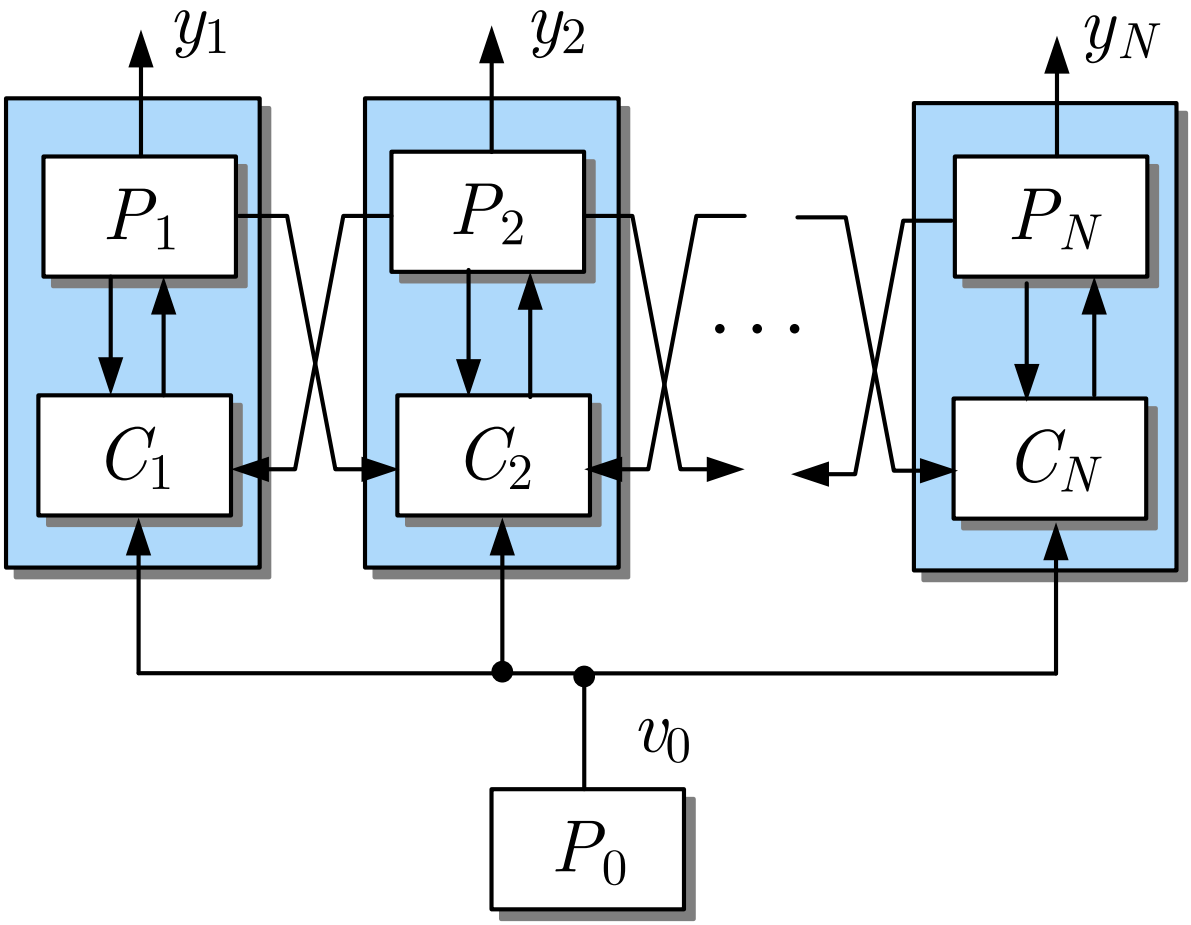

Fig. 11: Irrigation system with networked controller

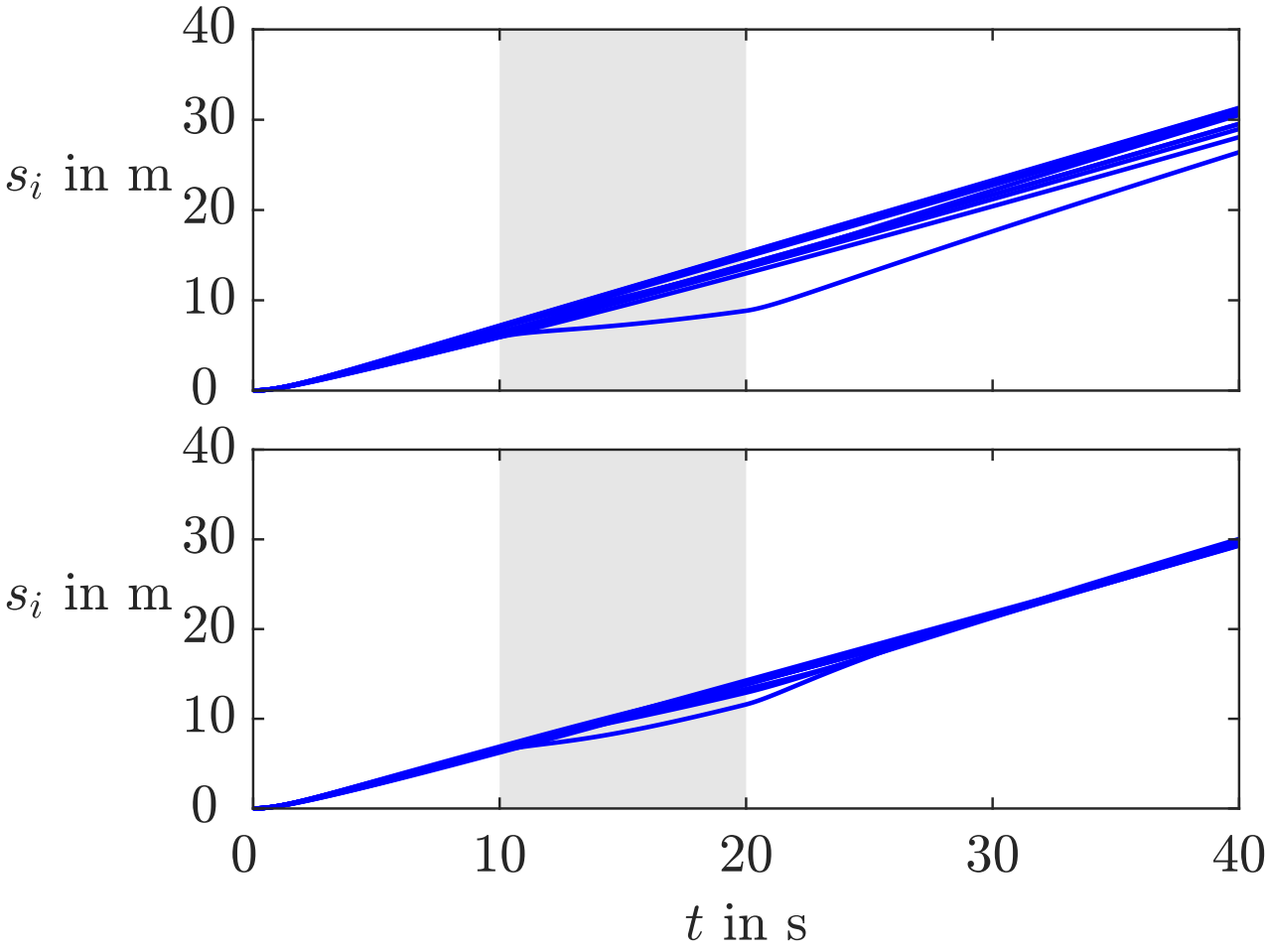

Fig. 12: Behaviour of the disturbed irrigation system with networked controller

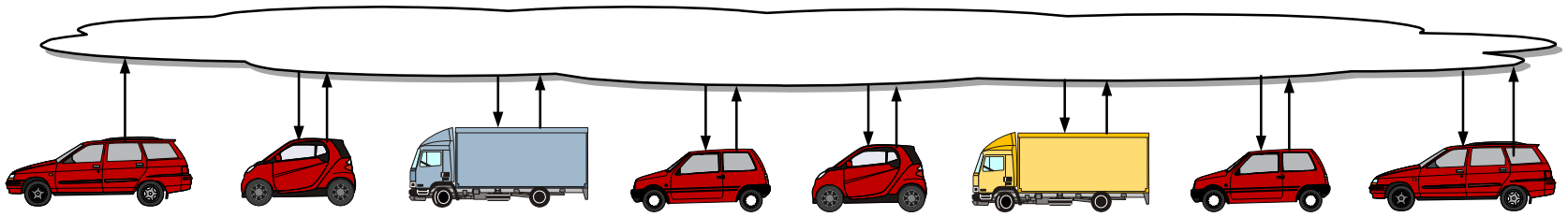

Fig. 0. Vehicle platoon

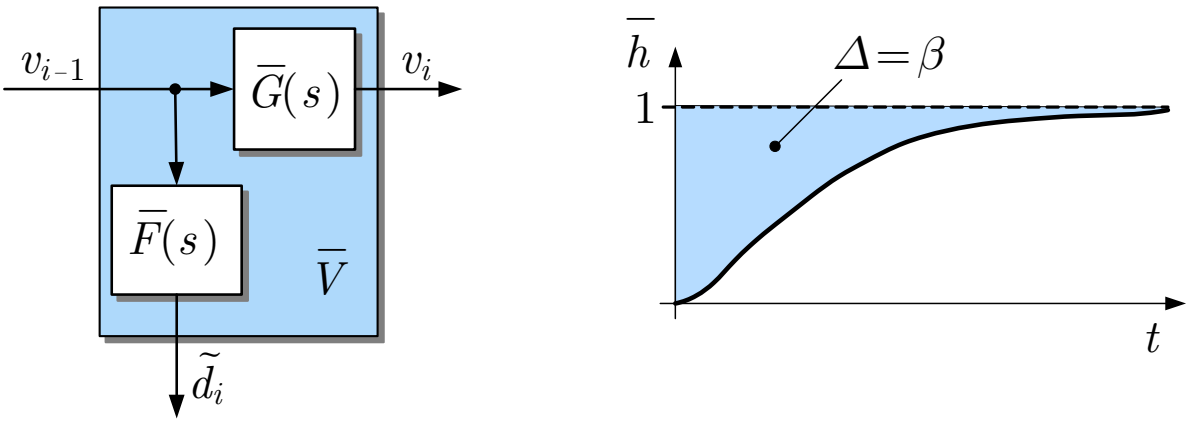

Fig. 1: Controlled vehicle

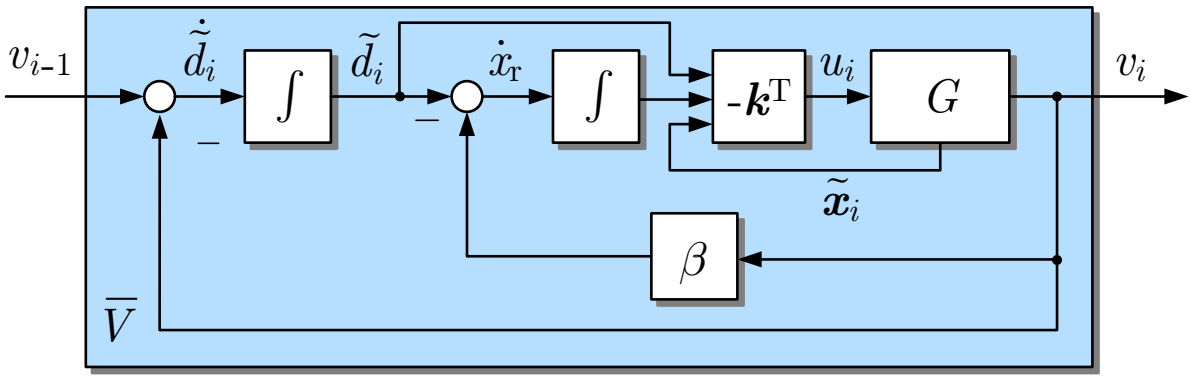

Fig. 2: Controlled vehicle

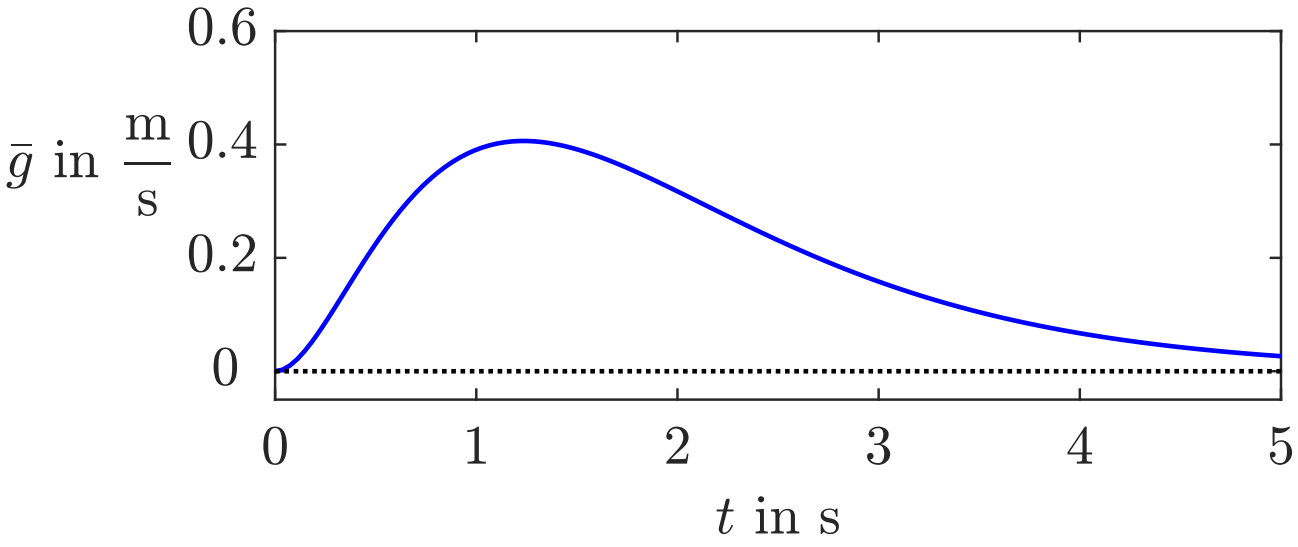

Fig. 3: Impulse response of the controlled vehicle

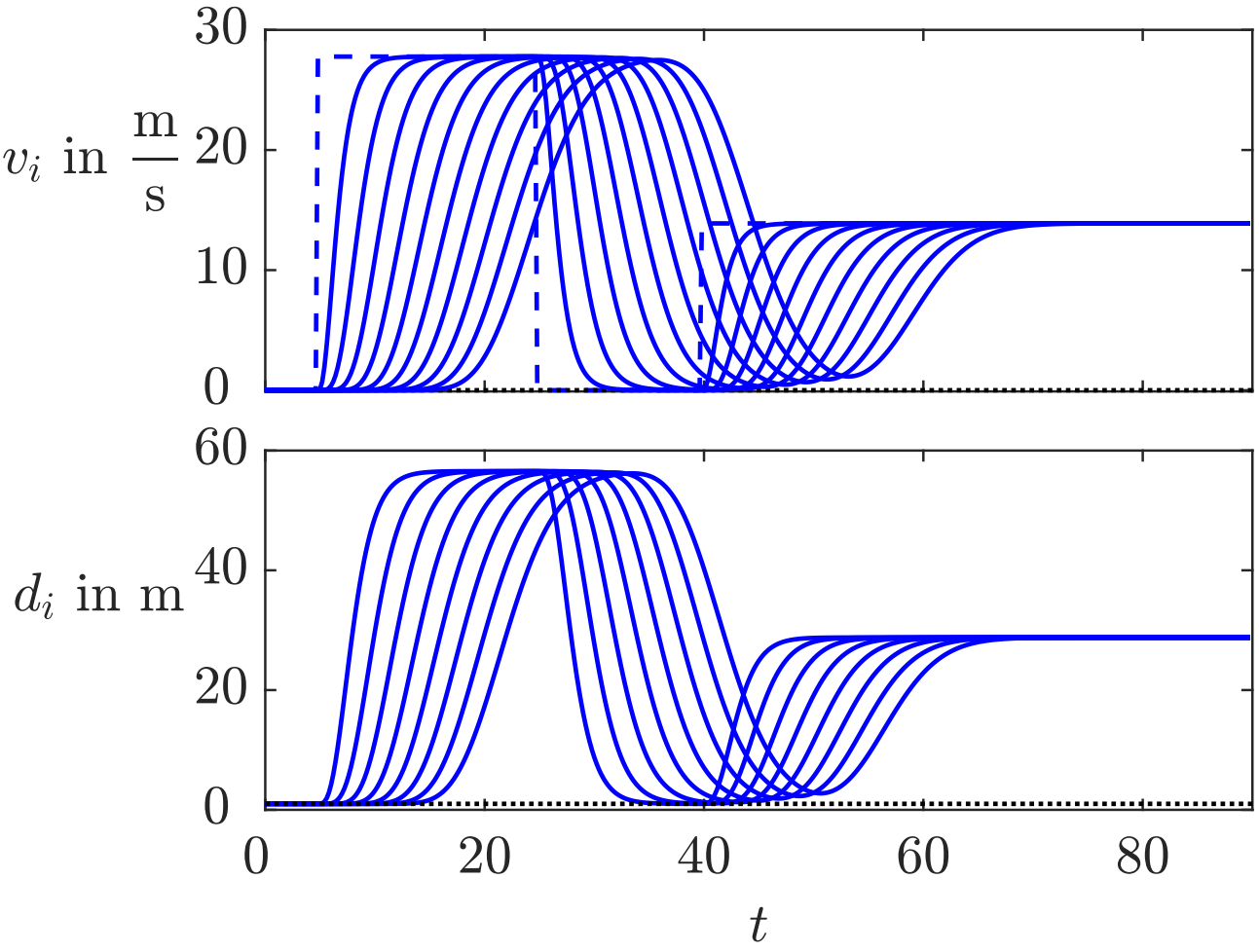

Fig. 4: Behaviour of a platoon of ten vehicles

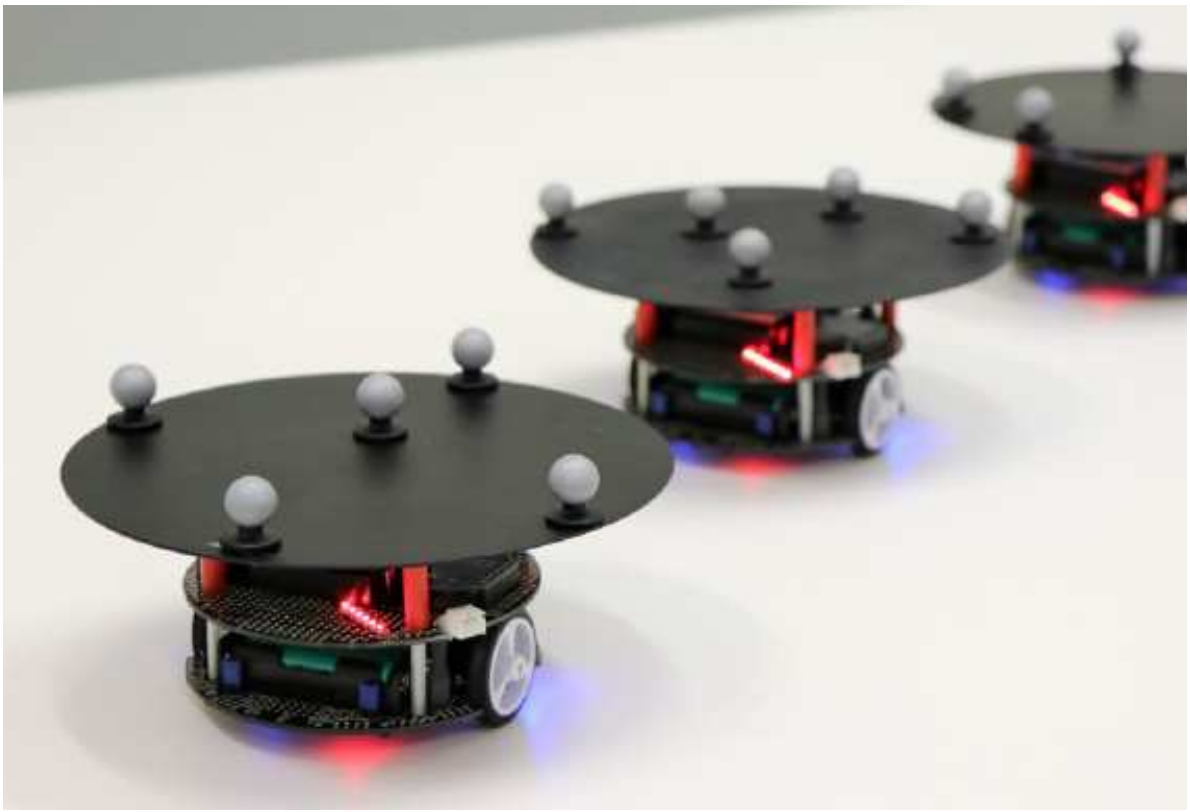

Fig. 5: Robots used for the experiments

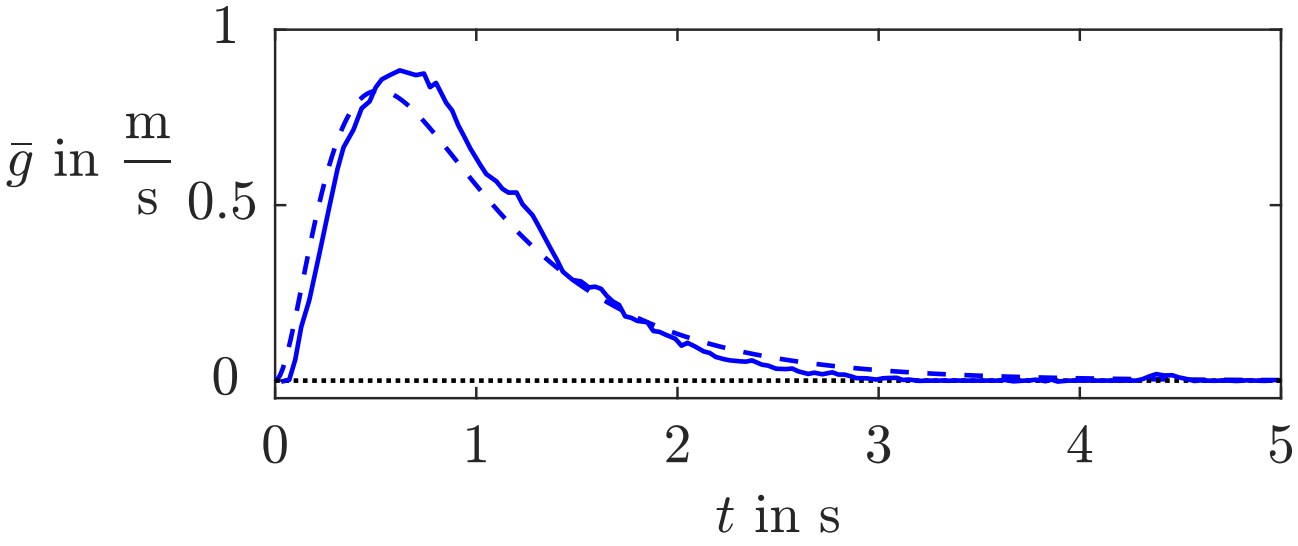

Fig. 6: Impulse response of the model of the controlled vehicle (- - -) and experimental data (—)

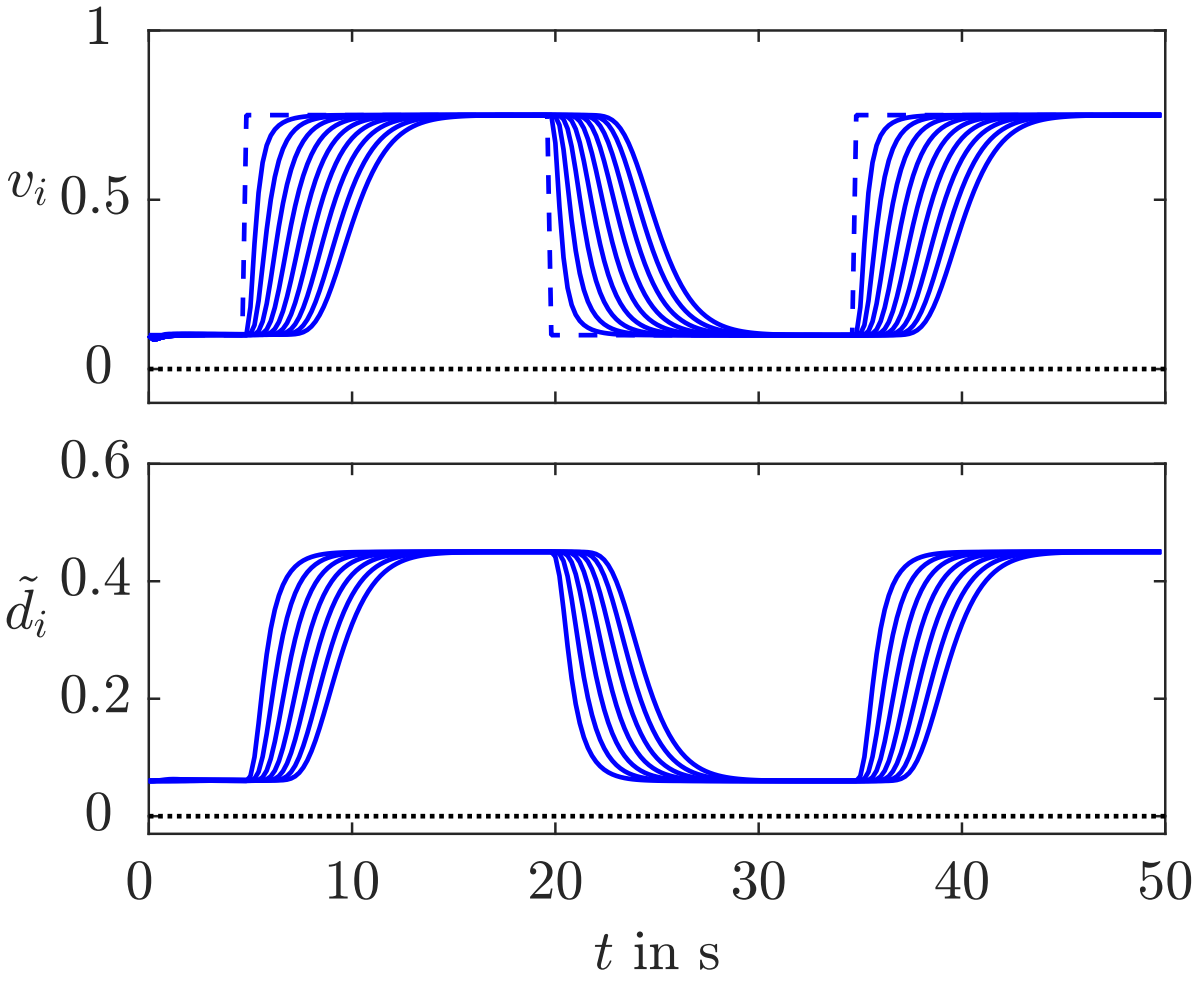

Fig. 7: Behaviour of a platoon with nine robots: Simulation results

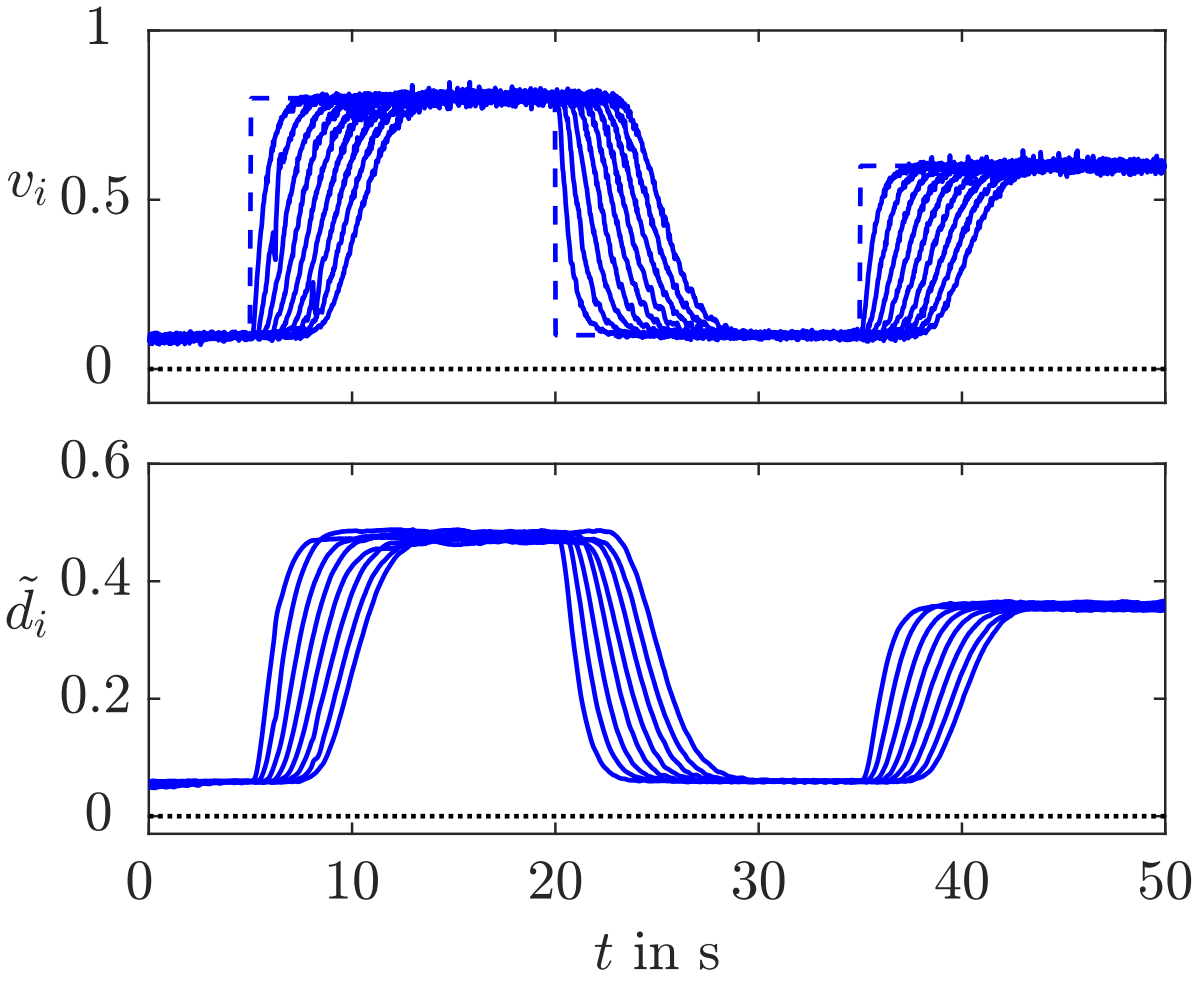

Fig. 7: Behaviour of a platoon with nine robots: Experimental results

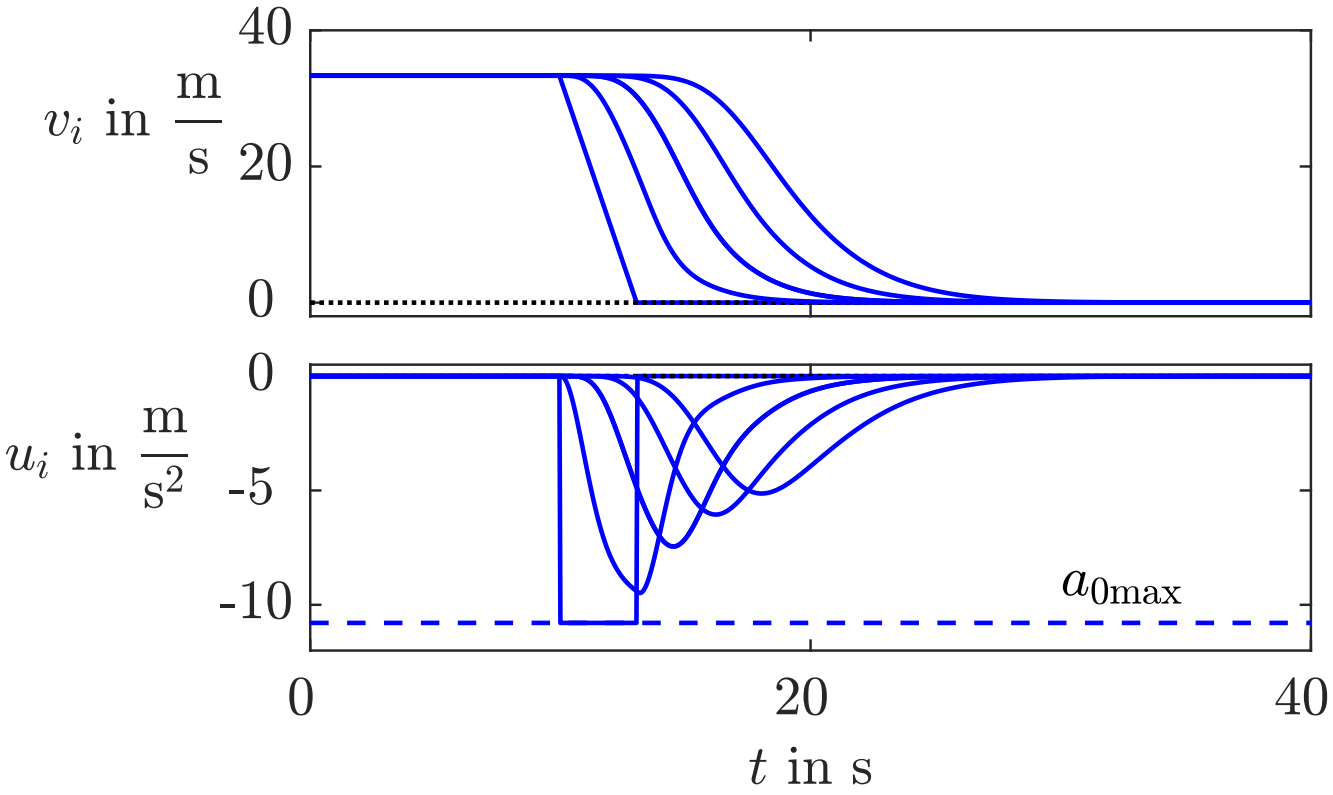

Fig. 8: Behaviour of the linear vehicle platoon

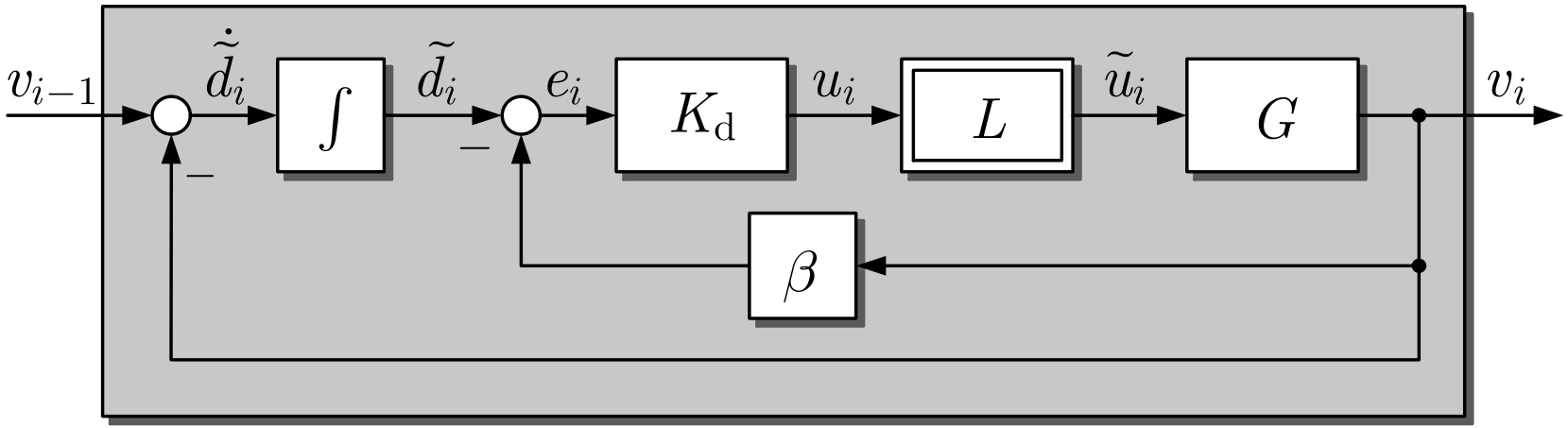

Fig. 9. Vehicle model with nonlinearity to represent the limited acceleration

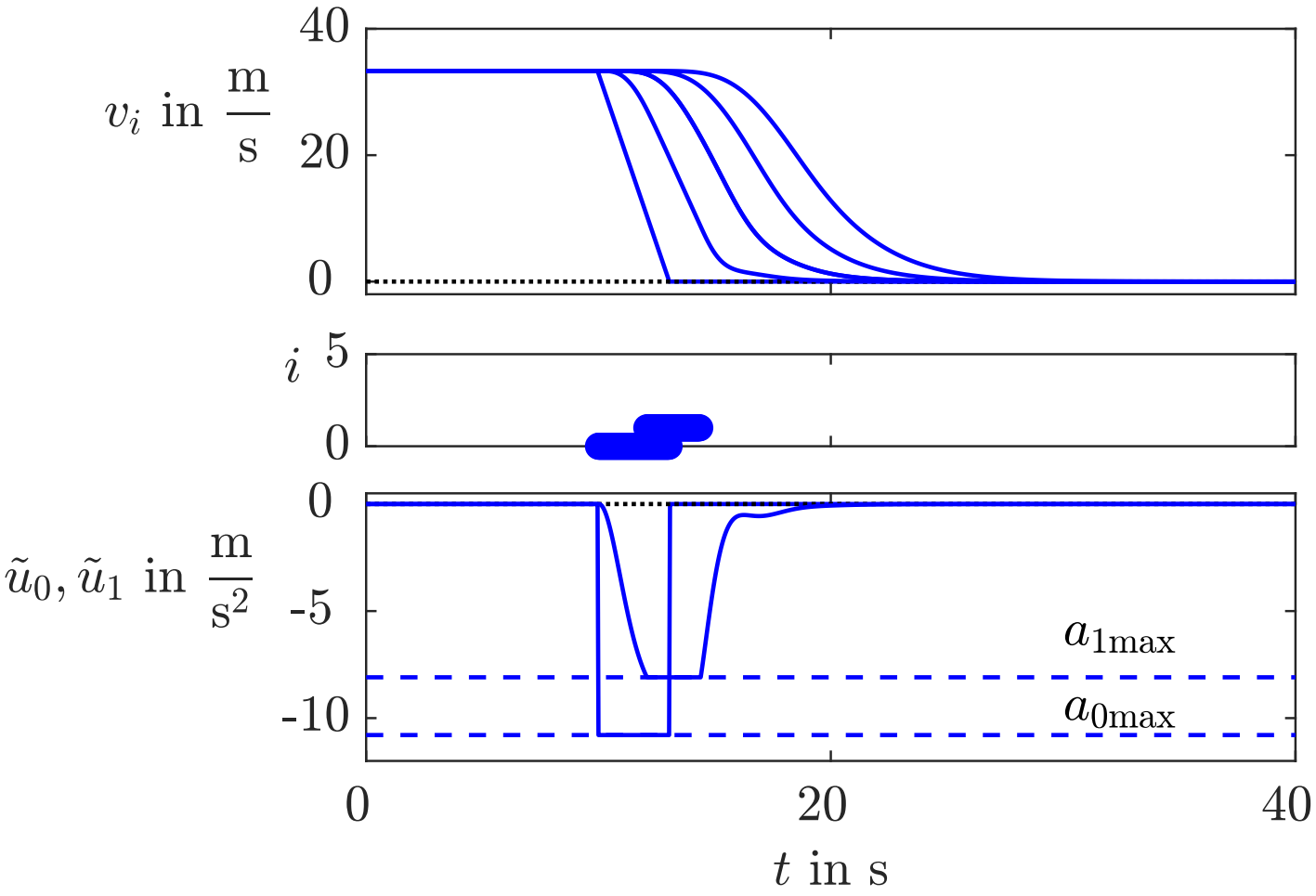

Fig. 10: Braking manoeuvre with nonlinear vehicles

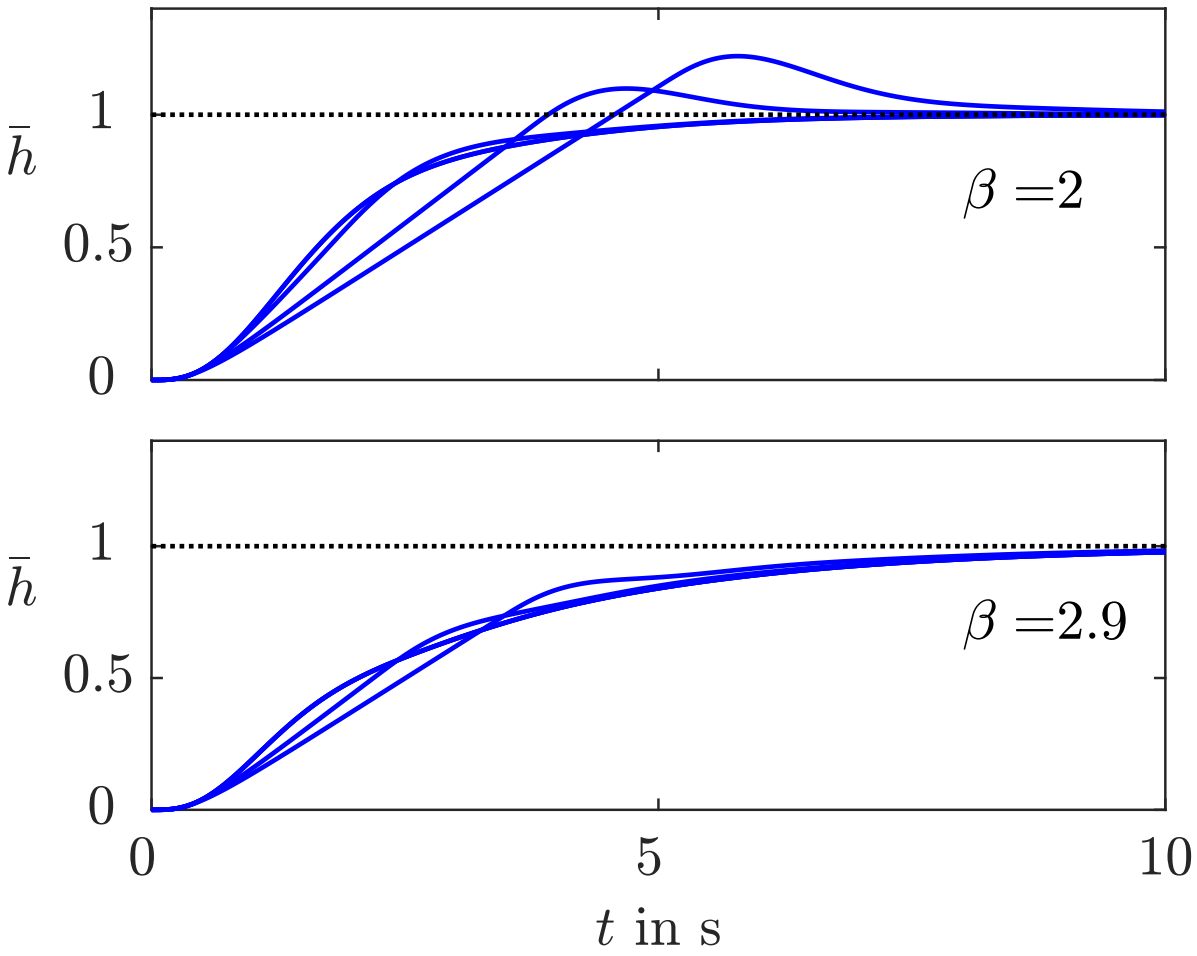

Fig. 11: Normalised response of the controlled vehicle to stepwise changes of the local reference velocity $v_{si}(t)$

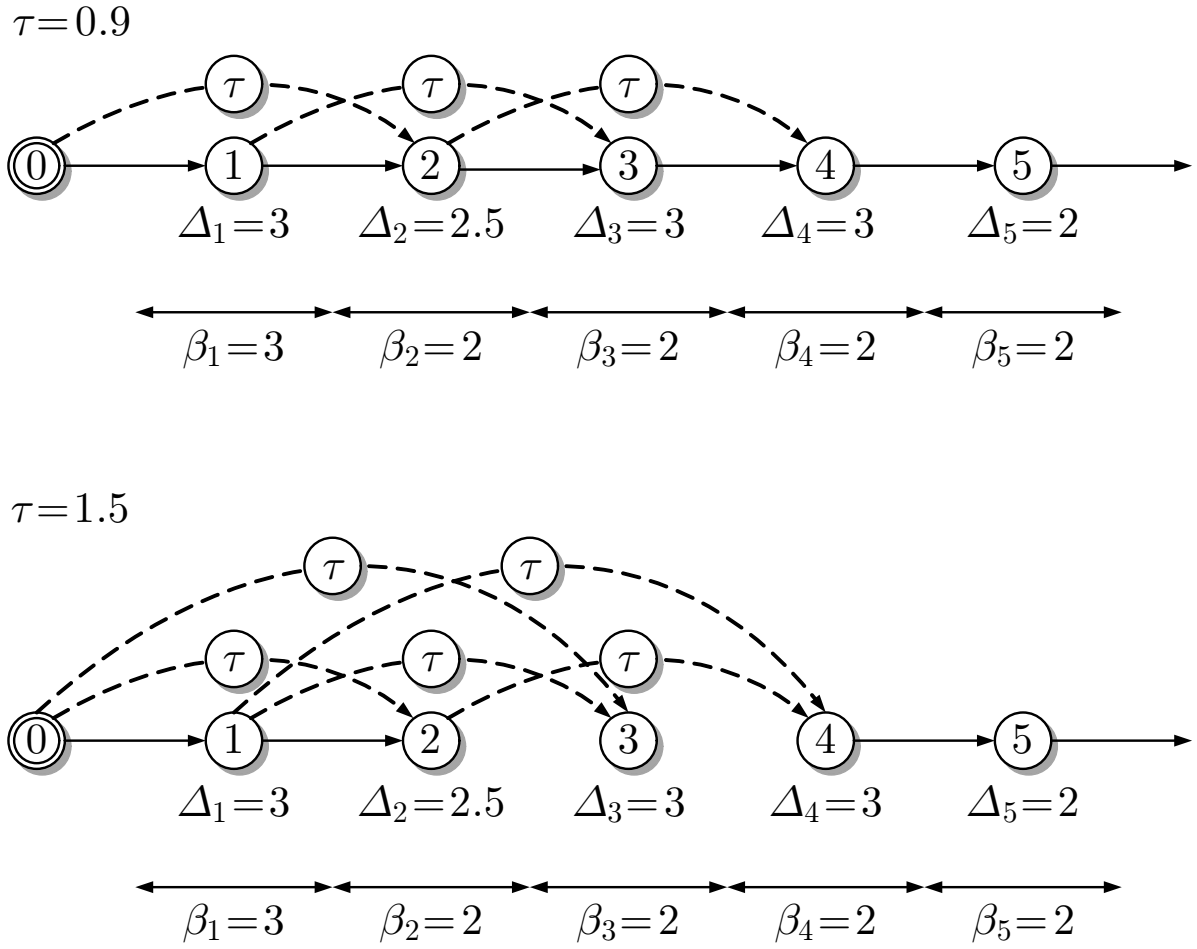

Fig. 12: Communication graph of the CACC with time delay

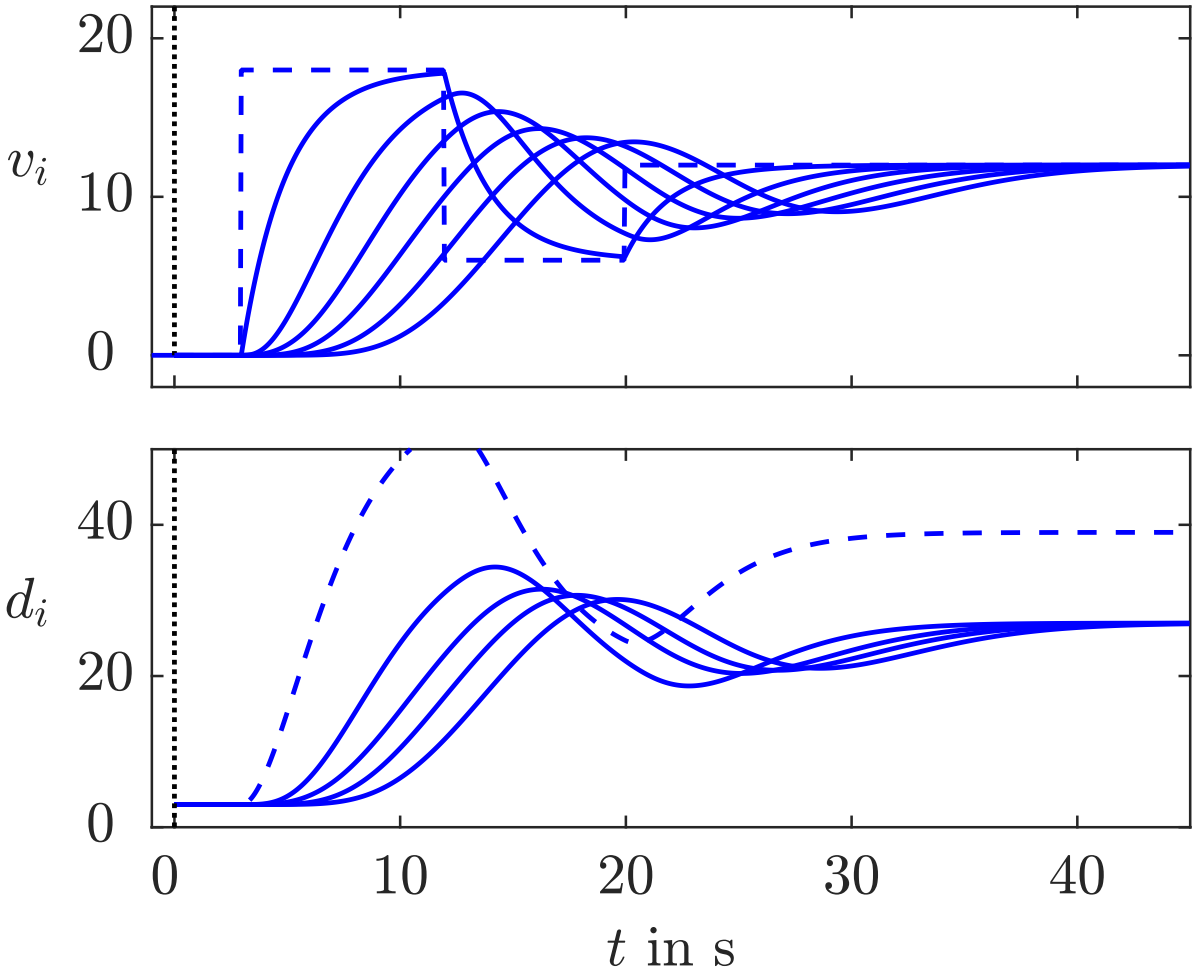

Fig. 13: Platoon with CACC without transmission delay

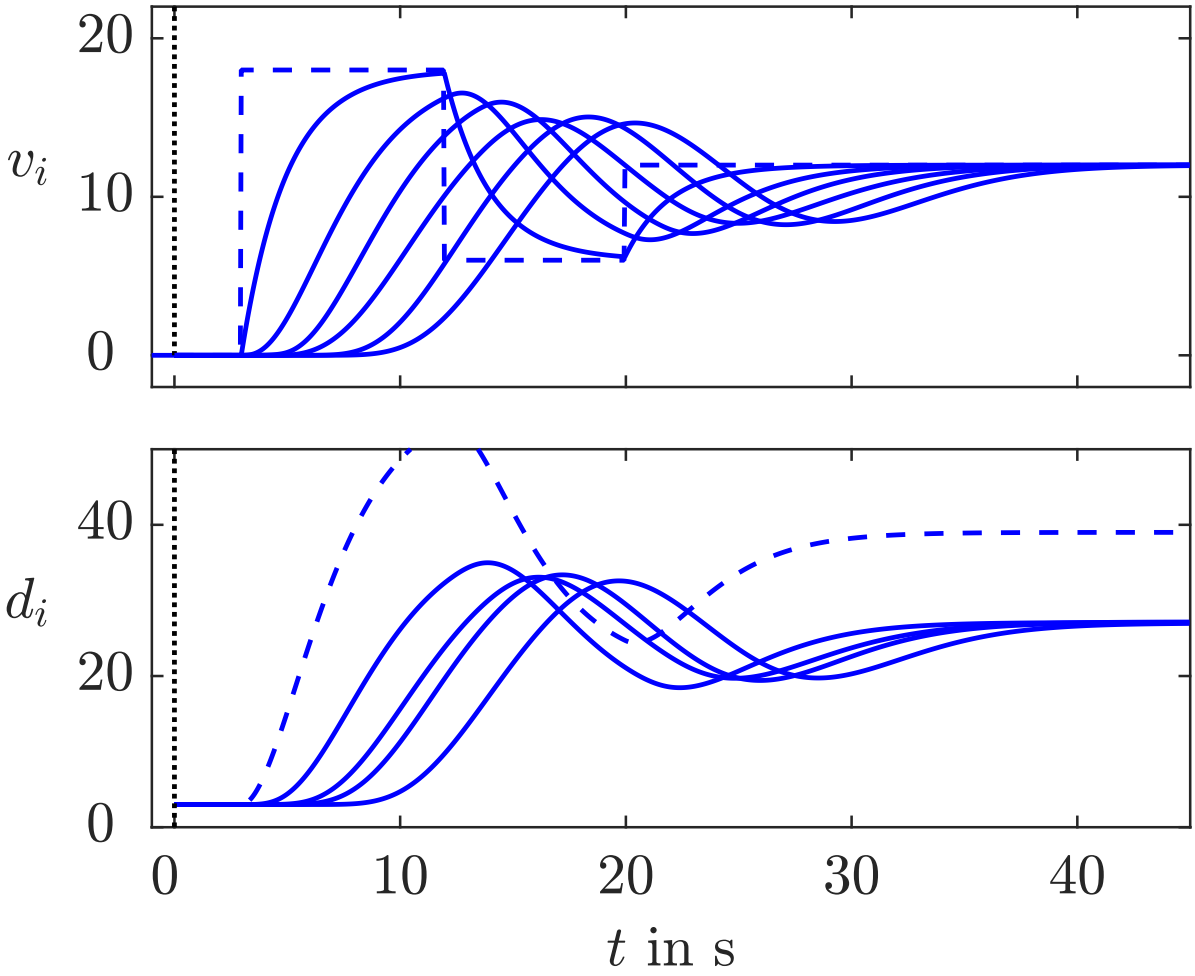

Fig. 13: Platoon with CACC with transmission delay $\tau = 1.5\,\mathrm{s}$

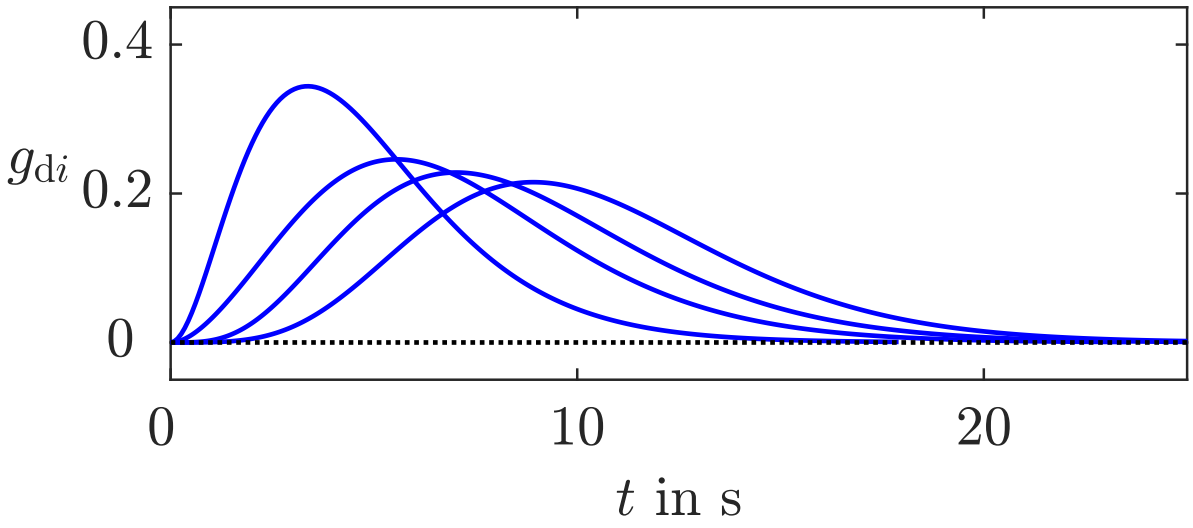

Fig. 14: Collision avoidance test without transmission delay

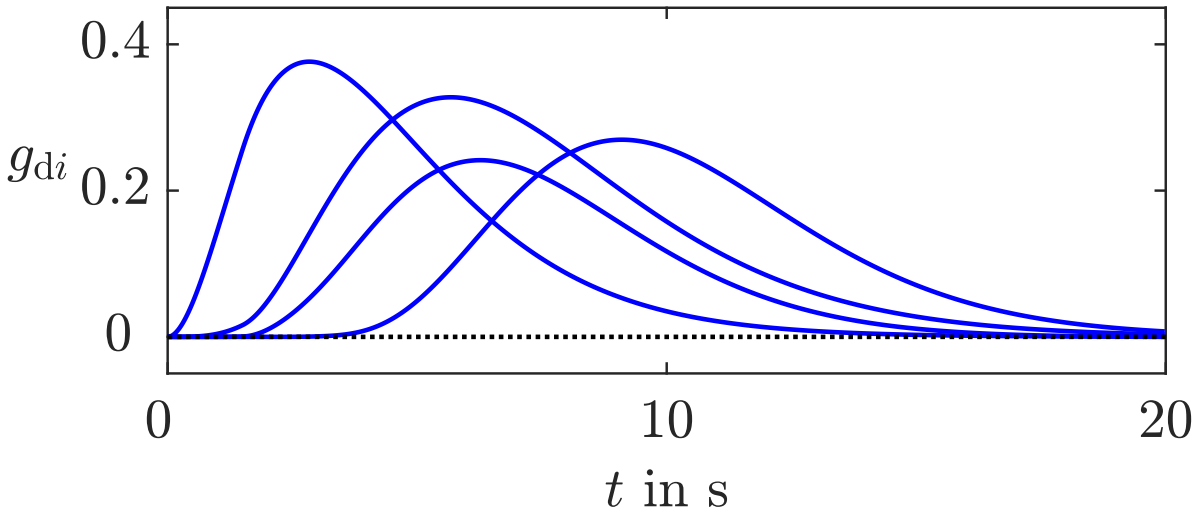

Fig. 14: Collision avoidance test with transmission delay $\tau = 0.9\,\mathrm{s}$

Fig. 0: μ-split braking

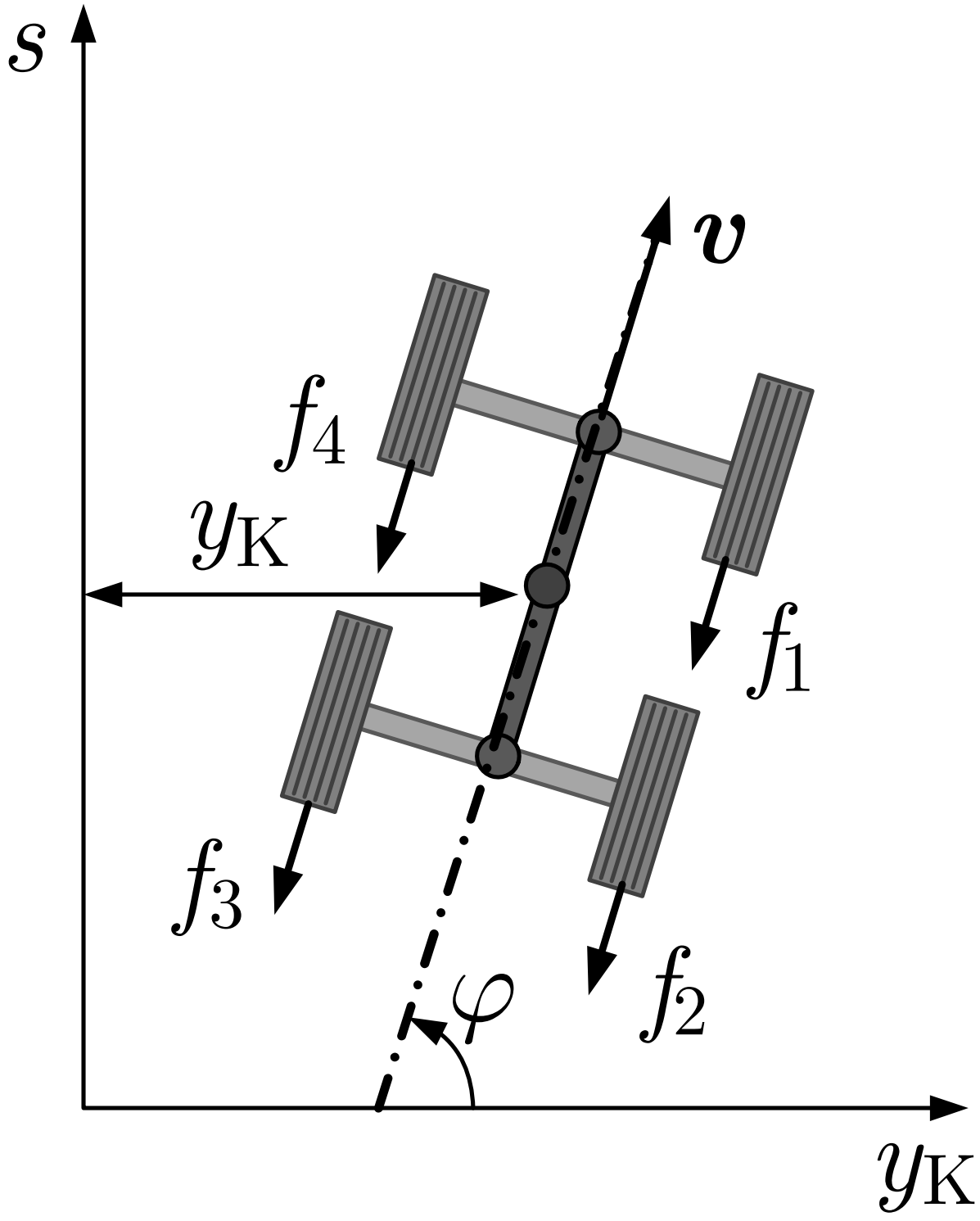

Fig. 1: Vehicle model

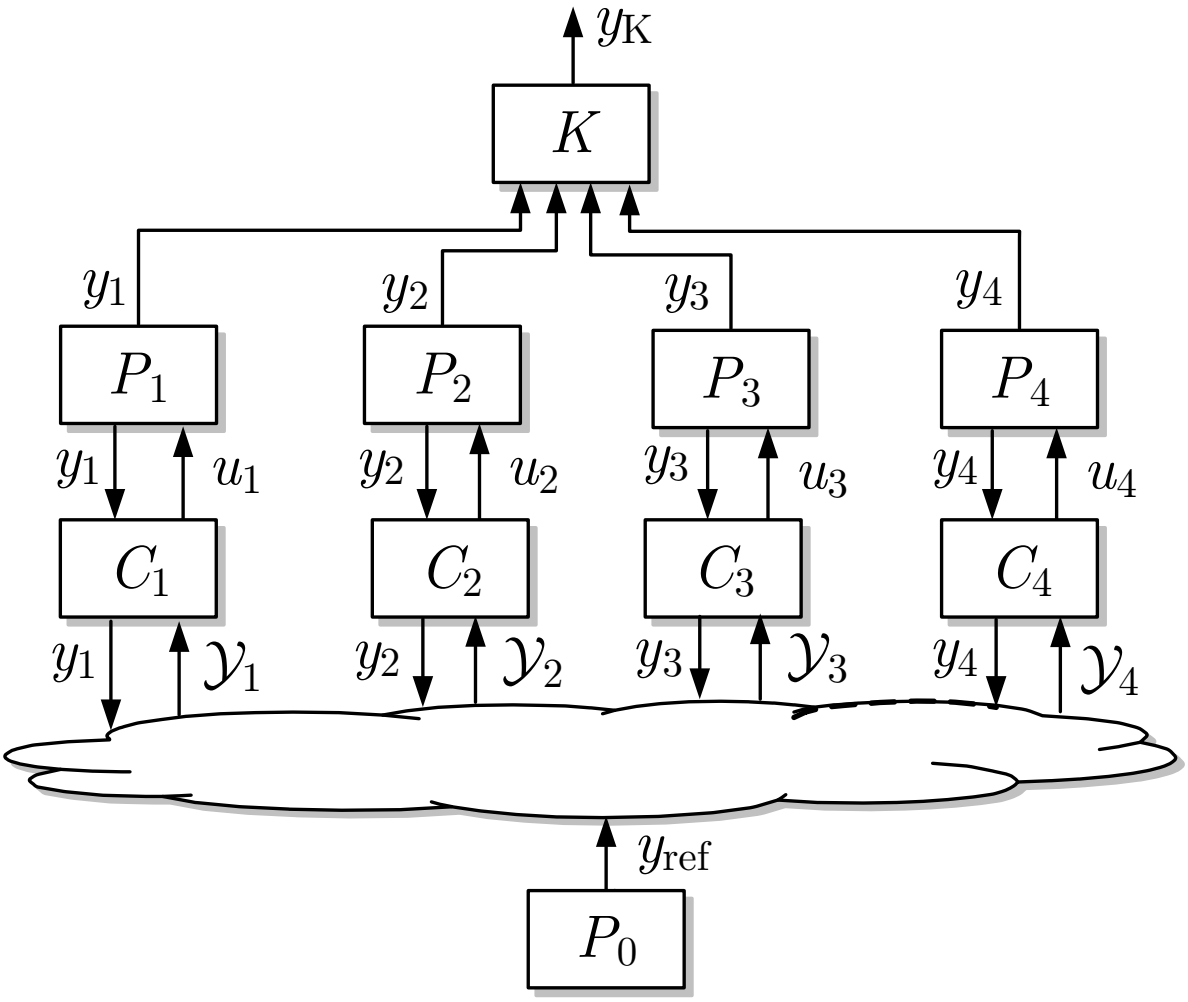

Fig. 2: Block diagram of the networked vehicle controller with the additional block K that generates the performance output $y_{\mathrm{K}}(t)$

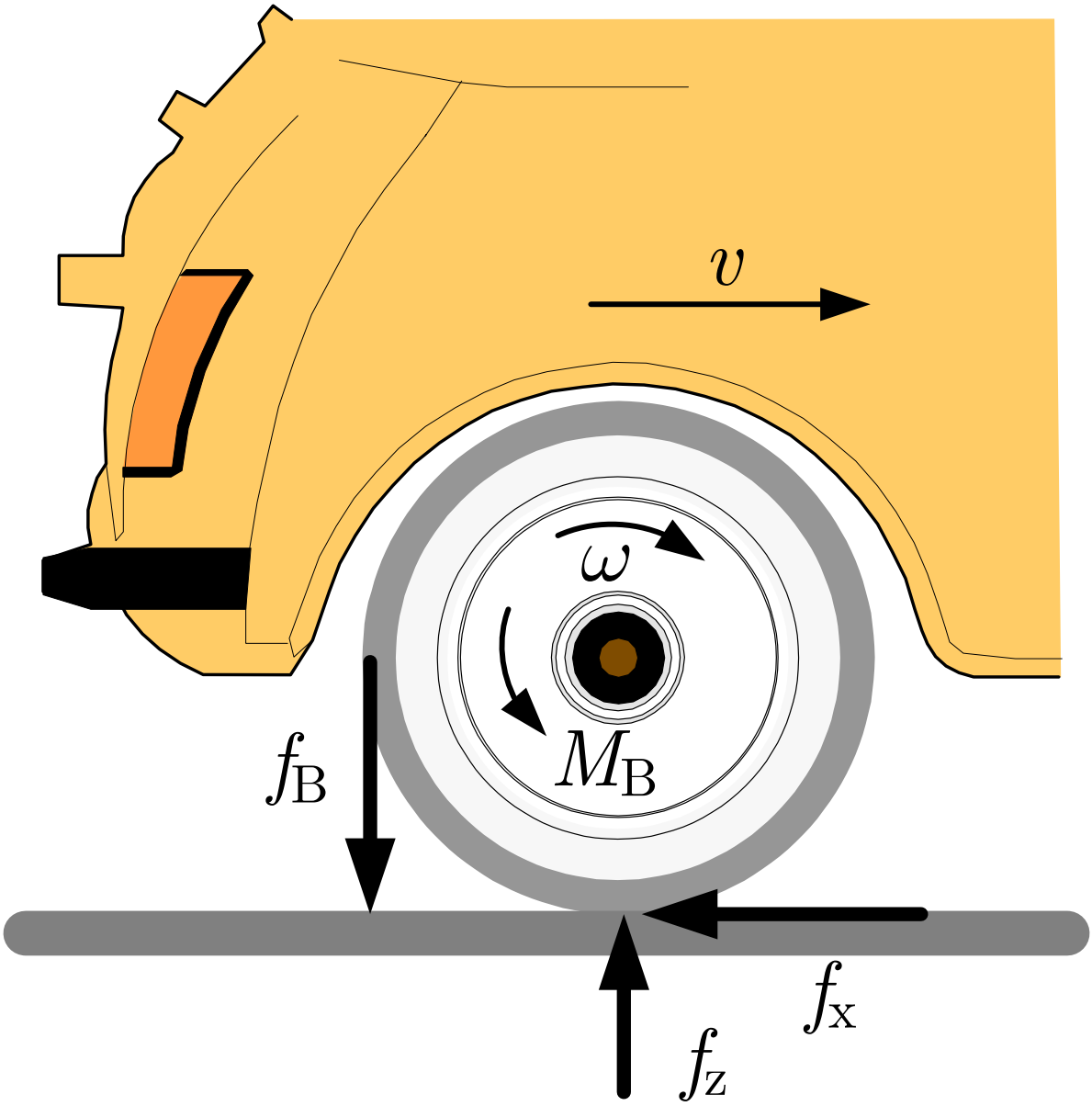

Fig. 3: Torques and forces acting on a wheel

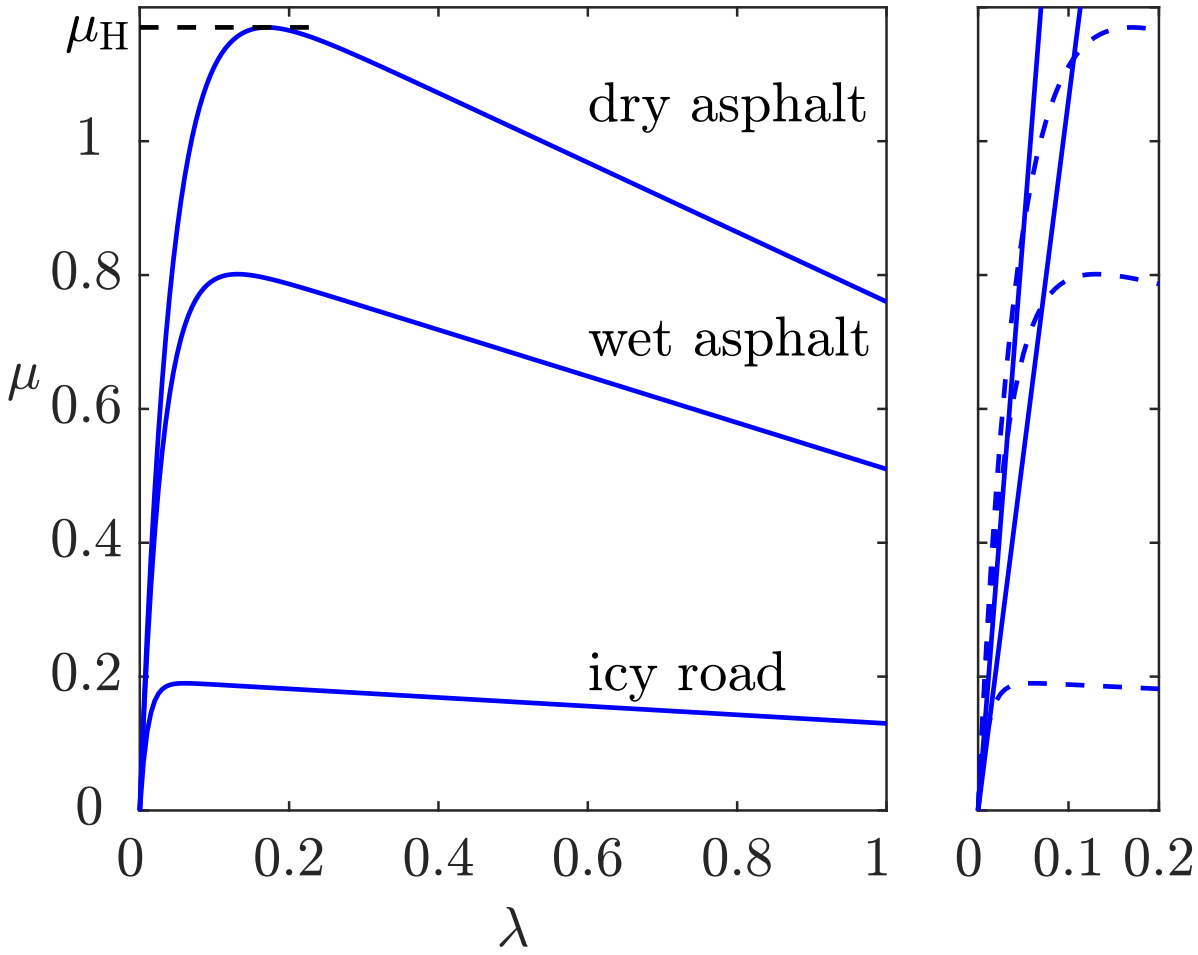

Fig. 4: Friction-slip curve (left) and its approximation (4) (right)

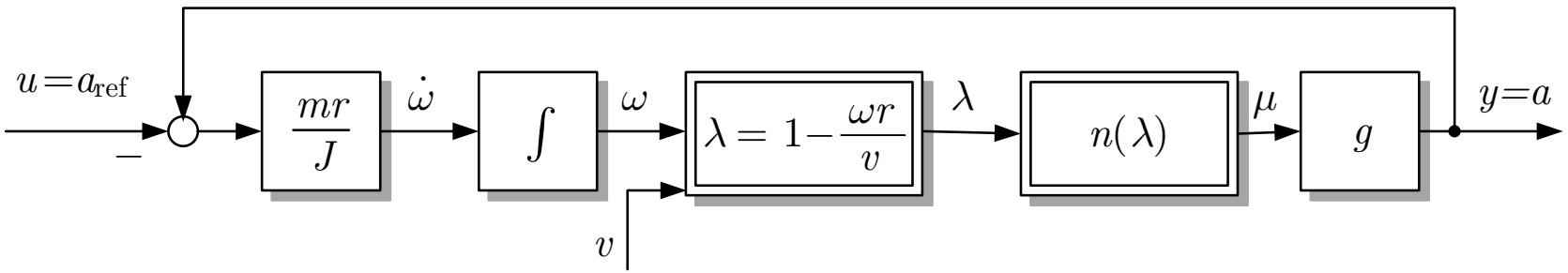

Fig. 5. Nonlinear model of the i-th wheel

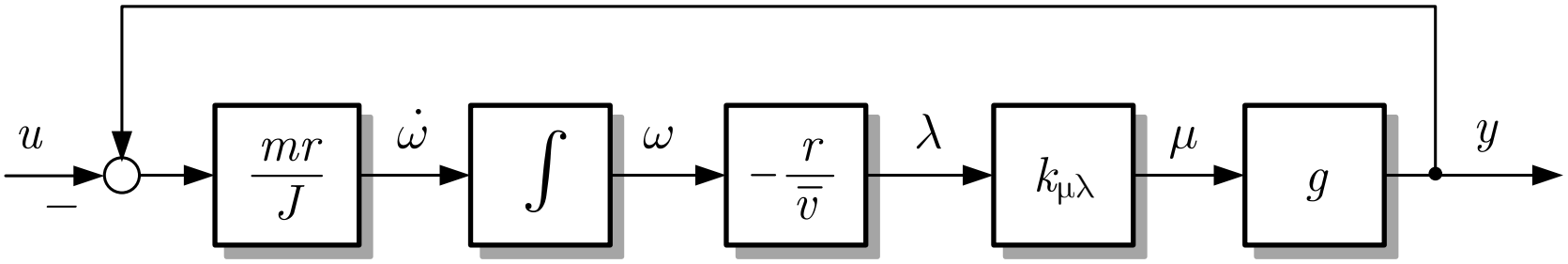

Fig. 6. Linearised model of the i-th wheel

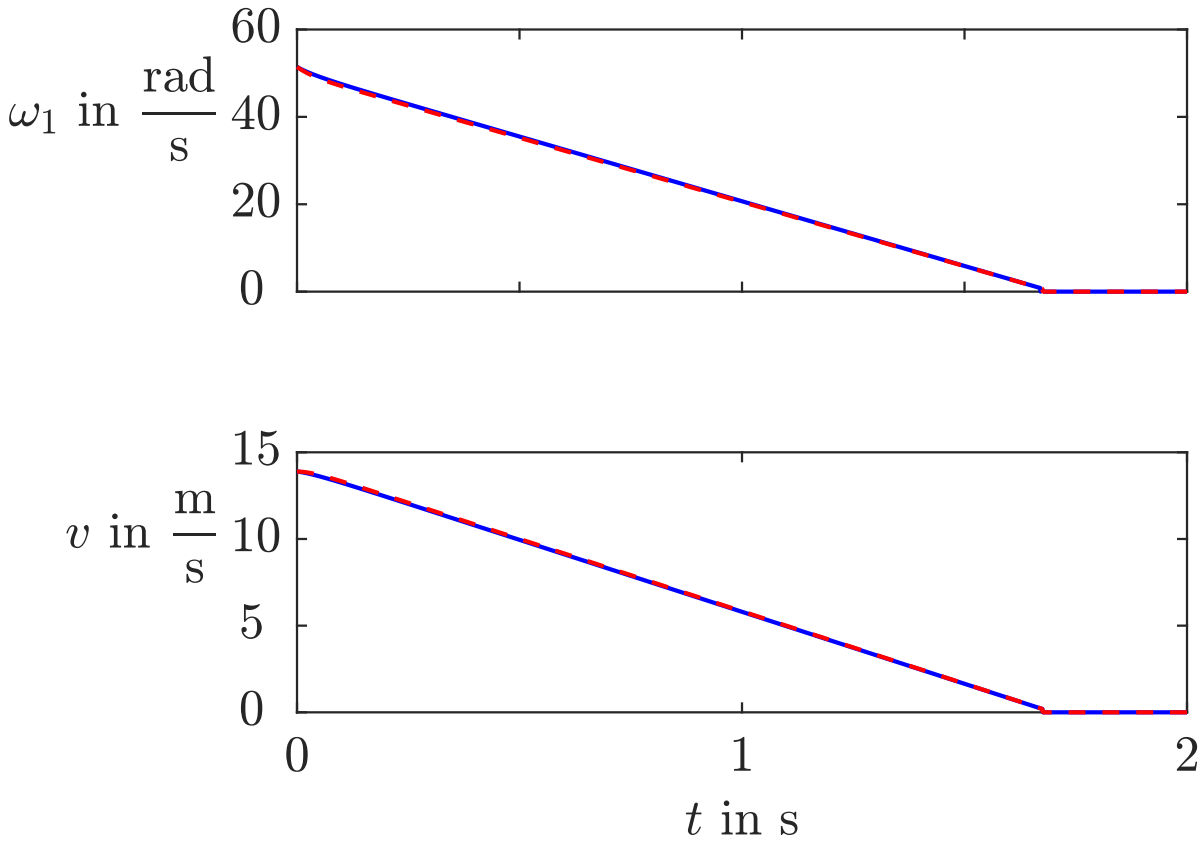

Fig. 7: Angular velocity of the four wheels and vehicle velocity in a braking manoeuvre

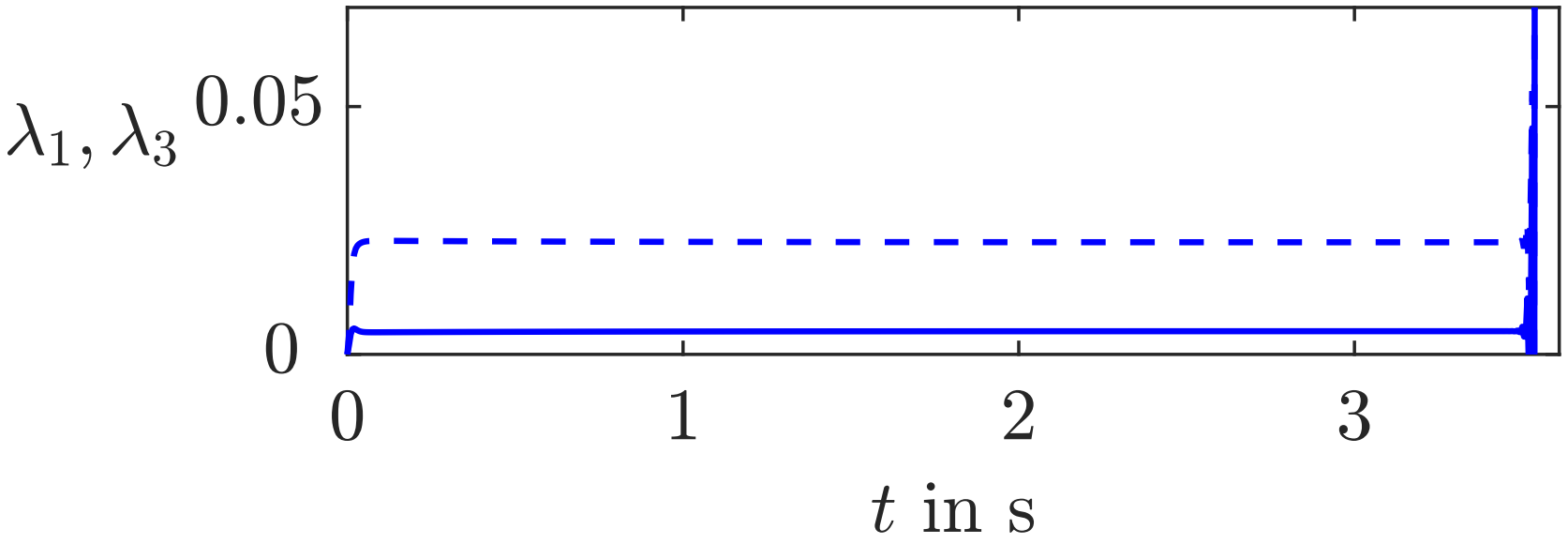

Fig. 8. Slip in the braking manoeuvre of Fig. 7

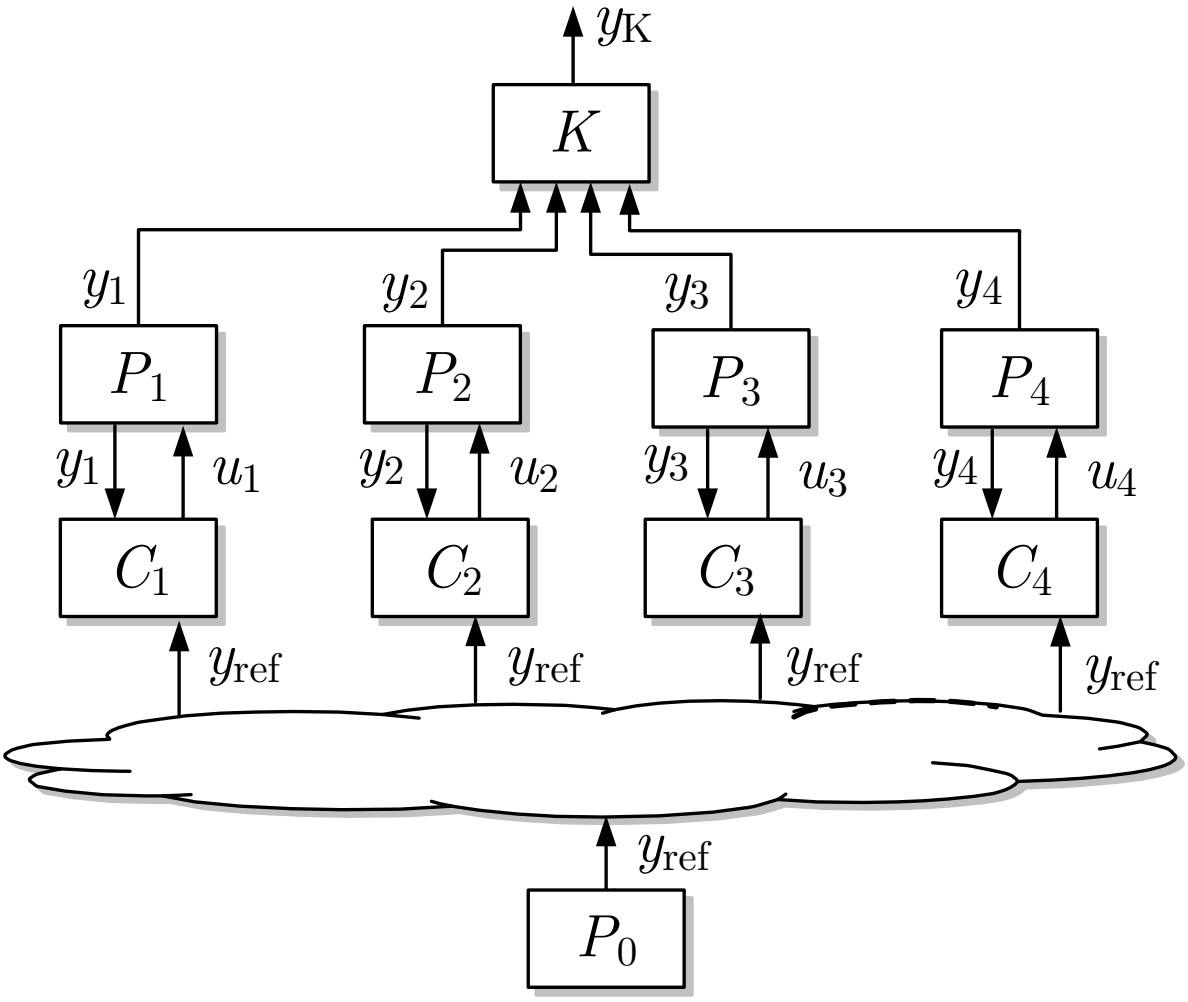

Fig. 9: Braking system with decentralised controller

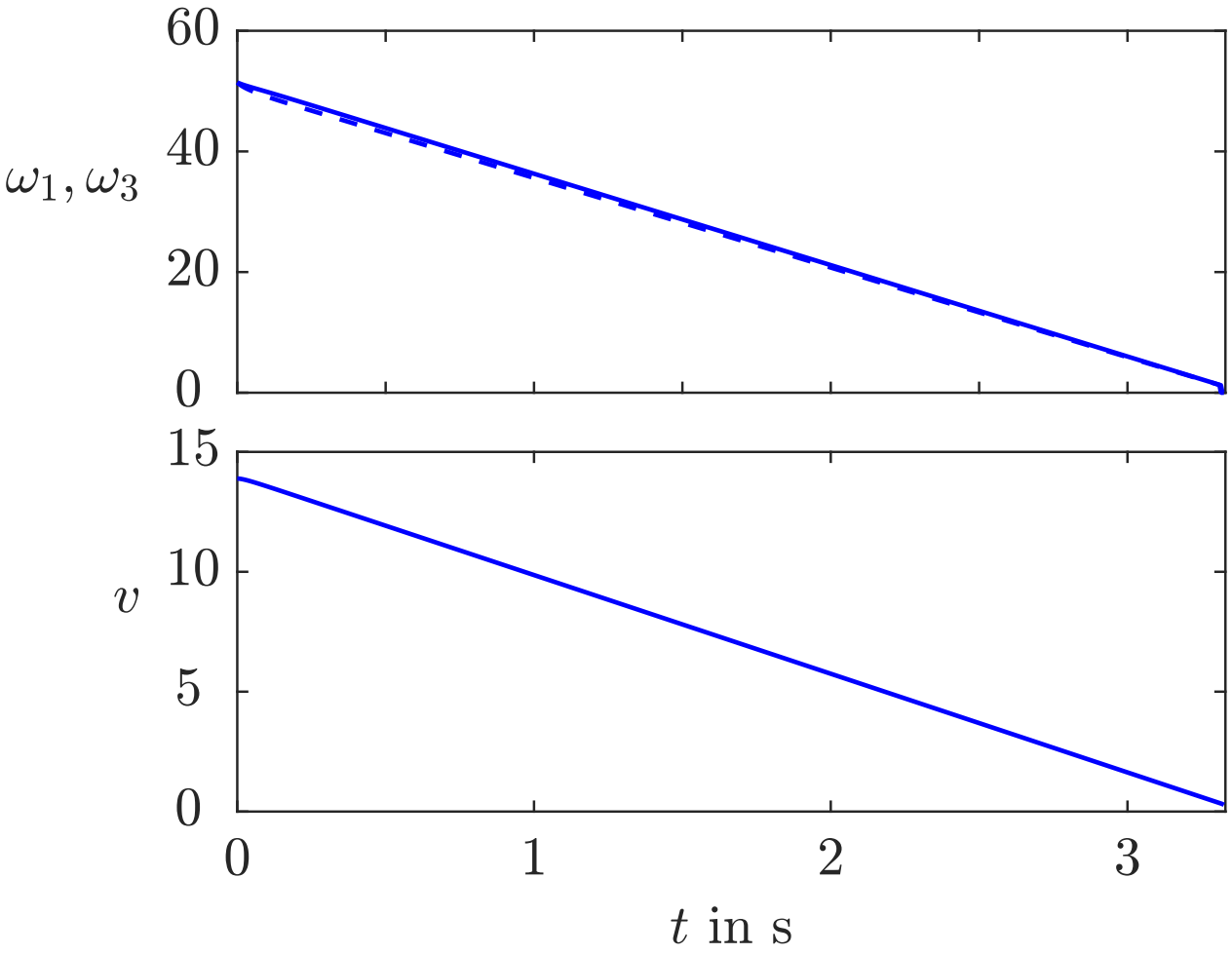

Fig. 10: Angular velocity and vehicle velocity in a braking manoeuvre with decentralised controller

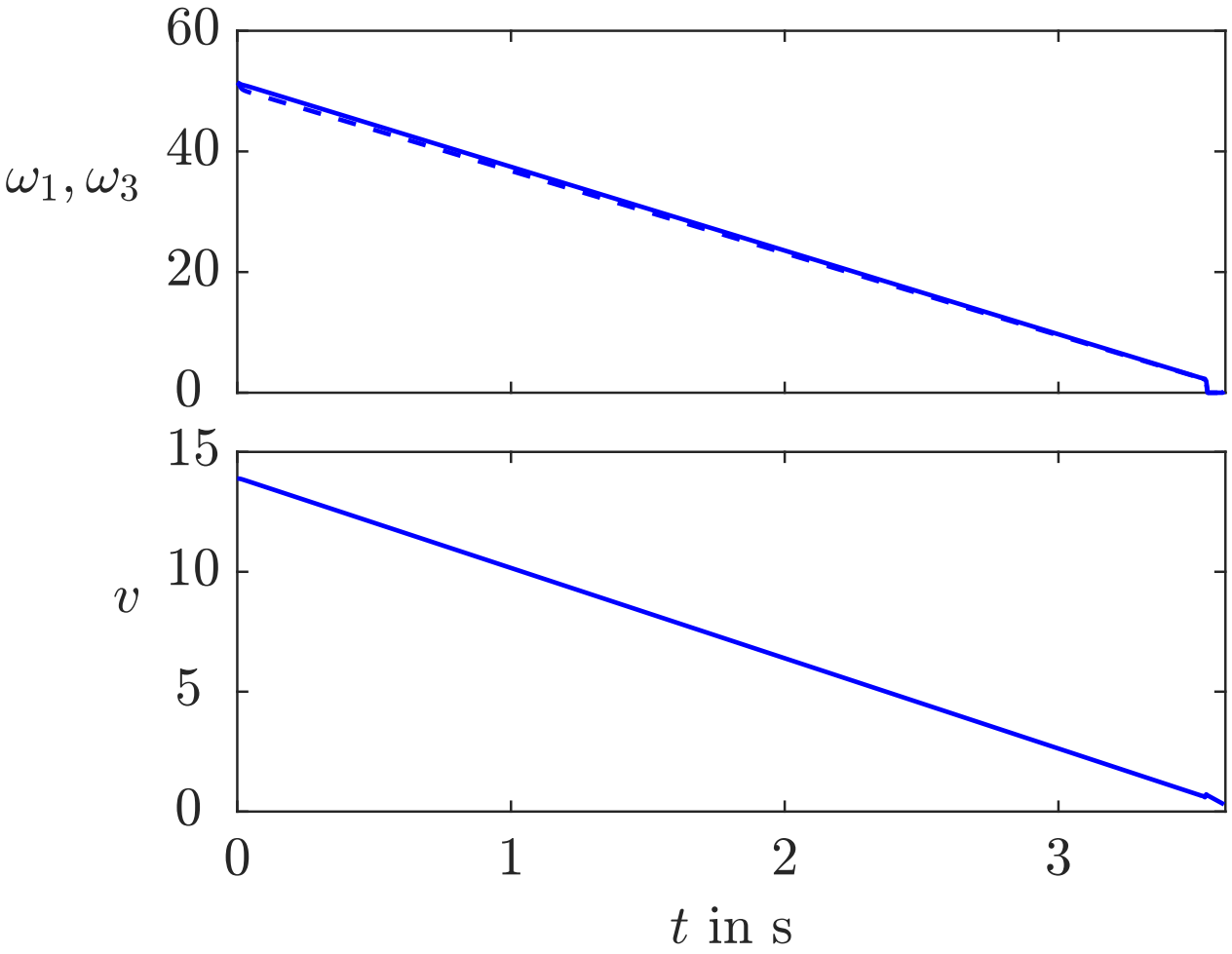

Fig. 10: Angular velocity and vehicle velocity in a braking manoeuvre with networked controller

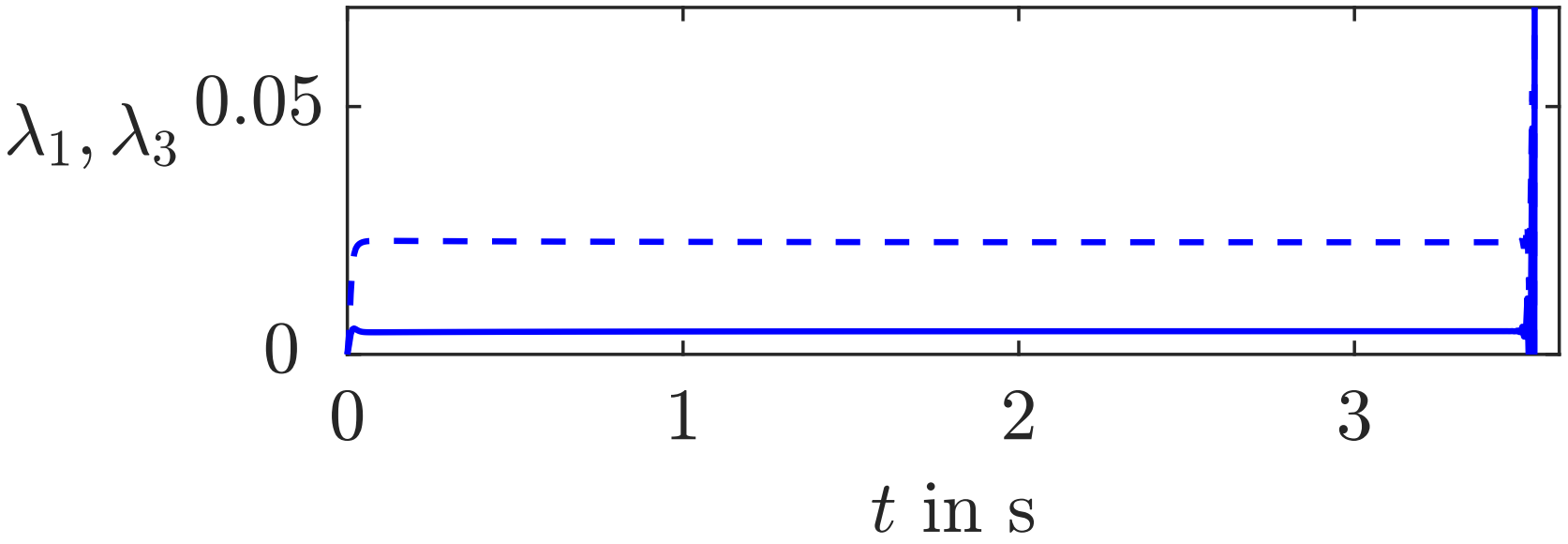

Fig. 11. Slip of the wheels with different road conditions

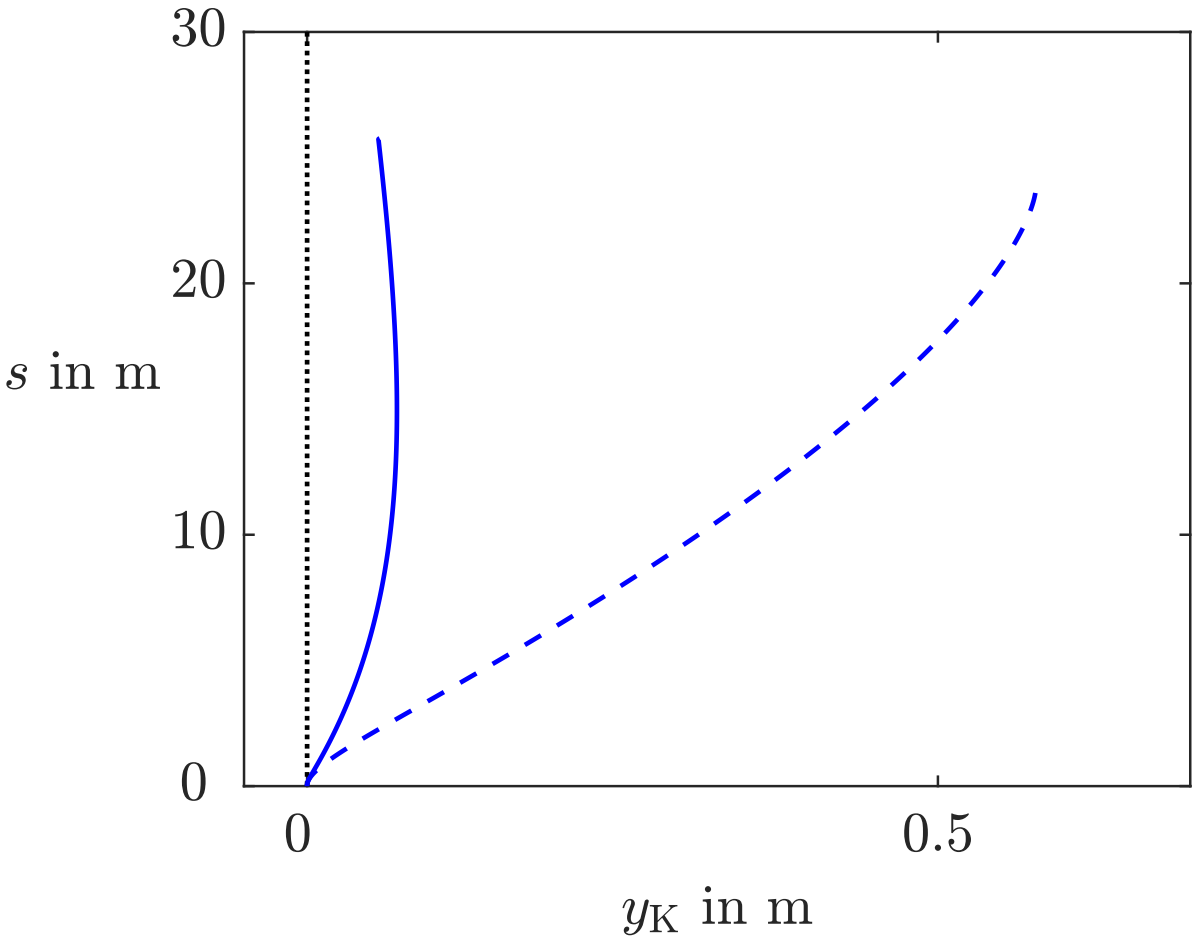

Fig. 12: Comparison of the vehicle movement for the decentralised controller (dashed line) and the networked controller (solid line) with constant road conditions

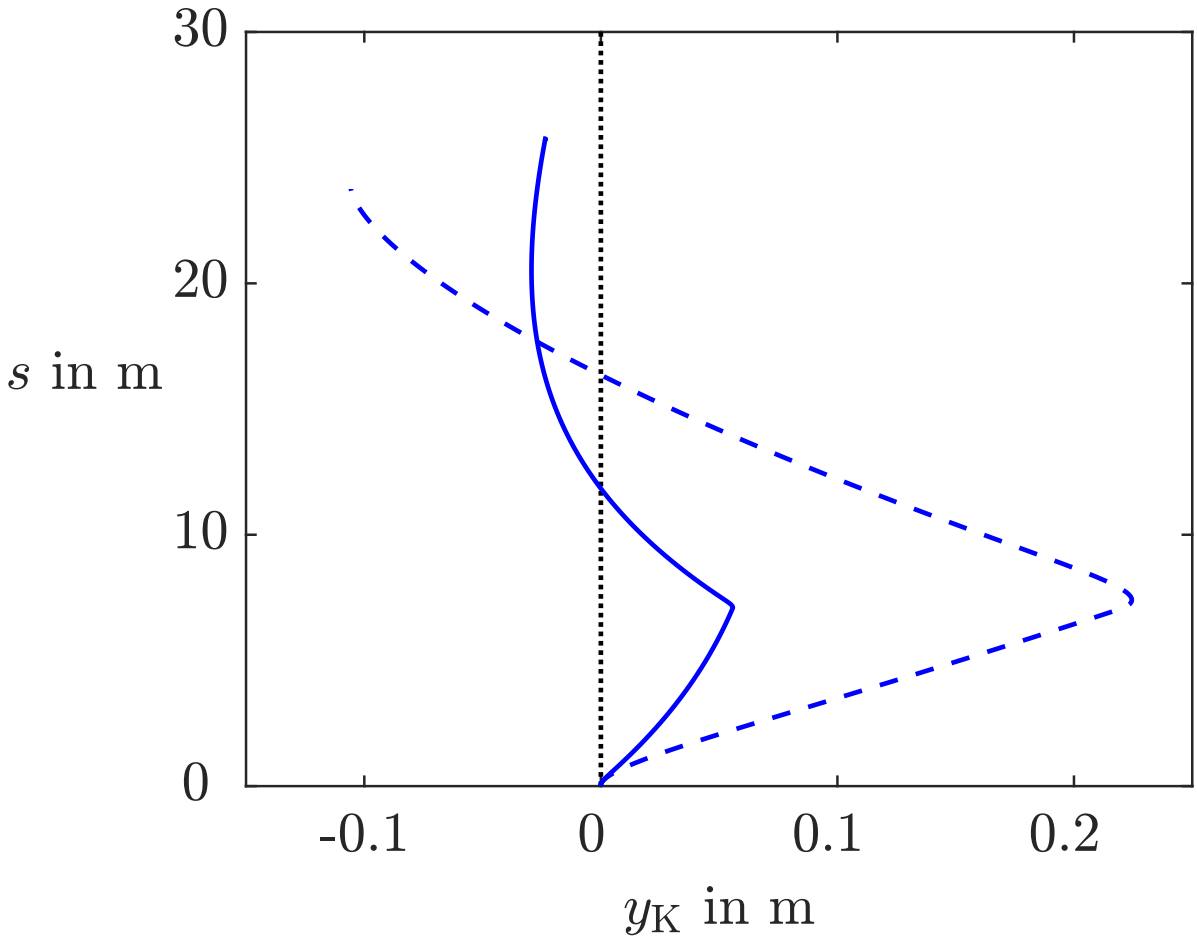

Fig. 12: Comparison of the vehicle movement for the decentralised controller (dashed line) and the networked controller (solid line) with changing road conditions

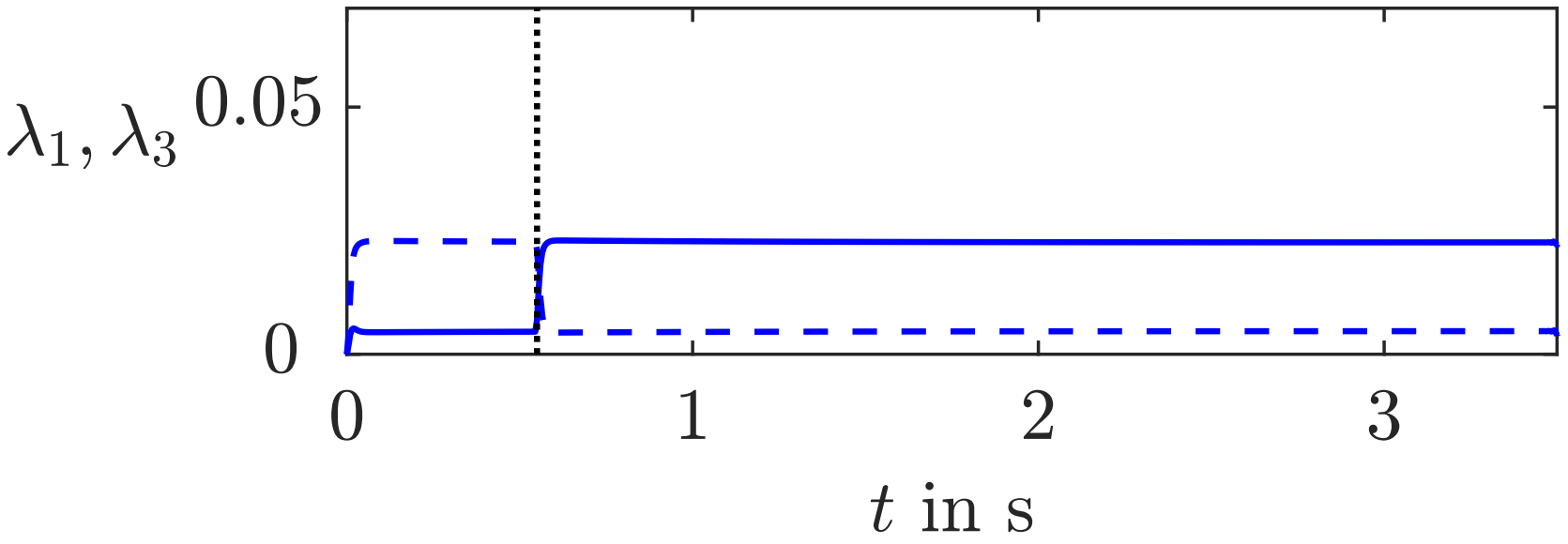

Fig. 13. Slip of the wheels with changing road conditions

Fig. 0: Part of the plan of the bike-renting stations in Paris

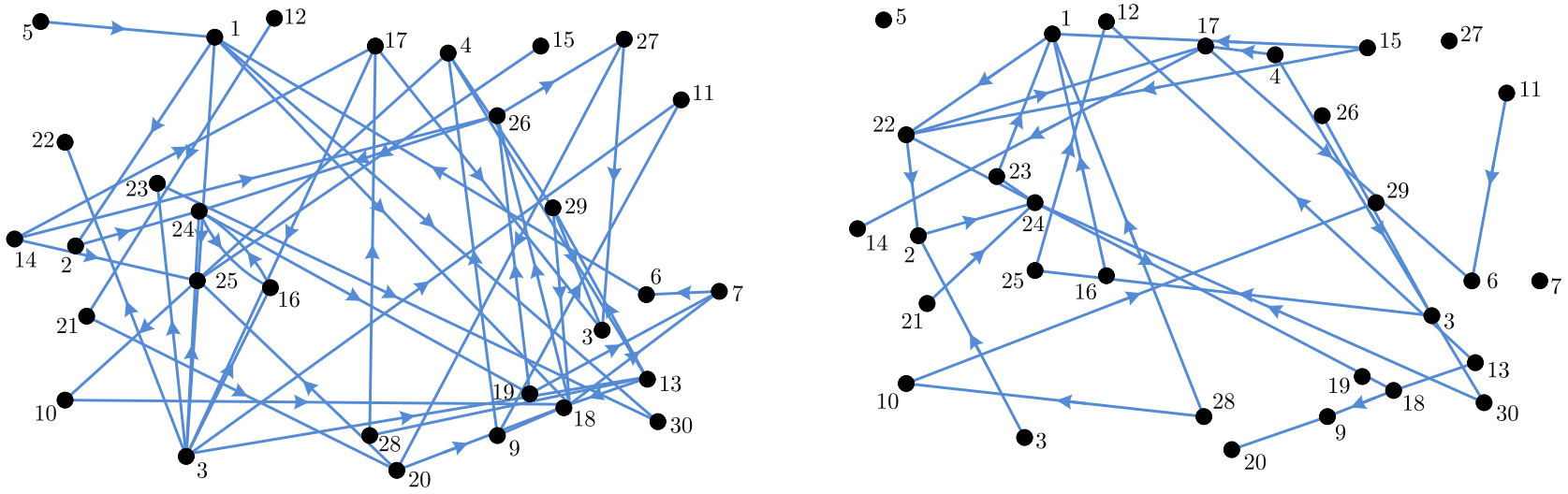

Fig. 1. Two realisations of the random graph for $p = 0.04$

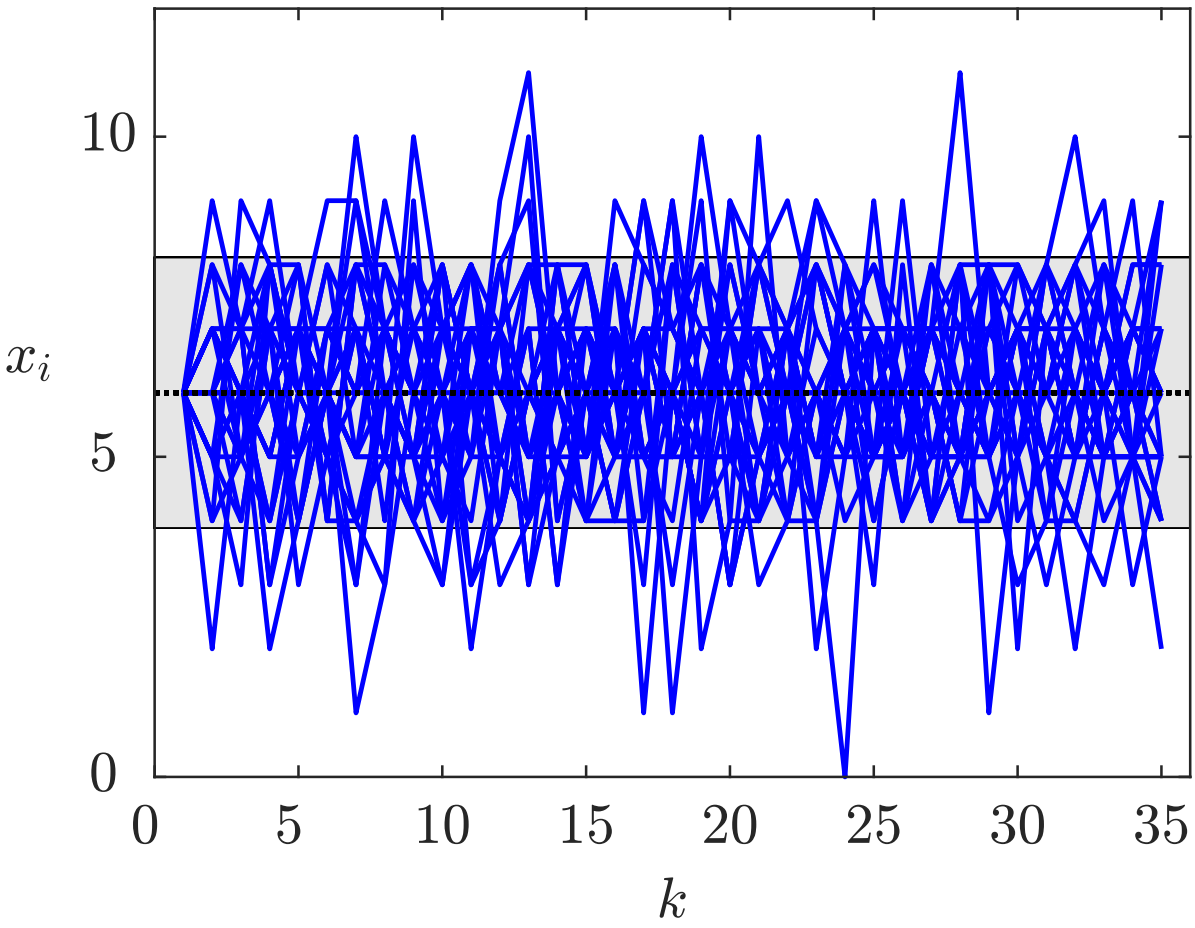

Fig. 2: Simulation result: Number of bikes stored in the docking stations in the centre of Paris between 5 a.m. ($k = 1$) and 10 p.m. ($k = 35$)

Fig. 0: Dice throwing

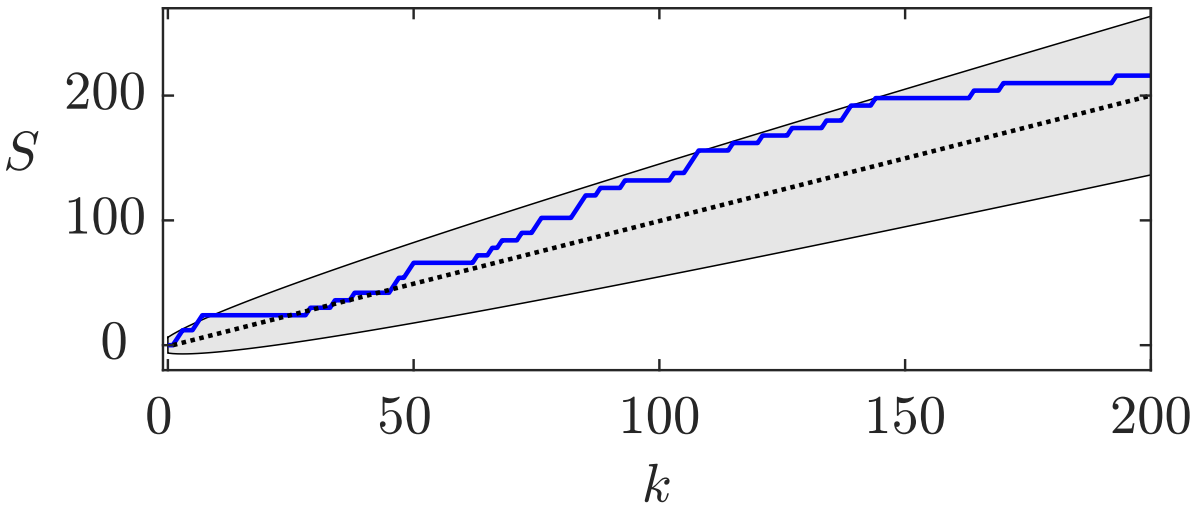

Fig. 1: Tolerance band and a realisation of $S(k)$

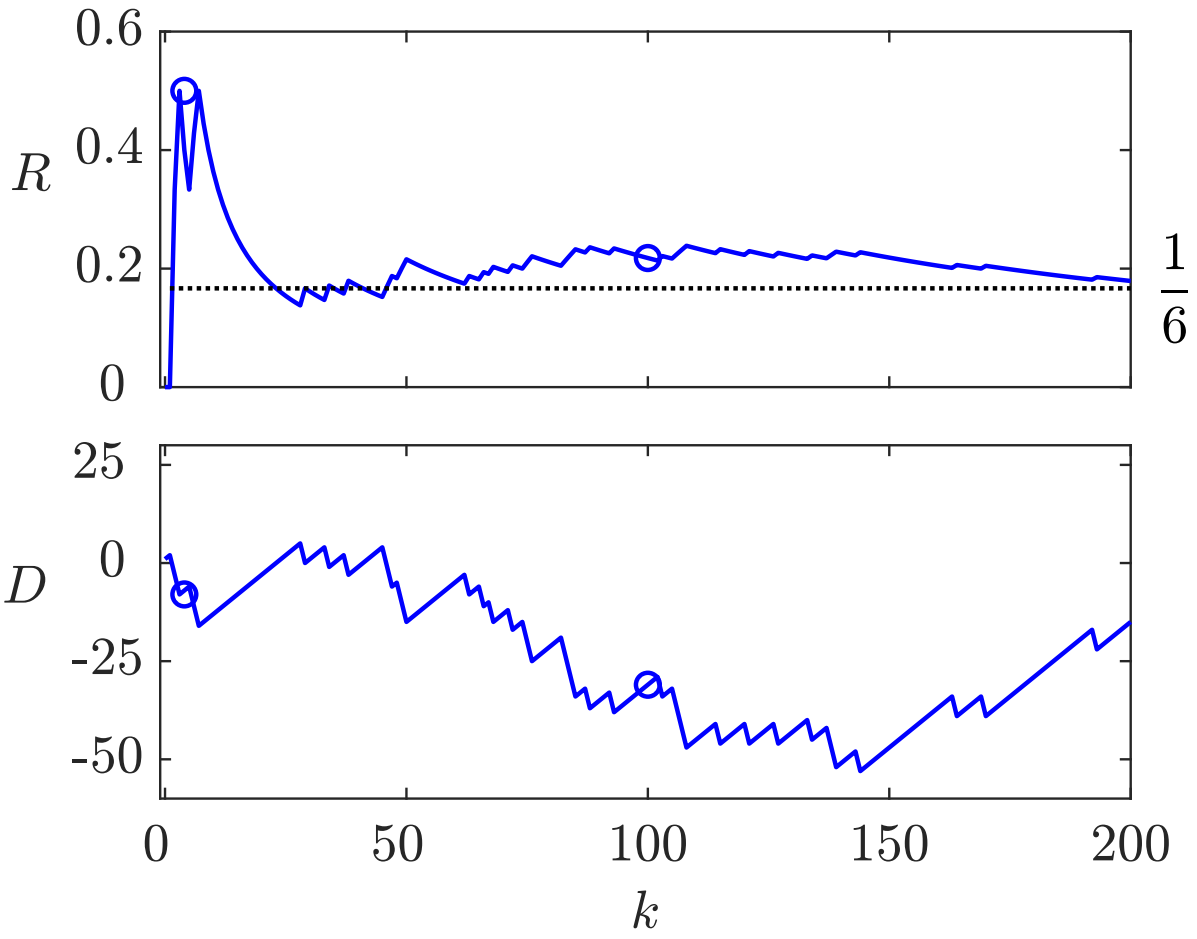

Fig. 2: A realisation of the random sequence $\{R(k), k \geq 0\}$

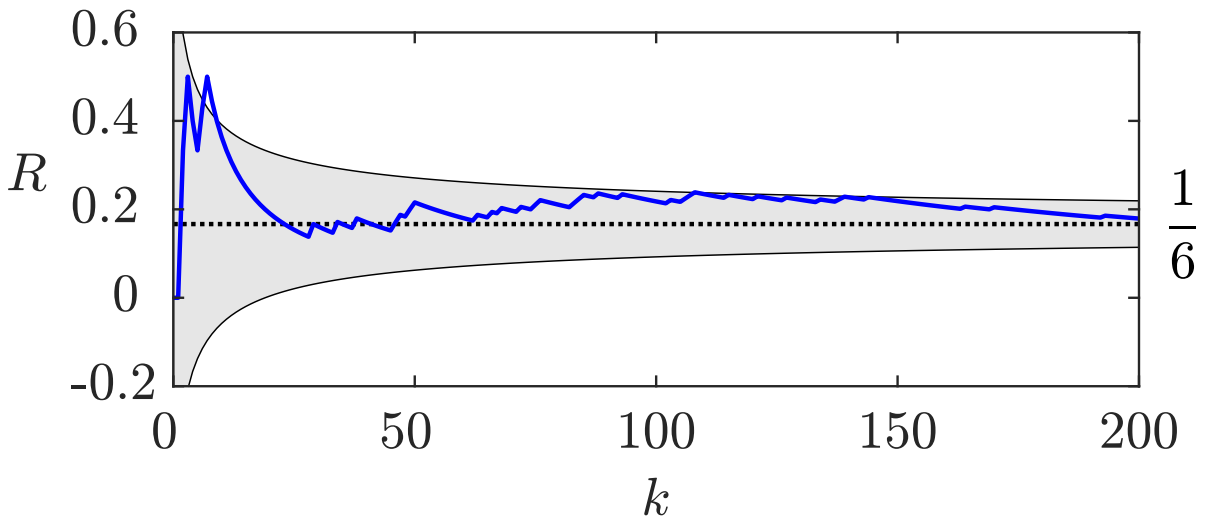

Fig. 3: Tolerance band around the expected value

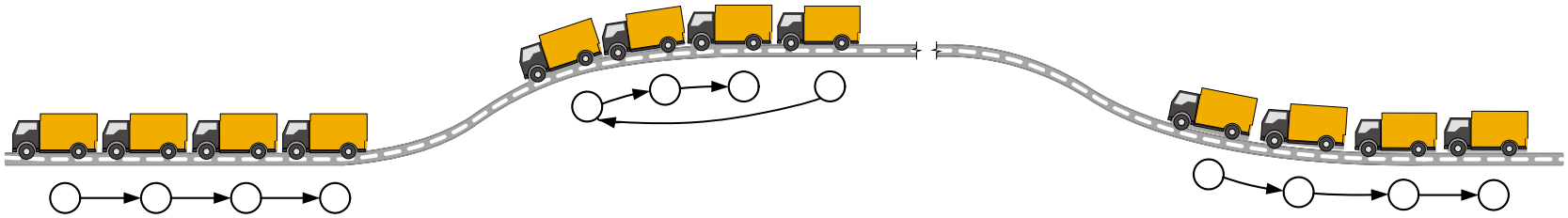

Fig. 0. Truck platoon in a hilly terrain

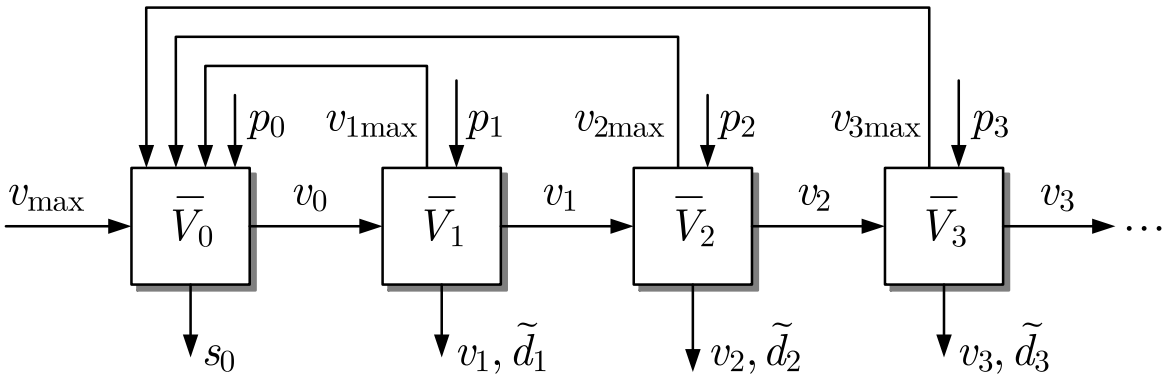

Fig. 1: Block diagram of the truck platoon

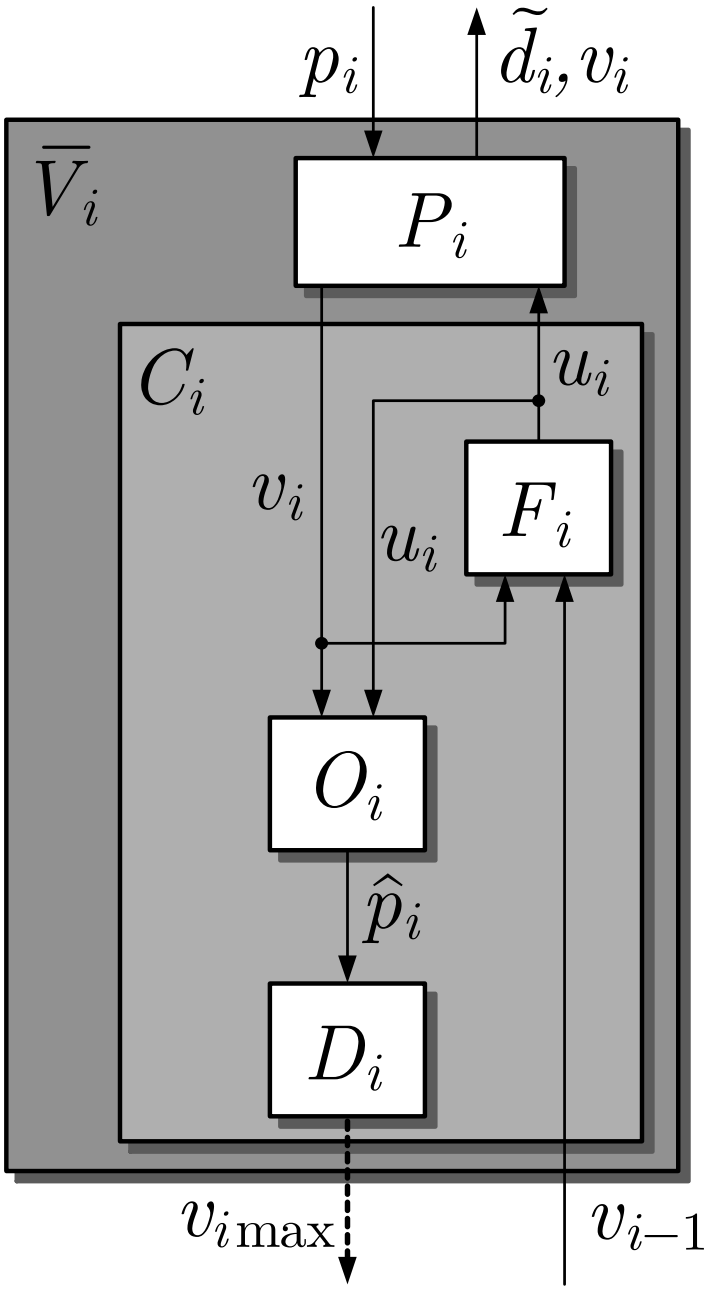

Fig. 2. Structure of the truck controller

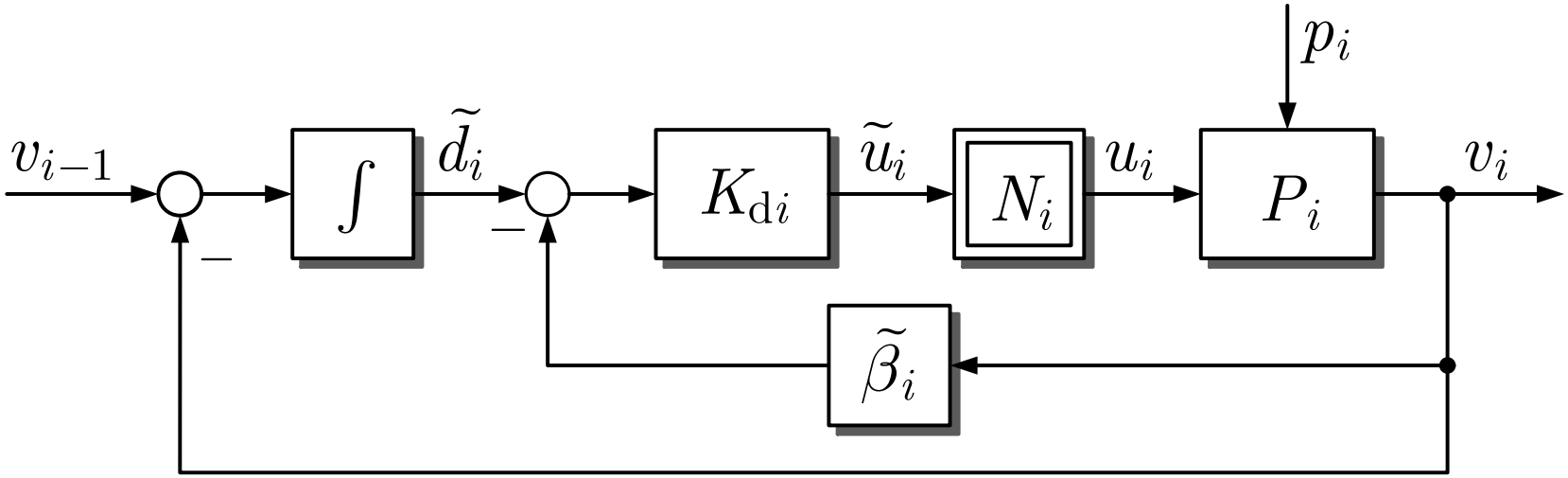

Fig. 3. Truck with distance controller

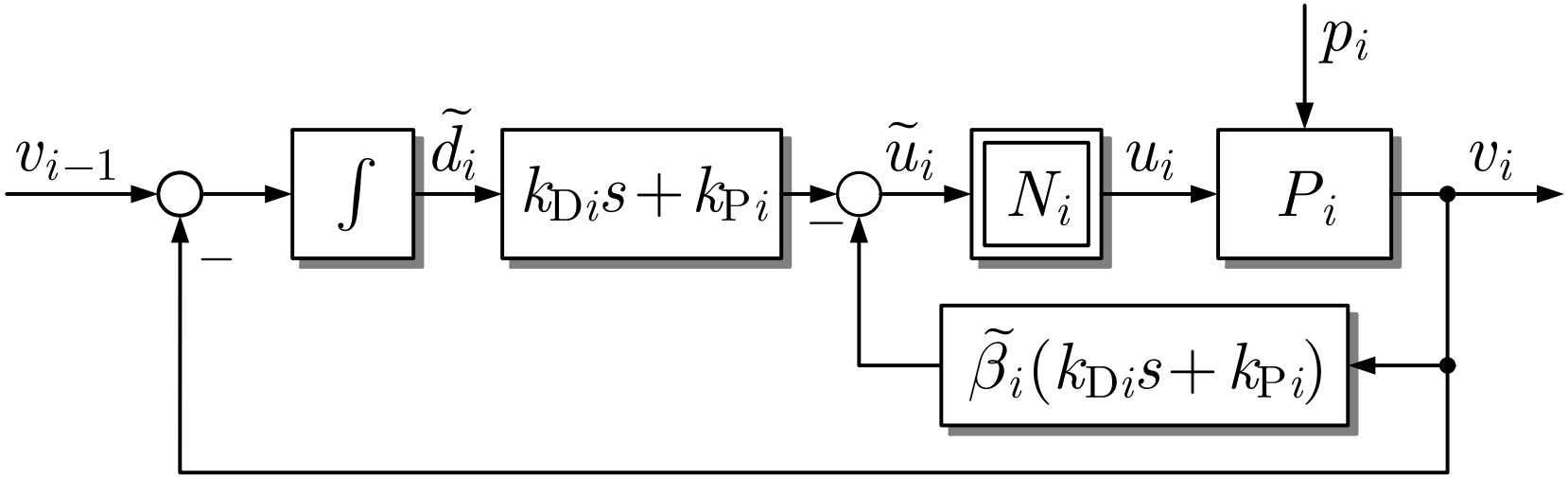

Fig. 4. Transformed distance control loop

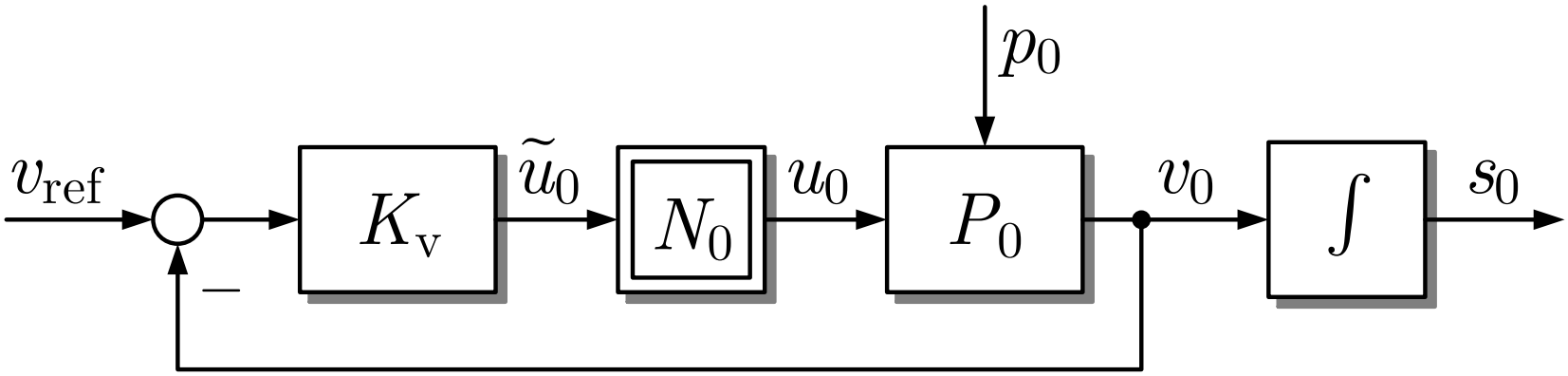

Fig. 5. First truck $\bar{V}_0$ with velocity controller

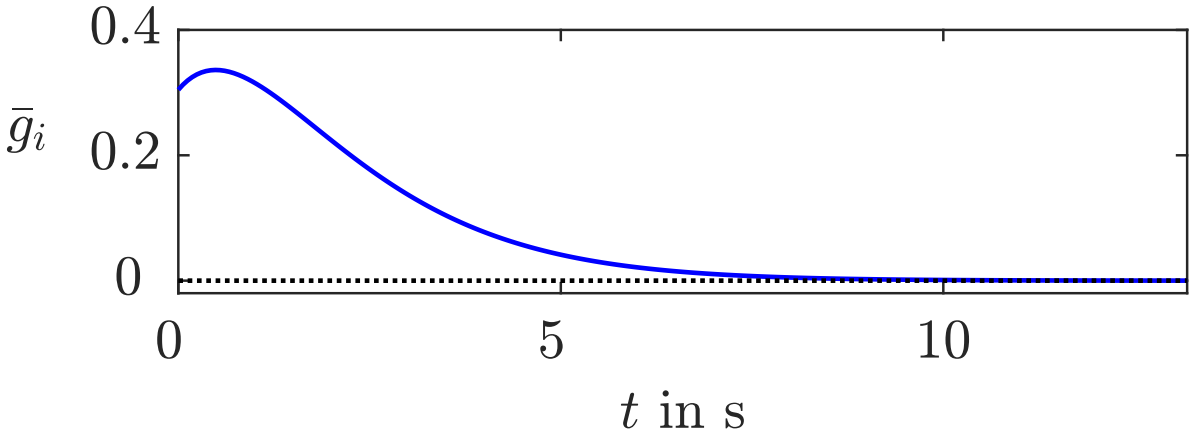

Fig. 6: Nonnegative impulse response of the linear trucks

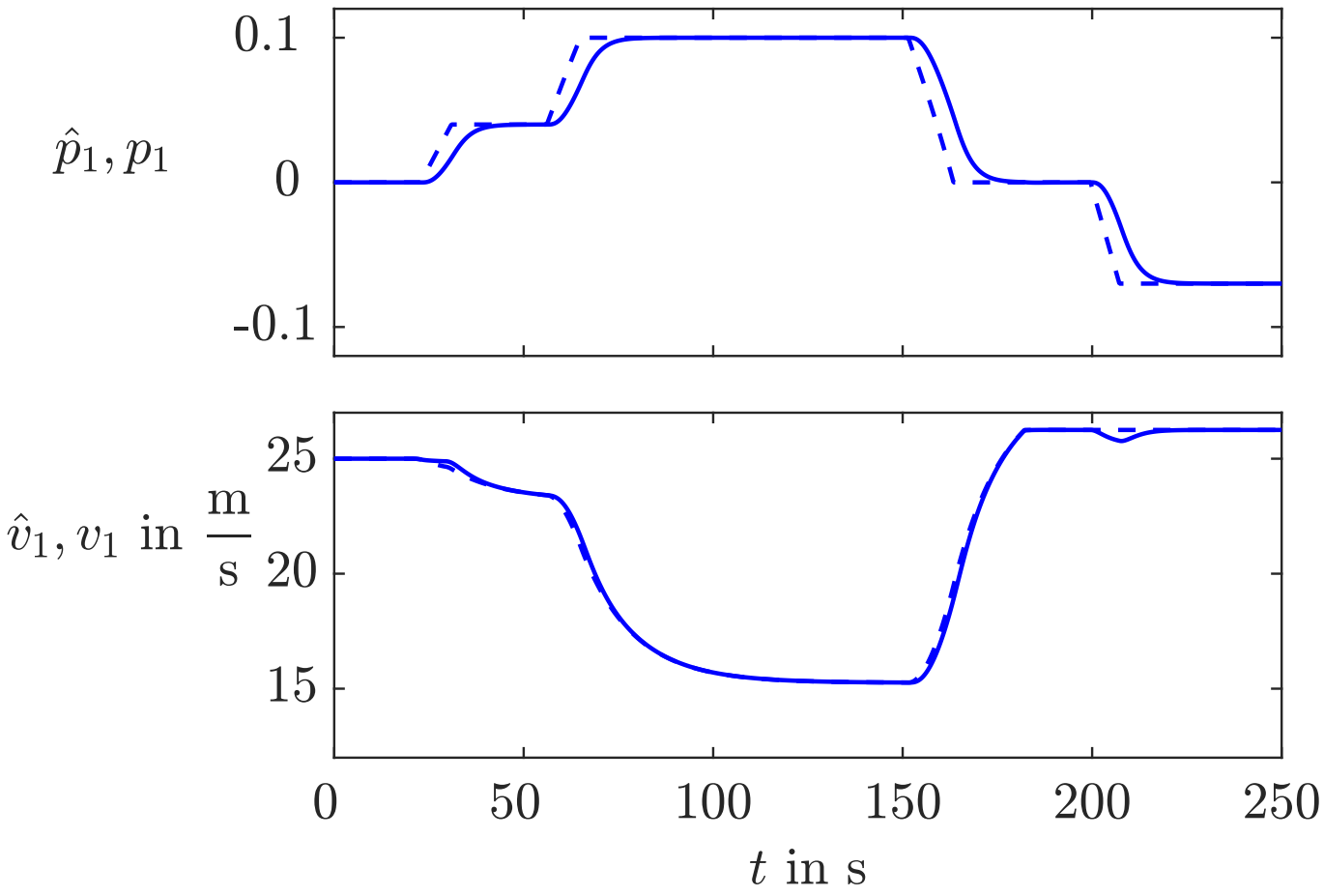

Fig. 7: True (- - -) and estimated (—) disturbance and velocity of the first truck

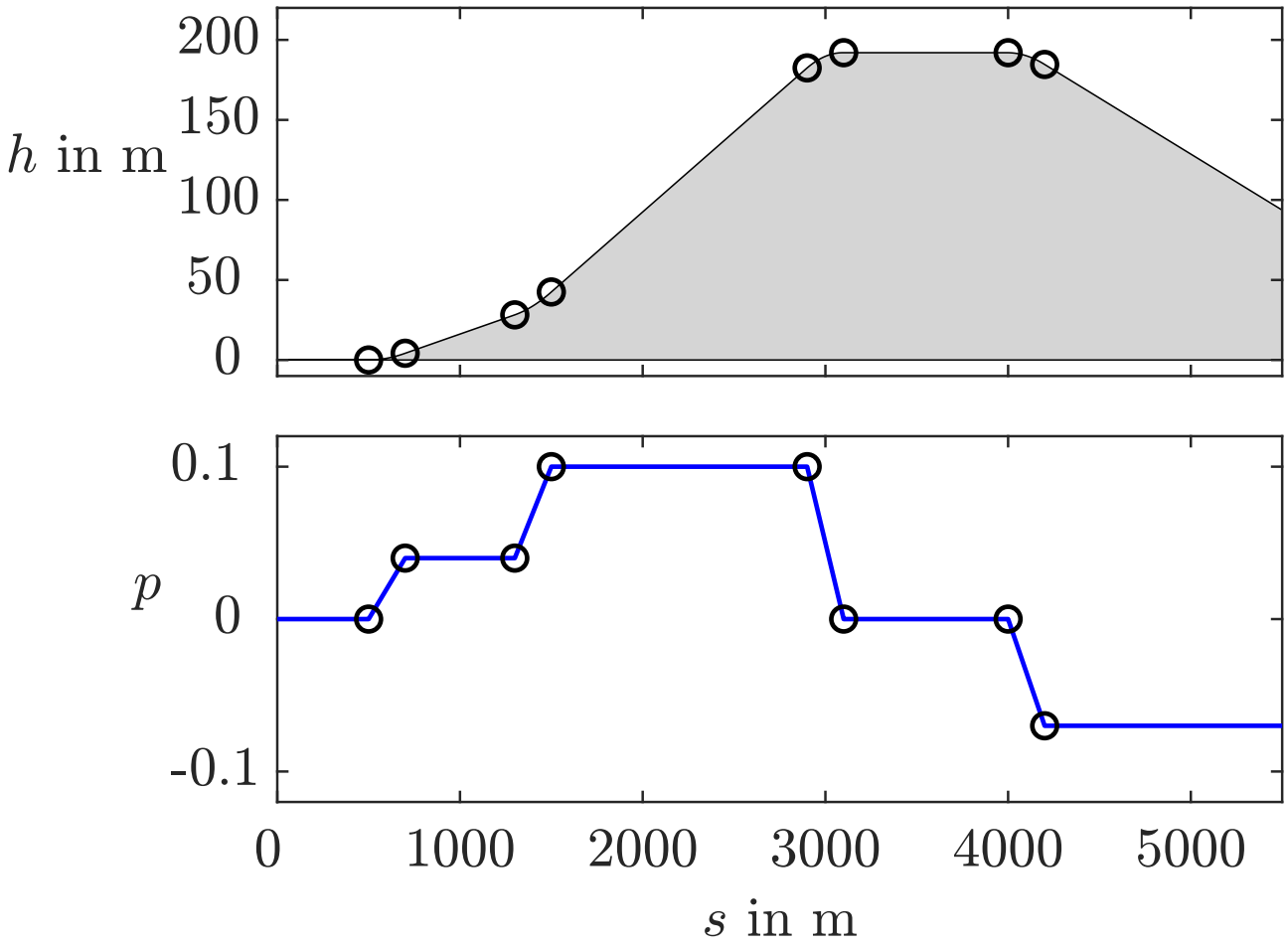

Fig. 8: Road profile and disturbance

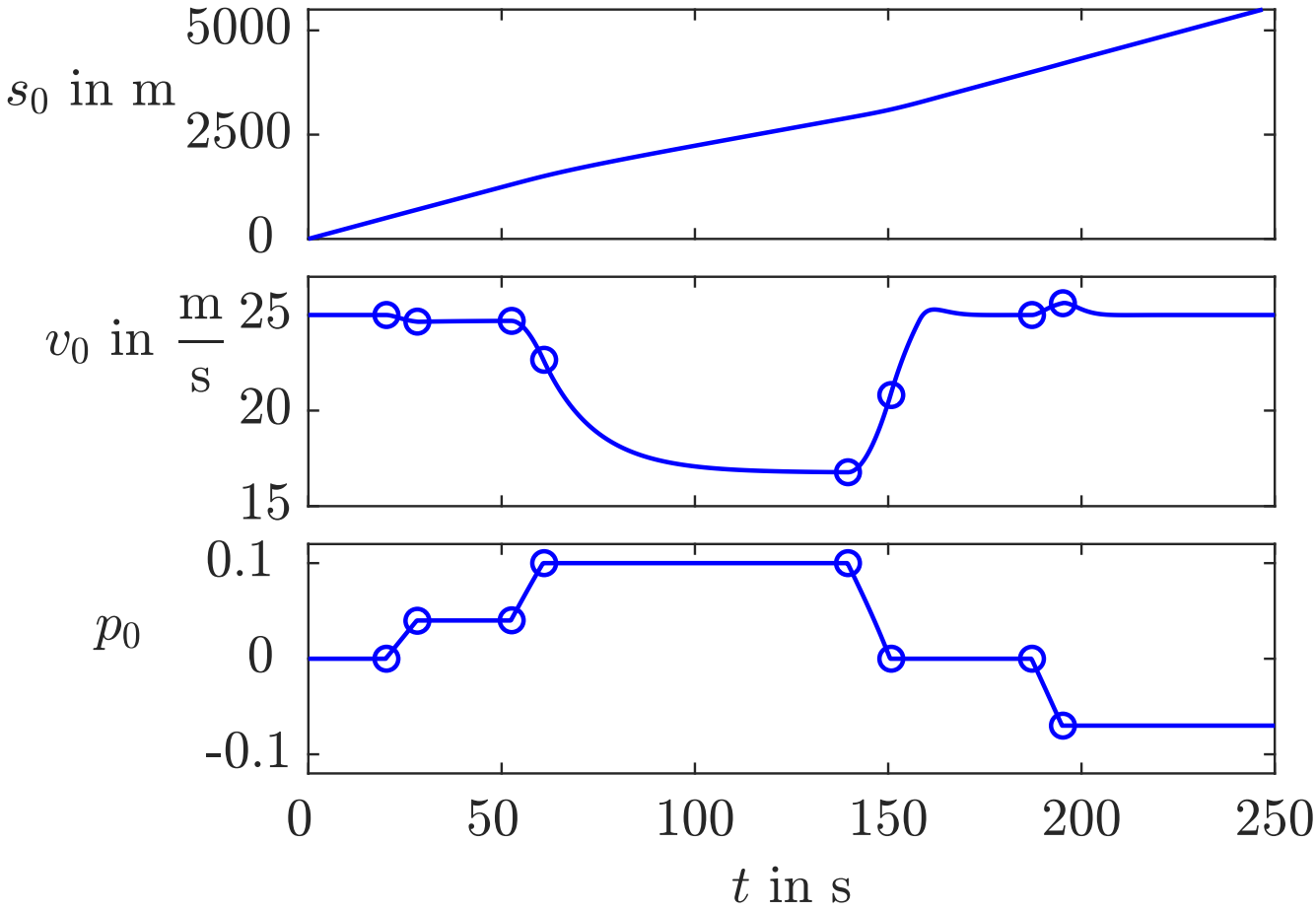

Fig. 9: Behaviour of the first truck for constant reference velocity $v_{\text{ref}}(t) = v_{\max}$

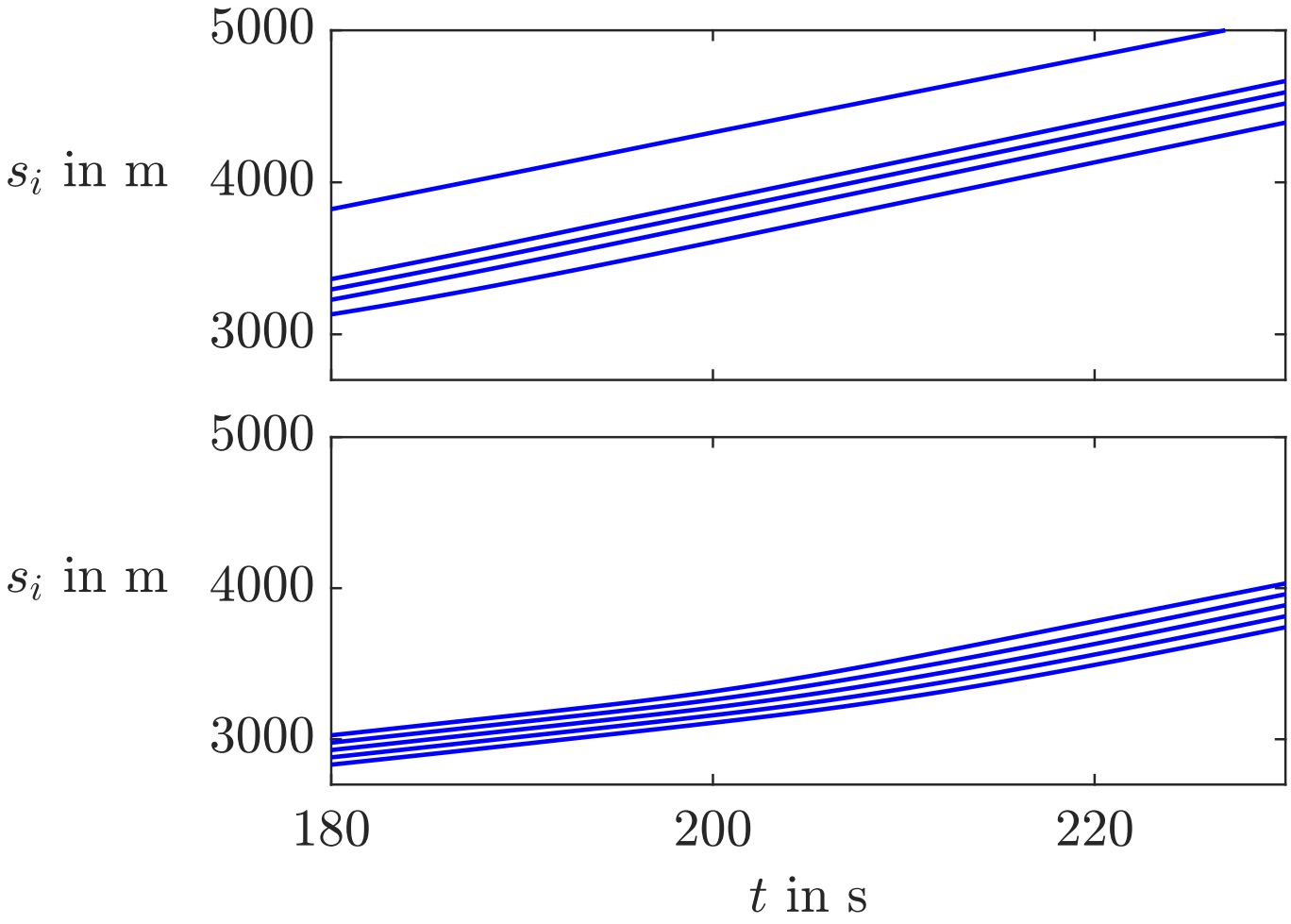

Fig. 10: Platoon behaviour with ACC (top) and with self-organised ACC (bottom)

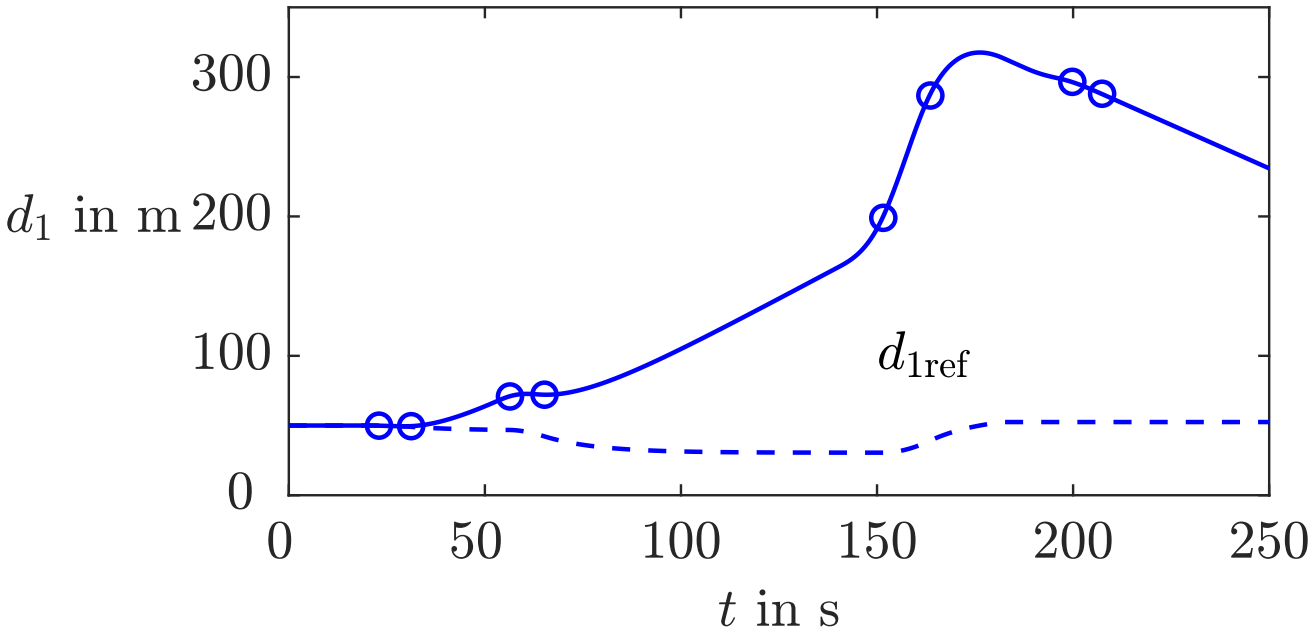

Fig. 11: Distance between the first two trucks with ACC

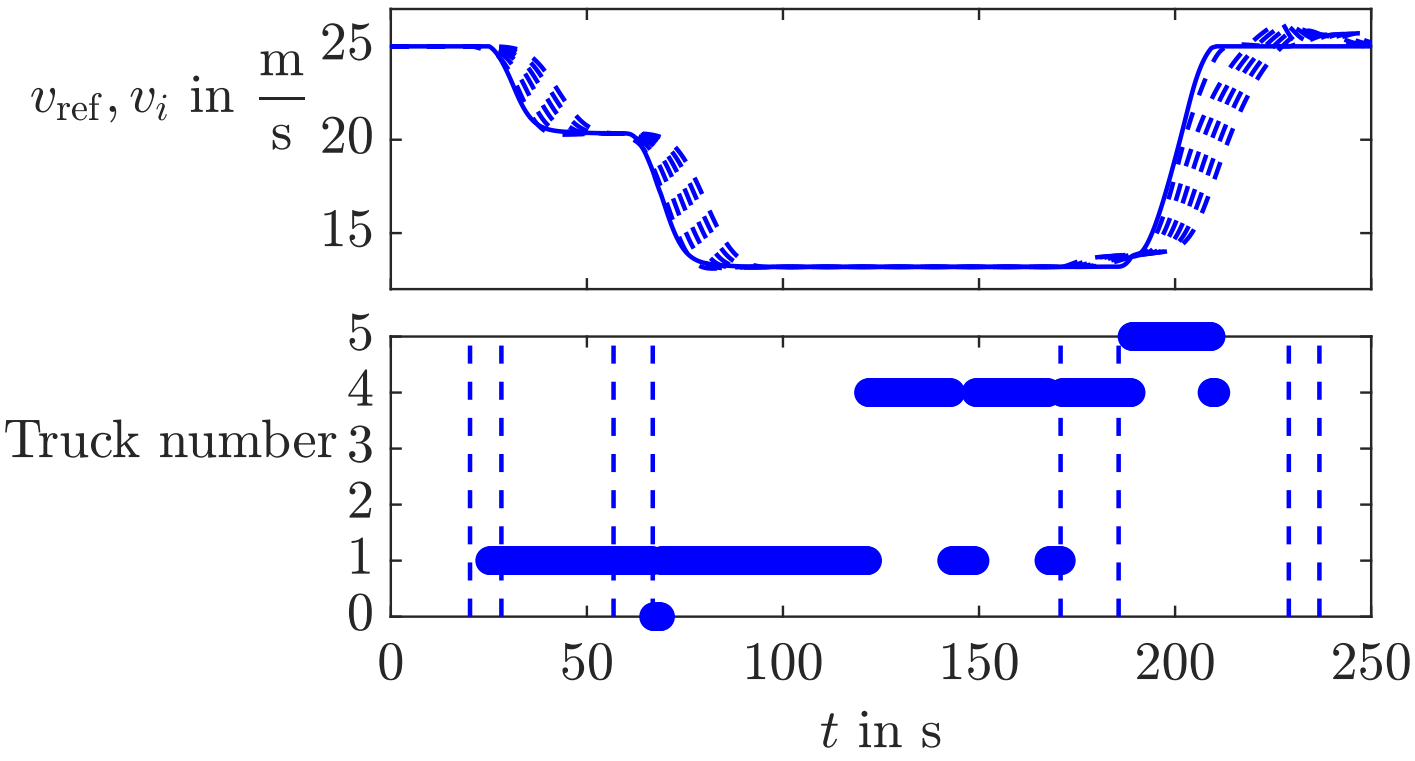

Fig. 12: Behaviour of the truck platoon with self-organised ACC

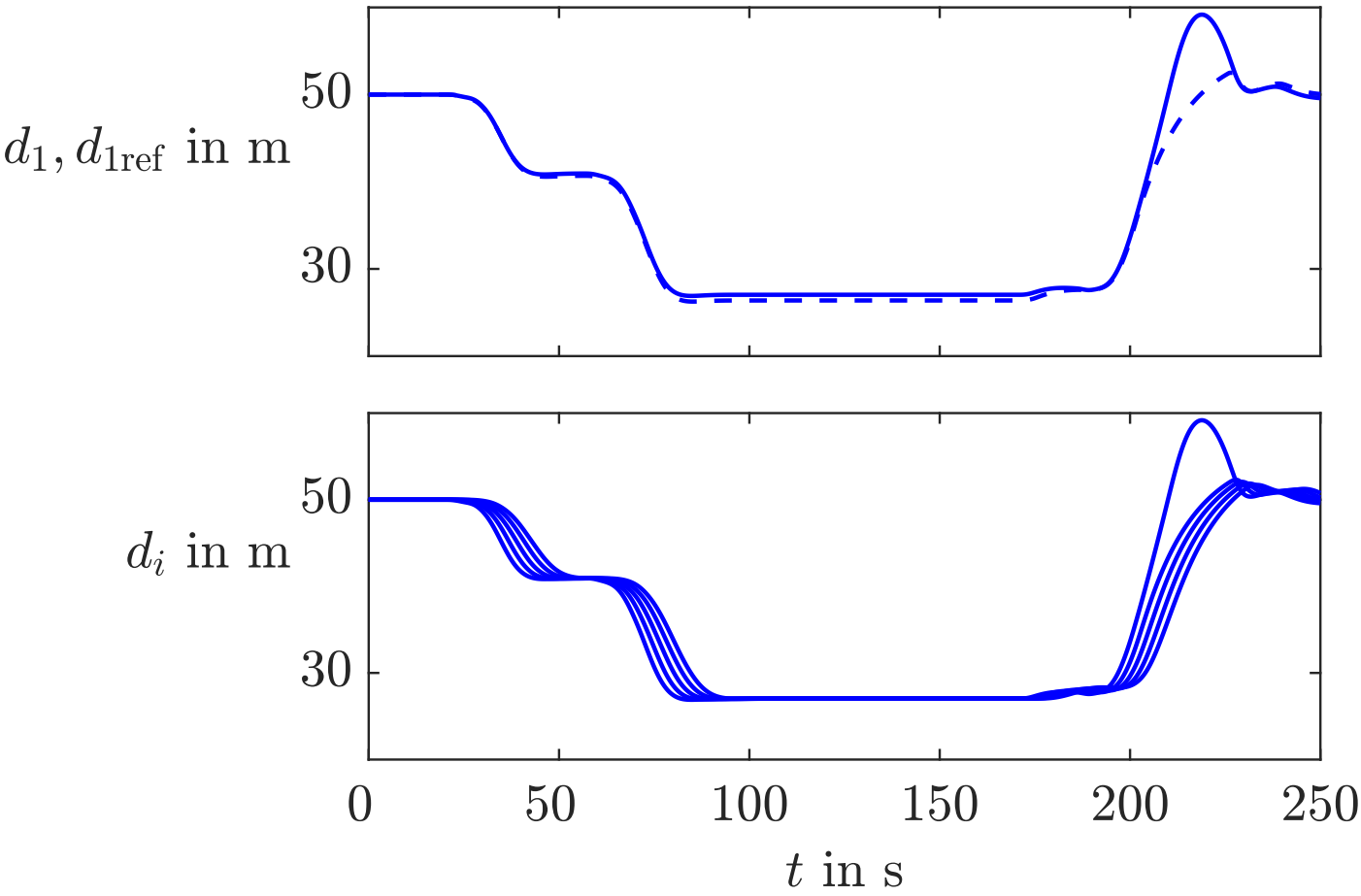

Fig. 13: Vehicle distances in the platoon with self-organised ACC

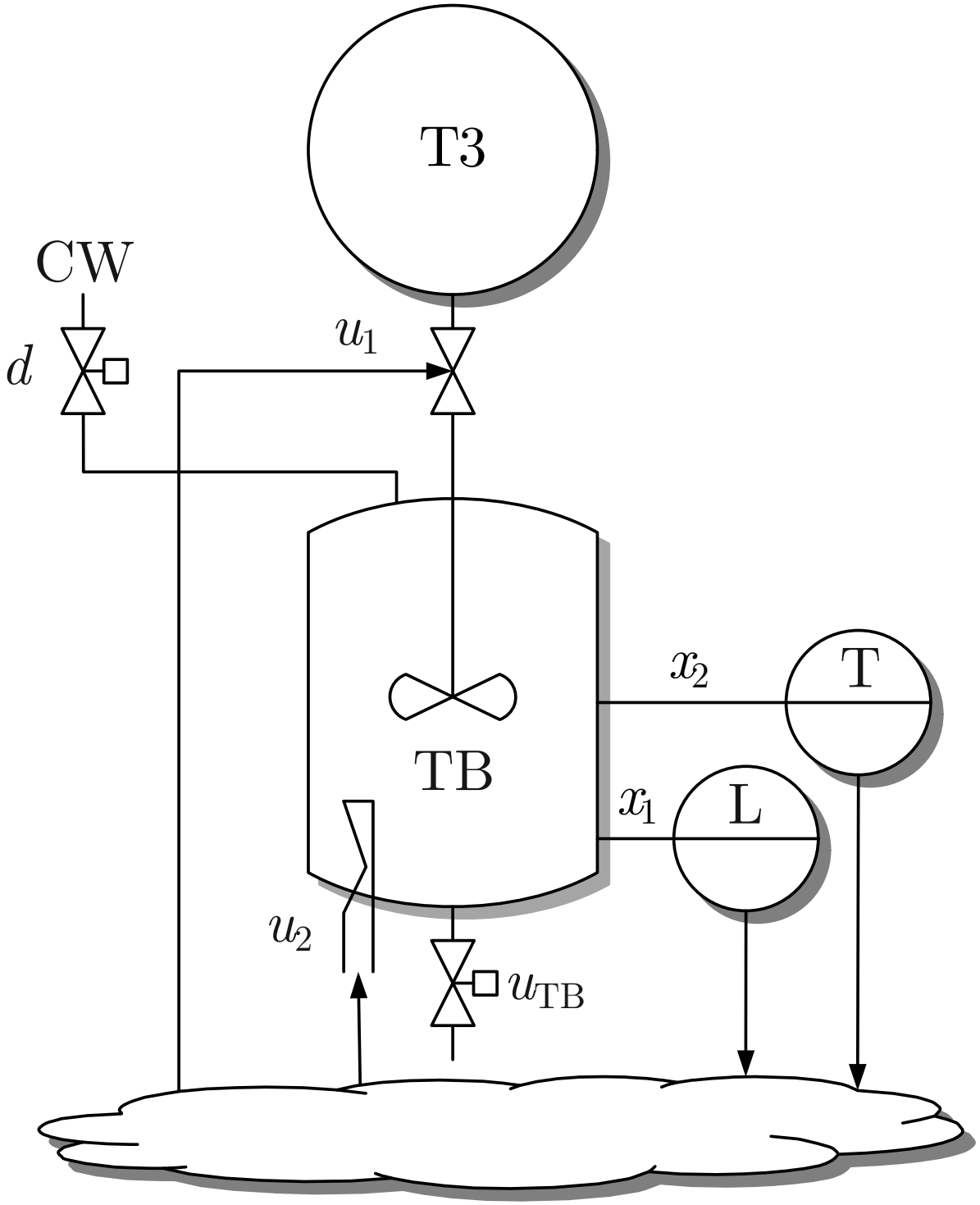

Fig. 0: A thermo-fluid process

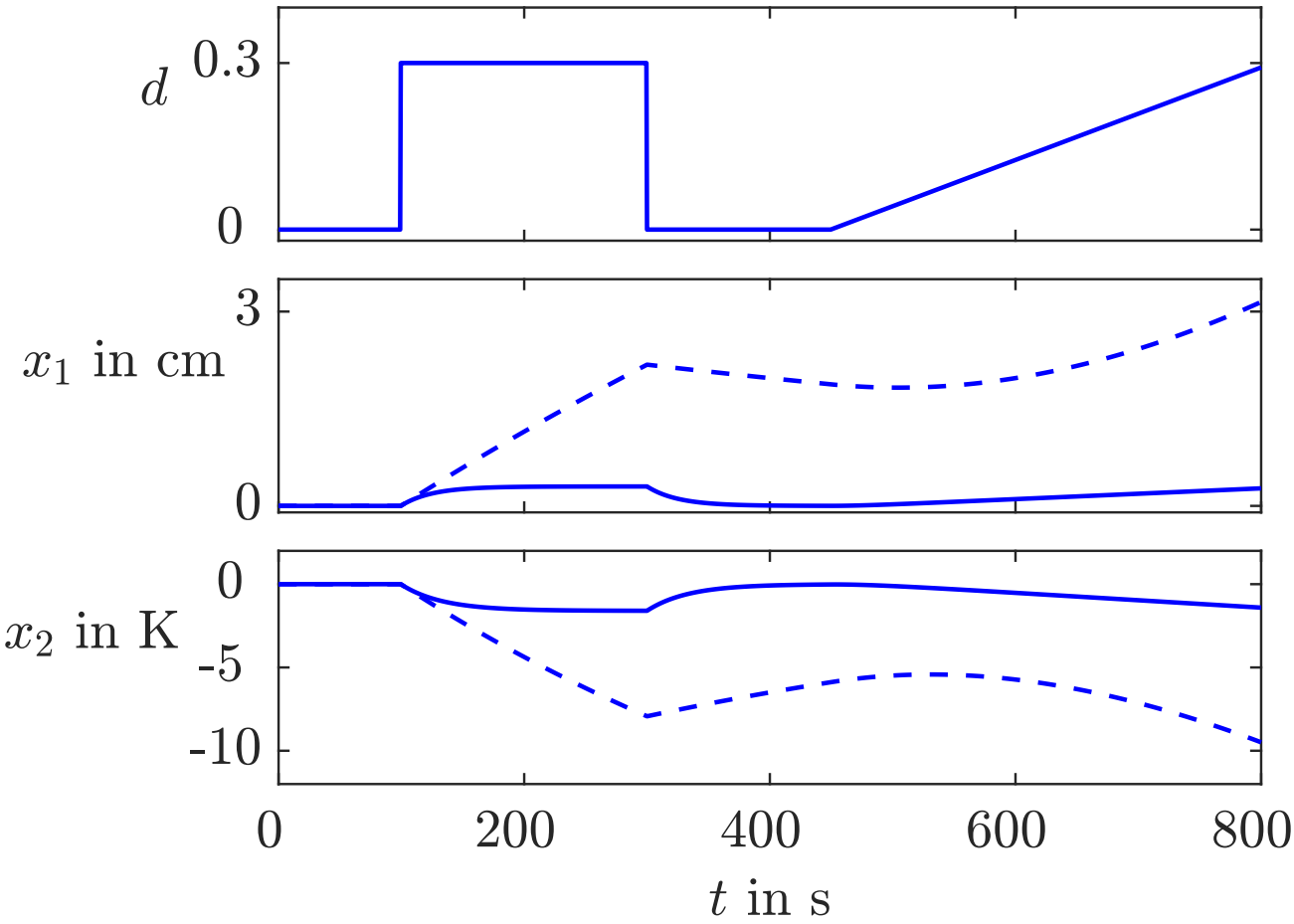

Fig. 1: Disturbance behaviour of the plant (- - -) and of the continuous closed-loop system (—)

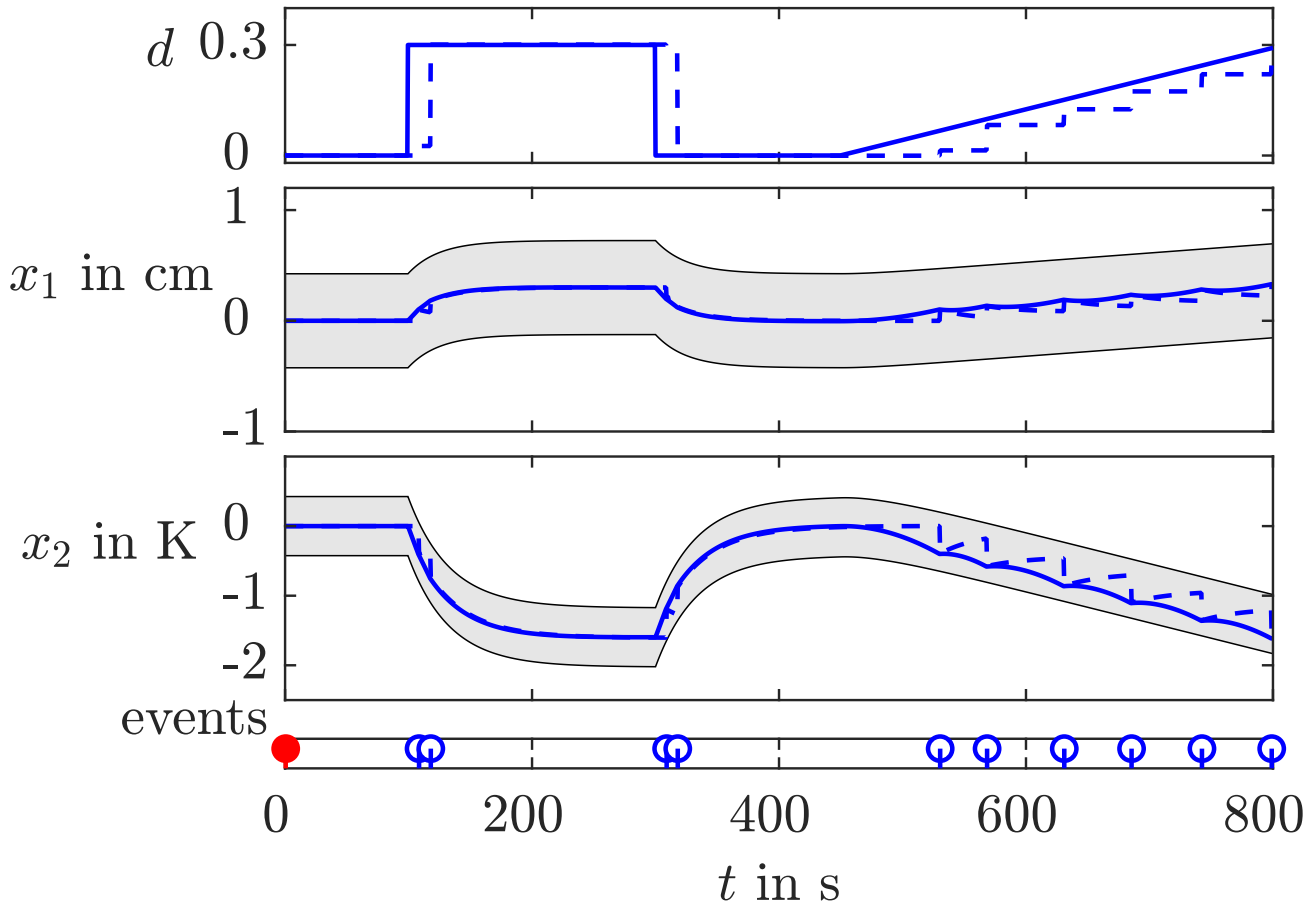

Fig. 2: Behaviour of the event-triggered control loop

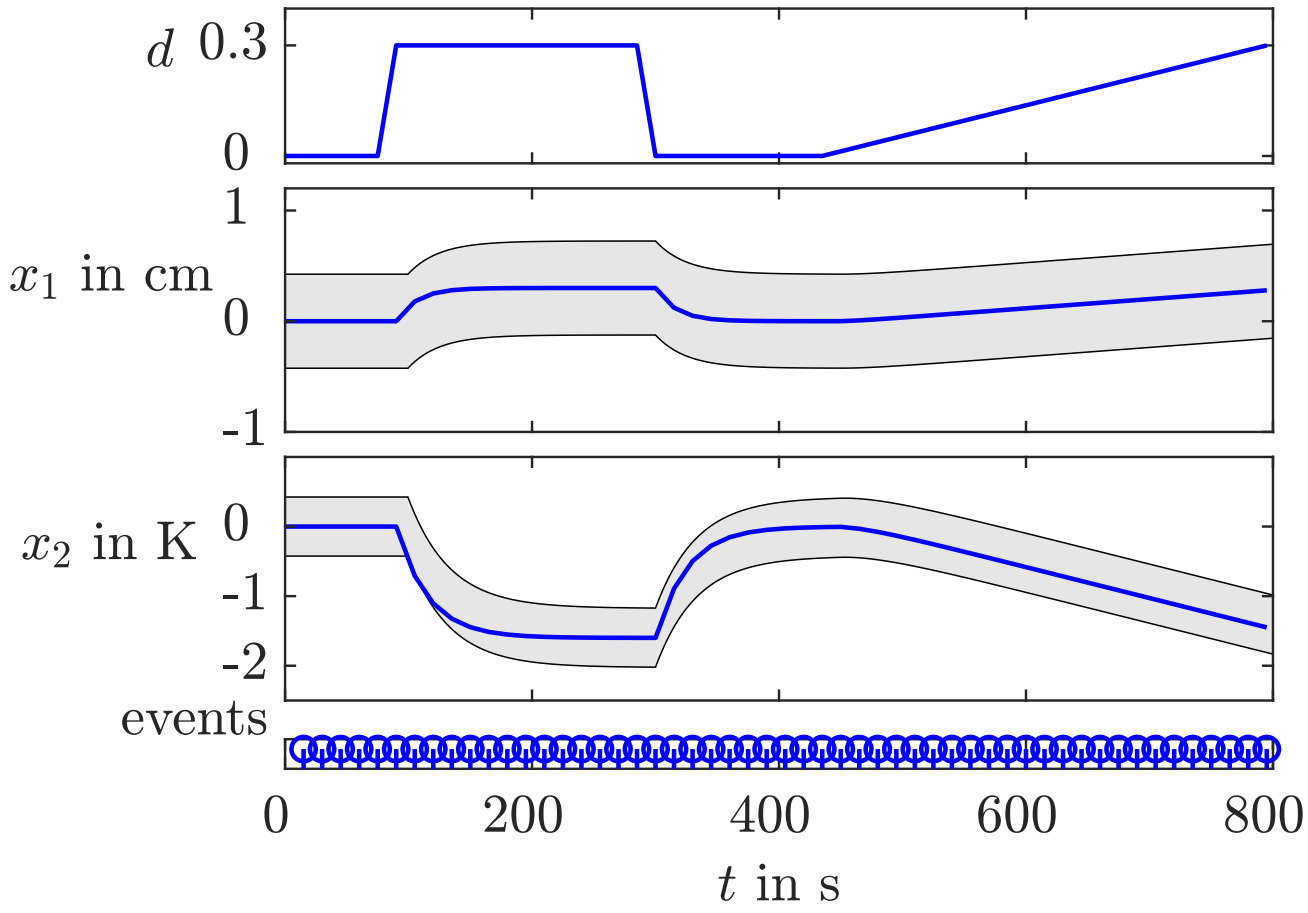

Fig. 3: Sampled-data control loop

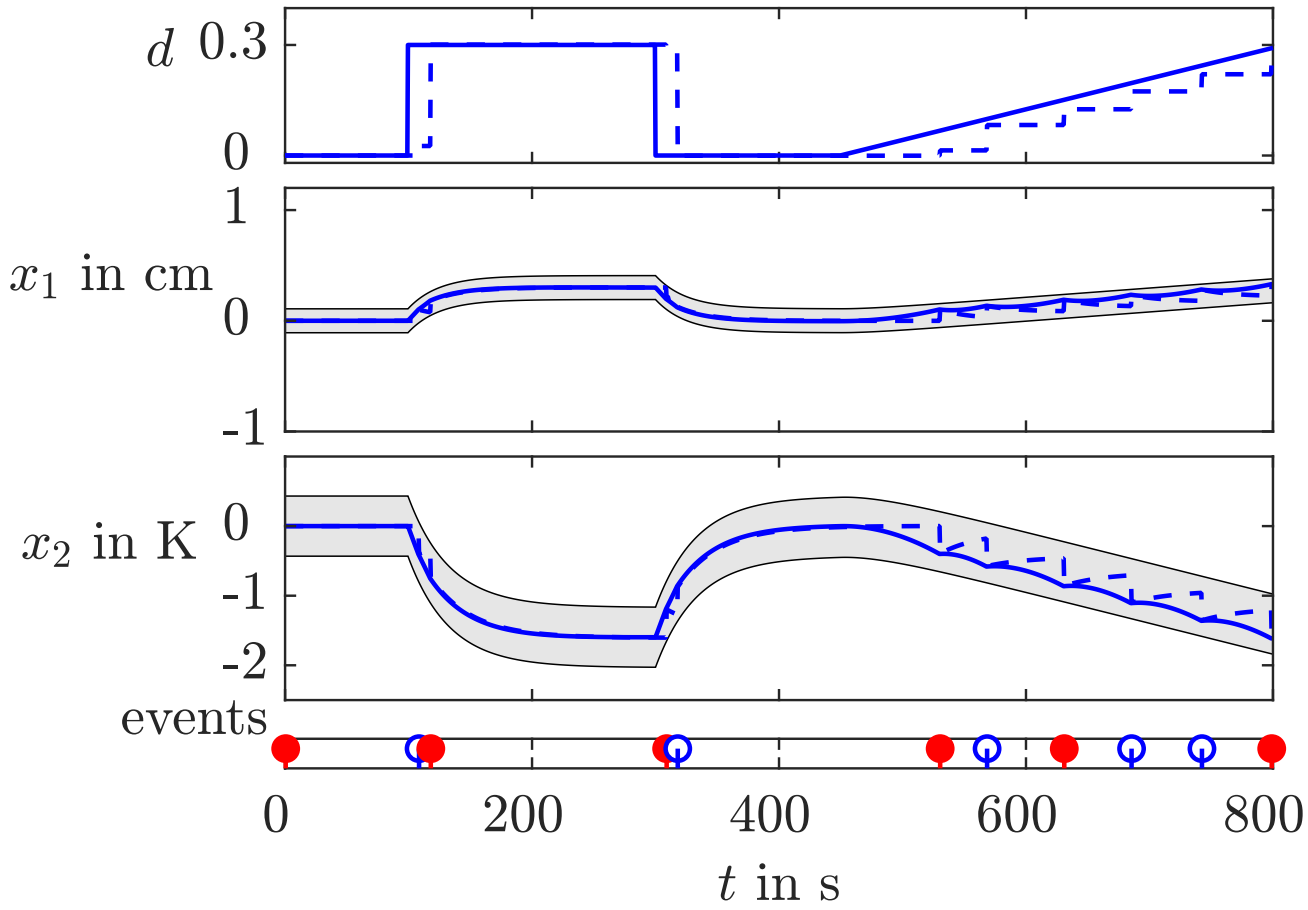

Fig. 4: Behaviour of the event-triggered control loop with scaled norms

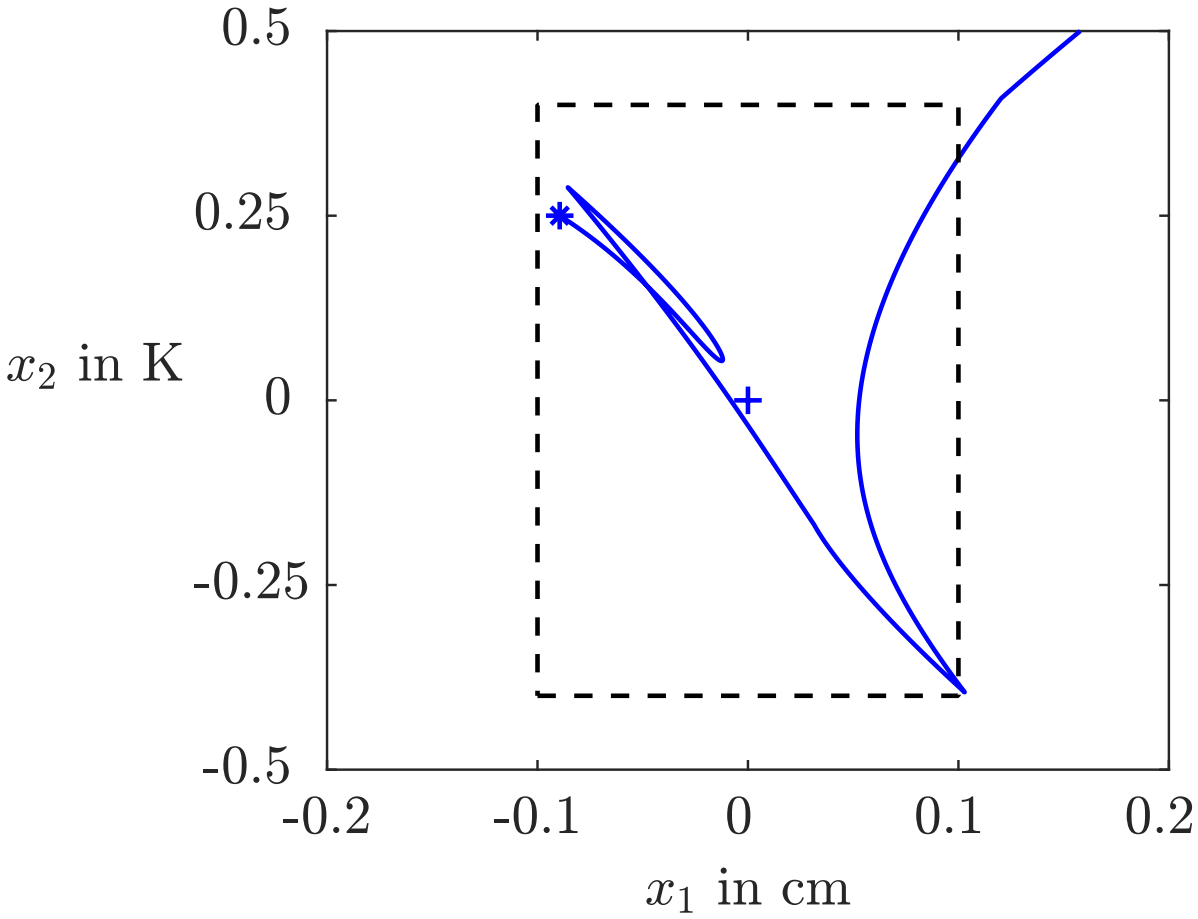

Fig. 5: Long-time behaviour of the event-triggered control loop

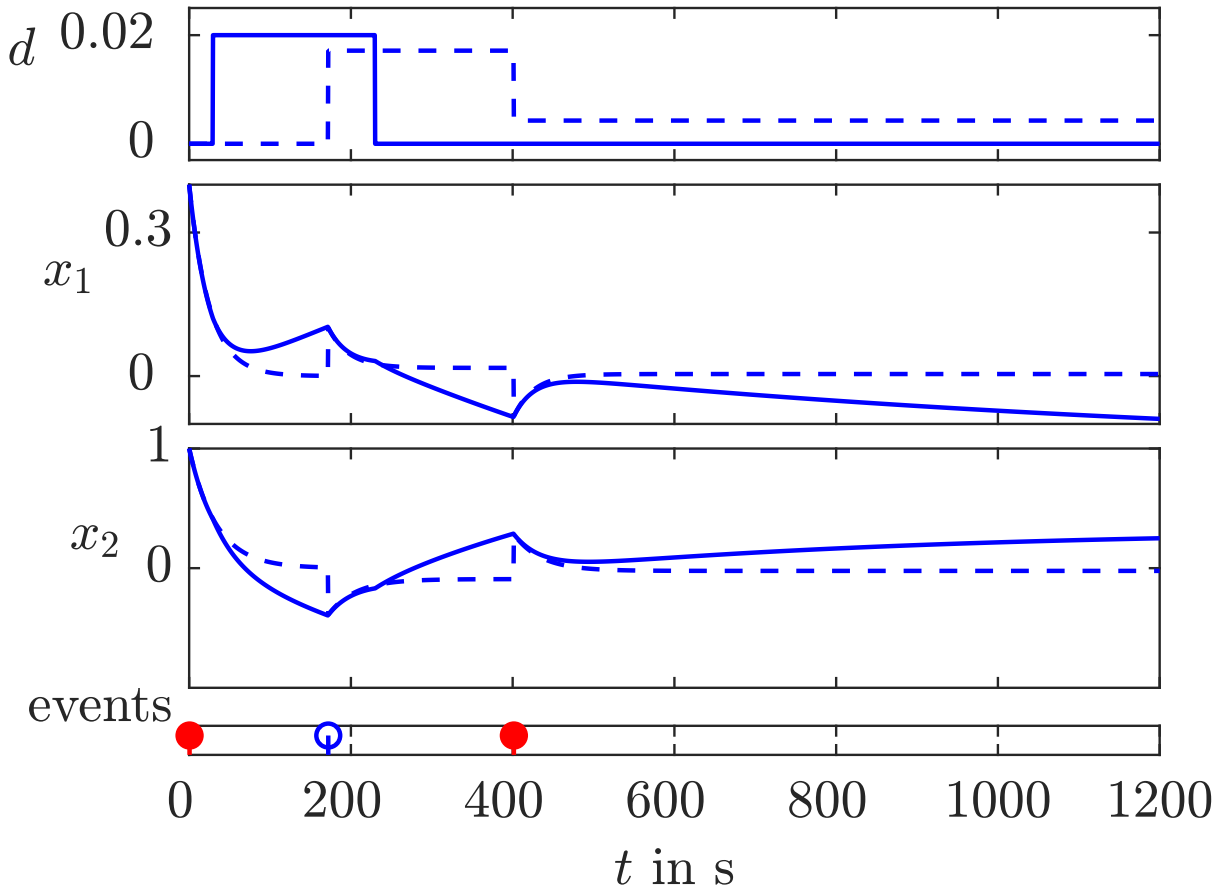

Fig. 5: Long-time behaviour of the event-triggered control loop

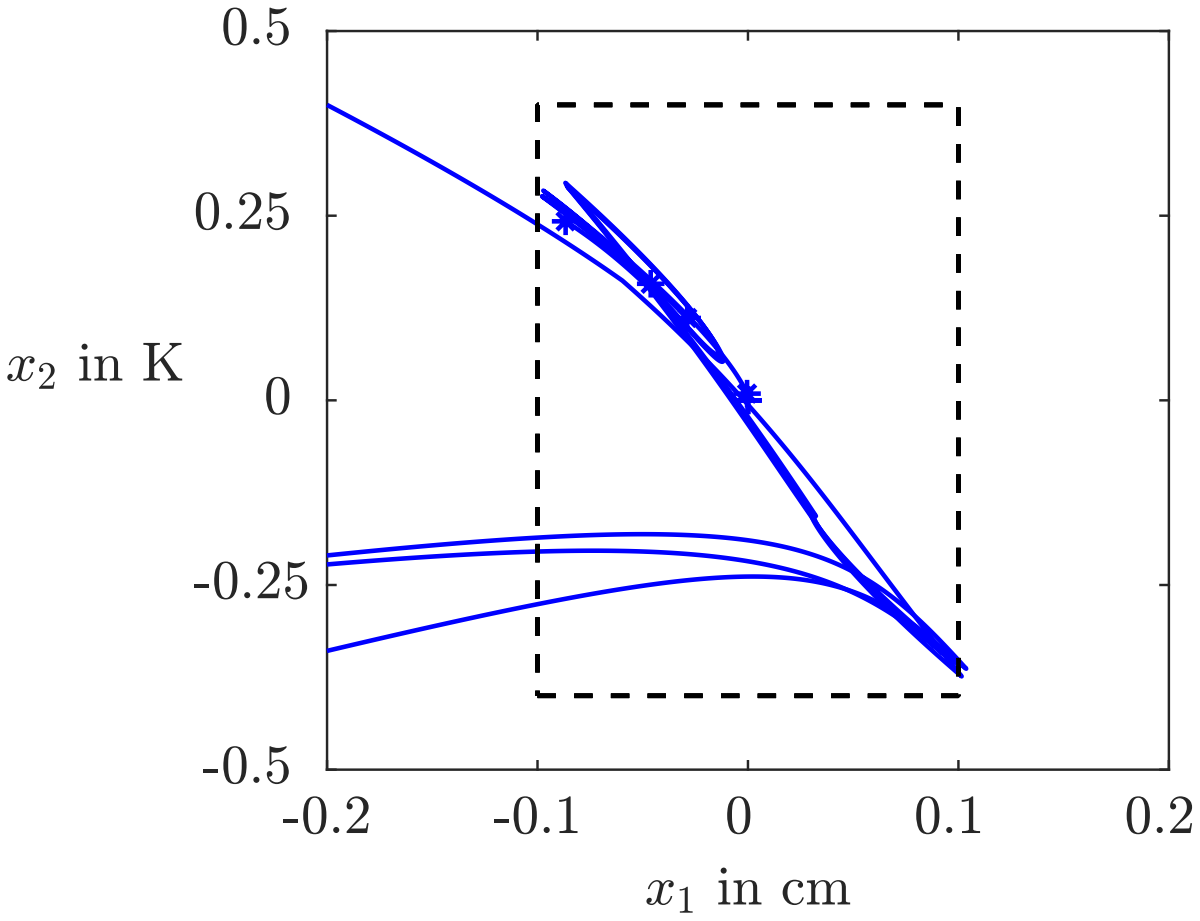

Fig. 6: Practical stability of the thermo-fluid process